VII. FUTURE CONDITIONS AND PROGNOSIS FOR RECOVERY

A. PURPOSE

The purpose of this section is to evaluate potential future air pollution impacts on sensitive receptors in Shenandoah National Park (SHEN) in response to various scenarios of emissions reductions. Simulation modeling was used to evaluate possible future changes in the extent of damage to aquatic, forest, and visibility resources in SHEN in response to changing levels of acidic deposition, ground-level (tropospheric) ozone (O_3) exposure, and ambient air quality, respectively. Alternative emissions scenarios were specified for aquatics and visibility projections on the basis of existing and substantially more stringent regulations, available emissions control technologies, and using the Regional Acid Deposition Model (RADM) to estimate future sulfate (SO_4^{2-}) air concentrations and deposition values at SHEN, as described in Section IV. Ozone exposure scenarios were based on measured 5-month SUM06 exposures for the period 1997 to 1999, and a suite of future exposure scenarios, ranging from about an 80% decrease to about a three-fold increase in the ambient 5-month SUM06 O_3 exposure. The effects modeling was conducted using the Model of Acidification of Groundwater in Catchments (MAGIC) for aquatic effects, the TREGRO model for growth of individual tree species, and the ZELIG gap succession model for forest stand composition and growth. Future visibility conditions were calculated for each of the emission scenarios based on expected reductions in fine SO_4^{2-} particle concentrations in the atmosphere, generated from RADM, and the known contribution of each particle type to light extinction.

The prognosis for future recovery of damaged resources in SHEN was also evaluated. In particular, this effort included a critical loads analysis of the effects of sulfur (S) deposition on aquatic resources, based on several chemical endpoint criteria and evaluation years.

B. 1990 CLEAN AIR ACT AMENDMENTS AND ALTERNATIVE EMISSIONS CONTROL SCENARIOS

Scenarios of future emissions were developed for this report following U.S. Environmental Protection Agency (EPA) methods regarding preparation of emissions inventory input into air quality modeling for policy analysis and rule making purposes (see, for example, Appendix A of U.S. EPA 1999). A base emissions inventory was created representing the future with economic assumptions obtained from the Bureau of Economic Analysis and emissions controls representative of the laws, rules, and regulations already on the books and final as of the date of

preparation of the inventory. These various control constraints include Federal, state and local requirements for emissions control for a wide variety of environmental and human health goals.

This report relies upon EPA projected emissions developed for the Heavy-Duty Engine and Vehicle Standards and Highway Diesel Fuel Rulemaking for the 1996, 2010 and 2020 base emissions for all sources other than electricity generation. Electricity generation emissions were modeled using the Integrated Planning Model (IPM) to develop the base emissions estimates for electricity generation for 2020. Additional control constraints were applied to the generation system nationwide to reflect the various levels of additional control considered. In addition, a control scenario was developed by E.H. Pechan and Associates under EPA contract for stationary point sources, representing the limit of current commercially available control technology. Finally, a set of mobile source emissions estimates were developed by Dyntel Corp., under contract to the EPA, reflecting the limit of technology for highway automobiles and light duty trucks based upon a California Air Resources Board (CARB) analysis of this sector (CARB 2001).

The 1990 base case and future emissions estimates were thus developed for this assessment based on existing regulations and future economic assumptions. Four emissions scenarios, described in more detail in Section IV.B, were implemented:

Scenario 1. Base with NO_x State Implementation Plan (SIP) Call - Assumes reasonable economic growth and emissions limitations according to existing regulations as of summer, 2000. Projections are provided to 2010.

Scenario 2. Base Projected to 2020 - Same assumptions as Scenario 1, but projected to 2020 to allow for continued implementation of Tier II Vehicle Standards and full implementation of Title IV and Heavy Duty Diesel Vehicle standards.

Scenario 3. Additional Stringent Utility Controls - Adds to Scenario 2 additional Electric Generating Unit (EGU) controls.

Scenario 4. Additional Stringent Controls on Utility, Industry-Point, and Mobile Sources - Adds to Scenario 3 additional, non-EGU emissions reductions.

The annual deposition of S and nitrogen (N) projected at SHEN under each of the scenarios is provided in Table VII-1. The deposition of S and, to a lesser extent, N is projected to decline substantially from the 1990 base under all scenarios, as are the O_3 exposures and fine particle air concentrations (Table V-19).

Table VII-1. Annual deposition of sulfur and nitrogen projected by the Enhanced Regional Acid Deposition Model for the four scenarios.

Constituent	1990 Base	Scenario 1	Scenario 2	Scenario 3	Scenario 4
Total Sulfur[a] (kg-S/ha/yr)	12.96	8.66	8.20	4.06	3.25
Total Nitrogen[b] (kg-N/ha/yr)	7.63	5.70	4.88	4.40	3.98

[a] Total sulfur deposition includes wet deposition of SO_4^{2-} and dry deposition of gaseous SO_2 and particulate SO_4^{2-}.

[b] Total nitrogen deposition includes wet deposition of NO_3^- and NH_4^+ ; dry deposition of gaseous NO_2, HNO_3, and NH_3 ; and dry deposition of particulate NO_3^- and NH_4^+. Ammonium total deposition was assumed to remain constant at 2.16 kg-N/ha/yr.

C. FUTURE PROJECTIONS

1. Aquatic Ecosystems

a. Background

Computer models can be used to predict pollution effects on ecosystems and to perform simulations of future ecosystem response (Cosby et al. 1985a,b,c; Agren and Bosatta 1988). The MAGIC model, a lumped-parameter, mechanistic model, has been widely used throughout North America and Europe to project streamwater and lakewater response and has been extensively tested against the results of diatom reconstructions and ecosystem manipulation experiments (e.g., Wright et al. 1986; Sullivan et al. 1992, 1996; Sullivan and Cosby 1995; Cosby et al. 1995, 1996). It has been used extensively in the eastern and western United States and Europe to determine the deposition levels at which environmental damage would be expected to occur (c.f., Skeffington 1999, Bulger et al. 2000, Cosby and Sullivan 2001, Sullivan et al. 2002a).

To estimate the past and future status of Virginia's headwater brook trout streams under different acid deposition scenarios, Bulger et al. (2000) applied the MAGIC model to 60 streams, including 14 SHEN streams, chosen to be regionally representative with respect to acidification sensitivity. This analysis suggested that only about half of all trout streams in Virginia have suitable acid-base chemistry for supporting the relatively acid-tolerant brook trout (*Salvelinus fontinalis*) and that acidic deposition is responsible for significant ecological damage in about one-third of the brook trout streams in Virginia.

The model projections by Bulger et al. (2000) suggested that neither a 40% nor a 70% reduction in S deposition would increase the number of streams that are suitable for brook trout in the year 2041. In fact, the results suggested that a 70% reduction in S deposition would be needed in the long-term just to maintain the current number of streams that are suitable for brook trout. Bulger et al. (2000) concluded that recovery of brook trout streams that have been lost due to acidification is not likely unless S deposition reductions in excess of 70% are achieved. In addition, many other ecologically important species, including blacknose dace (*Rhinichthys atratulus*), minnows, darters and aquatic insects, will be eliminated under conditions that are tolerable for brook trout.

Based on such model projections and the results of other research (c.f., Kaufman et al. 1988, Feldman and Connor 1992, SAMAB 1996, Kauffman et al. 1999, Moeykens and Voshell 2002), it appears that aquatic biodiversity in western Virginia has been reduced by acidification. This is not surprising, given the large number of species regionally, some of which are acid-sensitive. Furthermore, rain water is generally too acidic (pH $\leq$ 4.8; Table V-16) to support any fish life without buffering, and dilute, low-acid neutralizing capacity (ANC) waters are common. The results of model simulations presented by Bulger et al. (2000) suggested that, under currently mandated reductions in acidifying pollutants, biodiversity loss in some of Virginia's headwater brook trout streams is likely to continue.

b. Modeling Methods for Aquatic Effects

Site Selection

Fourteen streams were selected for aquatic effects modeling, to represent the range of geologic sensitivity and streamwater ANC found in SHEN (Table VI-1). The 14 streams chosen are all of the streams in SHEN for which water quality data are available in sufficient quantity and of sufficient quality for use in calibrating MAGIC to a long-term database. These streams are routinely sampled as part of the Shenandoah Watershed Study (SWAS) and the Virginia Trout Stream Sensitivity Study (VTSSS). The frequency of sampling ranges from weekly (6 streams) to quarterly (8 streams) and all streams have at least 12 years of monitoring data available. Five streams are underlain by rocks from each of the siliciclastic and basaltic geologic sensitivity classes. Four streams represent the granitic sensitivity class. The siliciclastic watersheds included four streams having ANC between 0 and 16 μeq/L (Paine, Deep, Meadow,

and Twomile Runs), and one stream (White Oak Run) having ANC = 26 μeq/L. The streamwater ANC in the granitic watersheds ranged from 60 (North Fork Dry Run) to 102 (Hazel River) μeq/L, and for the basaltic watersheds ranged from 126 (White Oak Canyon Run) to 258 (North Fork of Thornton River) μeq/L.

Deposition and Meteorology Data

MAGIC requires as atmospheric inputs estimates of the annual precipitation volume (m/yr) and the total annual deposition (eq/ha/yr) of eight ions: Ca, Mg, Na, K, NH_4, SO_4, Cl, and NO_3. These total deposition data are required at each site for each year of the calibration period (the years for which observed streamwater data are used for calibrating the model to each site). Estimated total deposition data are also required for the 140 years preceding the calibration period as part of the calibration protocol for MAGIC, and for each year of any future scenario that will be run using MAGIC.

Total deposition of an ion at a particular site for any year can be represented as combined wet, dry, and in some cases cloud deposition. Inputs to the model are specified as wet deposition (the annual flux in meq/m^2/yr) and a dry and cloud deposition enhancement factor (DDF, unitless) used to multiply the wet deposition in order to get total deposition:

$$\text{TotDep} = \text{WetDep} * \text{DDF}$$

where:

$$\text{DDF} = 1 + \text{DryDep} / \text{WetDep}$$

Thus, given an annual wet deposition flux (WetDep) and the ratio of dry plus cloud deposition to wet deposition (DryDep/WetDep) for a given year at a site, the total deposition for that site and year is uniquely determined.

In order to calibrate MAGIC and run future scenarios, time-series of the total deposition at each site must be estimated for each year of: a) the calibration period; b) the historical reconstructions; and c) the future scenarios. The procedure used to provide these input data for this assessment was as follows.

Wet deposition input data were collected at Big Meadows by the National Atmospheric Deposition Program (NADP) and at White Oak Run and North Fork Dry Run by the University of Virginia. Wet deposition input data were averaged for the three sites over a five-year period centered on 1990. Averaging over a number of years reduces the likelihood that an "outlier" year (i.e., very wet or very dry) would have a large influence.[1] Dry deposition was estimated based on a DDF, which was calculated using NADP and Clean Air Status and Trends Network (CASTNet) data from Big Meadows, also as a five-year average, using those years for which a complete record was available (all except 1994 and 1996). These five-year average estimates of wet and dry deposition for S and N (Table VII-2), derived from sites within the park, were used to define the Reference Year deposition of S and N for the modeling study. These Reference Year deposition values of S and N were used for model calibration (including the historical reconstructions) and for simulation of future deposition scenarios as described below.

Table VII-2. Five-year average estimates of wet, dry, and total deposition of sulfur and nitrogen, which were used to calibrate the MAGIC model to watersheds modeled in SHEN for streamwater chemistry.

Monitoring Site	Precipitation (m/yr)	Wet Deposition (kg/ha/yr)[a]		
		NH_4^+-N	NO_3^-N	SO_4^{2-}-S
White Oak Run	0.99	1.05	2.47	7.24
N. Fork Dry Run	1.14	2.12	2.76	6.96
Big Meadows	1.39	2.02	2.66	7.03
Average	1.17	1.73	2.63	7.08
Monitoring Site		Dry Plus Cloud Deposition (kg/ha/yr)[b]		
		NH_4^+-N	NO_3^--N	SO_4^{2-}-S
Big Meadows		0.51	2.87	5.83
Estimate Applied to All Modeling Sites		Total Deposition (kg/ha/yr)		
		NH_4^+-N	NO_3^--N	SO_4^{2-}-S
	1.17	2.24	5.50	12.91

[a] Five-year average (1988-1992)
[b] Five-year average, based on years having complete data: 1991-1998, except 1994 and 1996

[1] Note that selection of the calibration period does not have an appreciable effect on model projections or estimates of critical loads. The model is run forward to the evaluation year, based on measured or projected deposition values.

Given the Reference Year deposition values, the deposition data for historical and calibration periods can be calculated using the Reference Year absolute values and scaled time series of wet deposition and DDF that give the values for a given year as a fraction of the Reference Year value. For instance, to calculate the total deposition of a particular ion in some historical year j:

$$\text{TotDep(j)} = [\text{WetDep(0)} * \text{WetDepScale(j)}] * [\text{DDF(0)} * \text{DDF Scale(j)}]$$

where WetDep(0) is the Reference Year wet deposition (meq/m^2/yr) of the ion, WetDepScale(j) is the scaled value of wet deposition in year j (expressed as a fraction of the wet deposition in the Reference Year), DDF(0) is the dry deposition factor for the ion for the Reference Year, and DDFScale(j) is the scaled value of the dry deposition factor in year j (expressed as a fraction of the DDF in the Reference Year). In constructing the historical deposition data, the scaled sequences of wet deposition and DDF were derived from simulations using the Advanced Statistical Trajectory Regional Air Pollution (ASTRAP) model (Shannon 1998).

Given the same Reference Year deposition values, the deposition data for the future deposition scenarios can be calculated using the Reference Year absolute values and a scaled time series of changes in total deposition to give the total deposition values for a given future year as a fraction of the Reference Year value. For instance, to calculate the total deposition of a particular ion in some future year j:

$$\text{TotDep(j)} = [\text{WetDep(0)} * \text{DDF(0)}] * \text{TotDep Scale(j)}$$

where WetDep(0) is the Reference Year wet deposition (meq/m^2/yr) of the ion, DDF(0) is the dry deposition factor for the ion for the Reference Year, and TotDepScale(j) is the scaled value of the total deposition factor in year j (expressed as a fraction of the total deposition in the Reference Year).

Deposition Inputs for MAGIC

Four deposition inputs are required for each of the eight deposition ions in MAGIC in order to set the total deposition for all years required in the calibrations and future simulations:

1) the absolute value of wet deposition at the site for the Reference Year (meq/m^2/yr);

2) the absolute value of DDF (calculated from the DryDep/WetDep ratios) for the site for the Reference Year, (unitless);

3) time series of scaled values of wet deposition and scaled values of DDF covering all historical years necessary to calibrate the model (scaled to the Reference Year);

4) time series of scaled values of future total deposition covering all future years of interest to the scenario runs (scaled to the Reference Year).

The *absolute value of wet deposition* is time and space-specific, varying geographically and from year to year. It is desirable to have the estimates of wet deposition take into account the geographic location of the site as well as the year for which calibration data are available. The Reference Year wet deposition (derived above) for the park provides a single value for the deposition of each ion for the whole park for the Reference Year. To provide an estimate of the spatial variation in wet deposition across the 14 modeling sites within the park, the Reference Year average deposition values were corrected for geographical location and elevation using scaled deposition data for each ion at each site derived from the spatially explicit deposition model of Lynch et al. (1996). The Lynch model is based on spatial and elevational interpolation of wet deposition values of each ion from the NADP monitoring network. The outputs of the Lynch model for each of the 14 modeling sites were averaged over the same five-year period (1988-1992) to provide spatial patterns of wet deposition within the park over the period used to define the Reference Year. The resulting spatially-dependent wet deposition data were used for each site when calibrating MAGIC (Table VII-3). This spatial extrapolation procedure insures that the average deposition values of each ion across the 14 sites (Table VII-3) are equal to the Reference Year deposition values for the whole park.

The *absolute value of the DDF* specifies the ratio between the absolute amounts of wet and total deposition. This ratio is less variable in time and space than is the estimate of total deposition. That is, if in a given year the wet deposition goes up, then the total deposition usually goes up also (and conversely). Estimates of the DDF used for MAGIC may, therefore, be derived from a procedure that uses park-wide data (i.e., lacks spatial resolution). As described previously, the DDF values for S and N were derived from observed data for the Reference Year at a single site within the park, Big Meadows. The same DDF was used for S and N for all 14 modeling sites (Table VII-3). DDF values for chloride (Cl^-) and the base cations were calculated by assuming that Cl^- inputs and outputs should be in balance across the park. A single DDF (dry

Table VII-3. Wet and dry deposition input data for SHEN sites.[a]

Site[b]	Discharge (cm/yr)	Precip. (m/yr)	Yield (%)	Concentration in Precipitation (1990 Reference Year)								Dry Deposition Factor (DDF)							
				Ca	Mg	Na	K	NH^4	SO_4	Cl	NO_3	Ca	Mg	Na	K	NH^4	SO_4	NO_3	Cl
VT36	0.705	1.071	0.66	5.3	2.1	3.6	2.0	10.8	36.8	5.4	15.4	1.76	1.76	1.76	1.76	1.25	1.83	2.08	2.8
DR01	0.779	1.271	0.61	5.9	2.2	3.8	2.5	10.6	41.1	5.3	17.9	1.67	1.67	1.67	1.67	1.25	1.83	2.08	2.8
VT35 (PAIN)	0.814	1.213	0.67	6.0	2.3	4.0	2.6	10.4	41.4	5.6	18.3	1.68	1.68	1.68	1.68	1.25	1.83	2.08	2.8
VT53	0.885	1.332	0.66	6.0	2.4	4.1	2.7	10.4	41.4	5.7	18.5	1.68	1.68	1.68	1.68	1.25	1.83	2.08	2.8
WOR1	0.891	1.280	0.70	6.0	2.3	3.9	2.6	10.7	41.6	5.5	18.2	1.67	1.67	1.67	1.67	1.25	1.83	2.08	2.8
NFDR	0.649	1.343	0.48	5.0	2.0	3.6	1.9	10.4	35.3	5.3	14.5	1.76	1.76	1.76	1.76	1.25	1.83	2.08	2.8
VT58	0.744	1.172	0.63	5.4	2.1	3.5	2.0	10.7	37.1	5.3	15.4	1.73	1.73	1.73	1.73	1.25	1.83	2.08	2.8
VT59 (STAN)	0.750	1.188	0.63	5.6	2.2	3.8	2.3	10.5	39.6	5.4	17.0	1.70	1.70	1.70	1.70	1.25	1.83	2.08	2.8
VT62	0.712	1.163	0.61	5.0	2.1	3.6	2.0	10.8	36.3	5.4	15.1	1.76	1.76	1.76	1.76	1.25	1.83	2.08	2.8
VT75	0.578	1.123	0.51	4.8	2.0	3.7	1.9	10.4	34.6	5.4	14.3	1.78	1.78	1.78	1.78	1.25	1.83	2.08	2.8
VT66	0.526	1.066	0.49	4.6	2.0	3.9	1.9	10.1	33.6	5.5	13.8	1.80	1.80	1.80	1.80	1.25	1.83	2.08	2.8
VT51	0.522	1.107	0.47	4.7	2.0	3.9	2.0	10.3	34.7	5.5	14.4	1.79	1.79	1.79	1.79	1.25	1.83	2.08	2.8
VT60 (PINE)	0.530	1.053	0.50	4.8	2.0	3.7	1.9	10.6	35.3	5.5	14.6	1.78	1.78	1.78	1.78	1.25	1.83	2.08	2.8
VT61	0.517	1.055	0.49	5.2	2.1	3.7	2.0	10.7	36.5	5.5	15.2	1.76	1.76	1.76	1.76	1.25	1.83	2.08	2.8

[a] Yield and reference year deposition data were adjusted as necessary to produce mass-balance for chloride.
[b] For stream names, see Table VI-2. Intensively studied sites include Paine Run (PAIN), Staunton River (STAN), and Piney River (PINE).

enhancement) of Cl^- inputs was calculated for the whole park such that the average mass balance (input-output) for Cl^- across all 14 sites was equal to zero. This same DDF was used for Cl^- for all 14 sites (Table VII-3). The added Cl^- was balanced by base cations. A DDF for each base cation at each site was calculated using the ratio of the four base cations in wet deposition at each site. The DDF's for base cations thus vary from site-to-site but result in an exact balance for the added Cl^- at each site (Table VII-3).

Similarly, the *time series of scaled sequences* used for MAGIC simulations do not require detailed spatial resolution. That is, if for any given year the deposition goes up at one site, it also goes up at neighboring sites within the park. Time series of wet deposition and DDF were derived from the ASTRAP model (Shannon 1998), which produced wet, dry, and cloud deposition estimates of S and oxidized nitrogen (NO_x) every five years starting in 1900 and ending in 1990 for the Big Meadows site as part of the Southern Appalachian Mountains Initiative (SAMI) project (Sullivan et al., 2002a). The ASTRAP model outputs are smoothed estimates of deposition roughly equivalent to a ten-year moving average centered on each of the output years. Modeling sites for this project were assigned the historical sequences of the ASTRAP Big Meadows output. The time-series of wet deposition and DDF from 1900 to 1990 were normalized to the 1990 values to provide scaled historical sequences for the MAGIC calibration and reconstruction simulations. The same scaled historical sequences of wet deposition and DDF for S and N were used at all 14 sites (Table VII-4). Historical sequences of base cation and Cl^- deposition were assumed to be constant.

Table VII-4. Assignment of historical deposition sequences at SHEN, based on ASTRAP modeled deposition. [a]

Scaled Sequence	Year													
	1850[b]	1900	1915	1920	1925	1935	1945	1950	1960	1965	1975	1980	1985	1990
Wet S	0.050	0.302	0.620		0.717	0.526	0.829	0.776	0.870	0.920	1.161		0.973	1.000
S DDF	1.112	1.112		1.138			1.154		1.106	1.048	0.977	0.970	0.972	1.000
Wet N	0.000	0.143	0.247		0.363	0.321	0.481	0.531	0.712	0.787	0.977		0.970	1.000
N DDF	0.989	0.989		1.054			0.988		1.000	0.976	0.960	0.960	0.995	1.000

[a] Sequence values were multiplied by wet deposition and DDF values that were measured or estimated for the reference year (1990) in order to estimate total deposition for past years.

[b] The 1850 values of these sequences are assumed for the historical reconstruction as follows: wet deposition sequences were assumed to decline to near zero and DDF sequences were assumed to remain constant at 1900 values.

Specification of Deposition for Future Projections

For a given scenario, the deposition in future years was specified as a fraction of the total deposition in the reference year. In that the future deposition changes were specified only as changes in total deposition, these were implemented in MAGIC by assuming that wet, dry and cloud deposition all change by the same relative amount. The percent changes in total S and N deposition calculated for the emissions control scenarios described in Section IV.B using the RADM model are given in Table VII-5. The modeled percent changes in S deposition are slightly smaller than percent changes in S emissions, whereas the model percent changes in NO_x deposition are slightly larger than percent changes in NO_x emissions (Table IV-4).

Table VII-5. Percent changes in sulfur and nitrogen deposition relative to 1990 base, calculated for emissions control scenarios.

Constituent	Scenario	All	1	2	3	4
	Year	1996	2010	2020	2020	2020
Sulfur		-20.2	-33.2	-36.7	-68.7	-74.9
Oxidized Nitrogen		+2.7	-35.2	-50.3	-59.0	-66.8
Reduced Nitrogen		+29.9	+26.1	+25.7	+29.6	+20.0

Protocol for MAGIC Calibration and Simulation at Individual Sites

The aggregated nature of the MAGIC model requires that it be calibrated to observed data from a system before it can be used to examine potential system response. Calibration is achieved by setting the values of certain parameters within the model that can be directly measured or observed in the system of interest (called fixed parameters). The model is then run (using observed and/or assumed atmospheric and hydrologic inputs) and the outputs (streamwater and soil chemical variables - called criterion variables) are compared to observed values of these variables. If the observed and simulated values differ, the values of another set of parameters in the model (called optimized parameters) are adjusted to improve the fit. After a number of iterations, the simulated-minus-observed values of the criterion variables usually converge to zero (within some specified tolerance). The model is then considered calibrated. If new assumptions (or values) for any of the fixed variables or inputs to the model are subsequently adopted, the model must be re-calibrated by re-adjusting the optimized parameters until the simulated-minus-observed values of the criterion variables again fall within the

specified tolerance. The model and its application methods for this assessment generally conform with the approach followed in the SAMI Assessment (Sullivan et al., 2002a) and are further described in Appendix F.

Calibration Data

The calibration procedure requires that streamwater quality, soil chemical and physical characteristics, and atmospheric deposition data be available for each stream. The water quality data needed for calibration are the concentrations of the individual base cations (Ca^{2+}, Mg^{2+}, Na^{+}, and K^{+}) and acid anions (Cl^{-}, SO_4^{2-}, NO_3^{-}) and the stream pH. The soil data used in the model include soil depth and bulk density, soil pH, soil cation-exchange capacity, and exchangeable bases on the soil (Ca^{2+}, Mg^{2+}, Na^{+}, and K^{+}). The atmospheric deposition inputs to the model must be estimates of total deposition, not just wet deposition.

Ideally, the MAGIC water quality calibration data would be the volume-weighted annual average values of each water quality variable. However, the eight VTSSS streams included in this study do not have discharge data available, and only have water quality data on a quarterly basis. It is thus not possible to derive a volume-weighted annual average value for the water quality variables at these sites. Discharge gauges and weekly water quality sampling at the other six sites allowed calculation of the volume-weighted annual average for those streams. Those averages were most similar to the spring quarter sample in each of the streams. Therefore, the spring quarterly data were selected for calibration at all sites (even in watersheds for which weekly water quality data were available) to ensure compatibility of calibration results across all streams. The averages of spring quarterly samples over the five year period from 1988-1992 were used for calibration at each site (Table VII-6).

Soils data for model calibration were derived as areally averaged values of soil parameters determined from four to eight soil pits excavated within each of the 14 watersheds in 2000. The soils data for the individual soil horizons at each sampling site were averaged based on horizon, depth, and bulk density to obtain single vertically aggregated values for each soil pit. The vertically aggregated data were then spatially averaged to provide a single value for each soil variable in each watershed. Details of the soils data used for calibration at each site are given in Table VII-7. The deposition values used for calibration are summarized in Tables VII-3 and VII-4.

Table VII-6. Streamwater input data for SHEN modeling sites.

Site	Bedrock Class[a]	Discharge (m/yr)	Streamwater Concentration (μeq/L or pH units)												
			Ca	Mg	Na	K	NH_4	SO_4	Cl	NO_3	ANC	pH	SBC[b]	SAA[b]	Calk[b]
VT36	S	0.705	24.7	41.6	21.9	27.0	0.0	90.9	23.1	1.2	-2.4	5.44	115.2	115.2	0.1
DR01	S	0.779	22.8	46.1	25.1	42.9	0.0	108.7	24.4	2.1	-0.8	5.46	136.9	135.2	1.6
VT35[c]	S	0.814	27.2	50.6	24.2	45.7	0.0	111.3	23.5	6.3	4.1	5.81	147.7	141.1	6.6
VT53	S	0.885	28.0	48.1	27.8	38.6	0.0	99.2	24.1	3.5	10.1	6.03	142.5	126.8	15.8
WOR1	S	0.891	30.0	51.8	22.8	38.7	0.0	79.9	22.0	14.9	19.8	6.03	143.2	116.8	26.4
NFDR[c]	G	0.649	84.8	49.2	73.7	10.1	0.0	100.5	30.5	26.5	49.7	6.47	217.7	157.6	60.2
VT59	G	0.750	59.6	25.1	61.3	9.4	0.0	41.4	23.9	2.0	69.7	6.67	155.4	67.3	88.1
VT58	G	0.744	53.7	33.5	59.4	9.5	0.0	40.6	23.2	4.6	71.4	6.73	156.0	68.5	87.6
VT62	G	0.712	56.5	40.7	62.1	10.1	0.0	38.9	24.7	3.9	80.8	6.66	169.4	67.6	101.8
VT75	B	0.578	101.5	79.6	49.8	4.8	0.0	52.2	29.2	28.1	110.7	6.75	235.8	109.6	126.2
VT66	B	0.526	108.9	84.6	58.0	5.1	0.0	52.1	31.3	26.4	127.8	6.80	256.6	109.9	146.8
VT51	B	0.522	132.5	130.0	66.5	18.0	0.0	131.2	32.8	17.2	155.6	7.11	347.1	181.2	165.9
VT60[c]	B	0.530	134.9	112.5	76.7	6.6	0.0	66.5	30.4	30.0	185.2	7.10	330.7	126.9	203.8
VT61	B	0.517	154.7	140.5	97.4	10.3	0.0	89.5	31.2	24.5	234.4	7.12	402.9	145.2	257.7

[a] Siliciclastic, S; Granitic, G; Basaltic, B

[b] SBC, sum of base cations; SAA, sum of mineral acid anions; Calk, calculated ANC.

[c] Intensively-studied sites include VT35 (Paine Run), VT59 (Staunton River), and VT60 (Piney River). For other stream names, see Table VI-2.

Table VII-7. Soils input data for SHEN modeling sites.

Site[b]	Bedrock Class[c]	Soil Chemistry[a]						
		Exchangeable Cations (%)				Base Saturation (%)	pH	CEC (meq/kg)
		Ca	Mg	Na	K			
VT35 (PAIN)	S	10.63	4.06	5.16	0.51	20.4	4.5	70.0
WOR1	S	2.84	1.77	2.86	0.46	7.9	4.4	76.6
DR01	S	5.49	5.34	2.61	0.42	13.9	4.5	85.4
VT36	S	8.40	2.28	2.93	0.45	14.0	4.4	64.0
VT53	S	18.25	5.55	3.71	0.14	27.6	4.4	82.5
VT59 (STAN)	G	19.56	4.66	3.11	0.24	27.6	4.9	101.9
NFDR	G	7.01	2.97	3.20	0.19	13.4	4.5	89.5
VT58	G	7.09	2.85	2.87	0.35	13.2	4.7	100.0
VT62	G	12.32	4.64	3.22	0.71	20.9	4.7	71.0
VT60 (PINE)	B	22.76	12.10	3.24	0.48	38.6	5.0	90.0
VT66	B	36.47	8.84	2.45	0.51	48.3	4.9	134.1
VT75	B	18.15	12.89	2.20	0.40	33.6	5.3	98.4
VT61	B	37.49	15.37	2.47	0.39	55.7	5.3	108.0
VT51	B	19.38	10.81	2.49	0.58	33.3	5.2	87.8

[a] The following parameter values were assumed for all sites: porosity, 50%; bulk density, 1400 g/m^3; depth, 90 cm.
[b] For stream names, see Table VI-2. Intensively studied sites include Paine Run (PAIN), Staunton River (STAN), and Piney River (PINE).
[c] Siliciclastic, S; Granitic, G; Basaltic, B

Calibration and Simulation Procedures

The procedures for calibrating and applying MAGIC to an individual site involve a number of steps, use a number of programs, and produce several discrete outputs. The input data required by the model (streamwater, watershed, soils, and deposition data) were assembled and maintained in data bases (electronic spreadsheets) for each landscape unit. When complete, these data bases were accessed by a program (MAGIC-IN) that generated the initial parameter files (xxx.PR) and optimization (xxx.OPT) files for each site. The initial parameter files contain observed (or estimated) soils, deposition, and watershed data for each site. The optimization files contain the observed soil and streamwater data that are the targets for the calibration at each site, and the ranges of uncertainty in each of the observed values.

The initial parameter and optimization files for each site were sequentially passed to the optimization program (MAGIC-OPT). This program produced three outputs as each site was calibrated. The first (xxx.OUT) is an ASCII file of results that was passed to statistical routines for analysis and summary of model goodness-of-fit for the site. The second (xxx.PR1 ... xxx.PR10) was the multiple calibrated parameter set used in the fuzzy calibration procedure to

assess model uncertainty (see below). The third (xxx.PAR) was the average parameter set for each site (average of the multiple calibration parameter sets) which represents the most likely responses of the site.

The multiple calibrated parameter set (xxx.PR1…xxx.pr10) for each site was used by the program MAGIC-RUN with estimates of historical or future deposition to produce two outputs: 1) reconstructions of historical change at the site; or 2) forecasts of most likely future responses for the applied future deposition scenario. Both of these outputs are in the form of electronic spreadsheets giving simulated values for all modeled variables for each year of each scenario at the site. The multiple calibrated parameter sets were also used with the same estimates of future deposition and the program MAGIC-RUN to produce an analysis of the uncertainty in model projections for that scenario. The results of the uncertainty analysis are in the form of an electronic spreadsheet giving simulated ranges (upper and lower values) for all modeled variables for each year of each scenario at the site.

The implementation of this protocol for calibration and simulation provides a structure for quality control and serves to document the calibration procedure, providing a degree of objectivity in the calibration process. The input data files and programs have been archived along with the MAGIC program. The assumptions involved in the calibration of MAGIC have thus become "fixed and documented". That is, anyone given the input files and programs will generate the same intermediate and final products. There are no subjective decisions made during the calibration of any site that may be forgotten, obscured or confused. The intent is to keep any subjective bias in calibration from affecting scenario simulations. A similar objective protocol was used for MAGIC applications in the National Acid Precipitation Assessment Program (NAPAP) and has been used in a number of regional studies in the United States and Europe.

Performance Analysis

The multiple calibration procedure for each site produced summary statistics (mean, standard deviation, maximum and minimum) for the observed values, the simulated values and the differences (simulated-observed values) of each of the 15 stream variables and each of the 7 soil variables simulated for each of the sites. In addition, plots of simulated versus observed values for stream variables were constructed (Figures VII-1 and VII-2). These analyses showed

that the model calibration results were not biased and did not contain unacceptably large residual errors.

Analysis of Uncertainty

The estimates of the fixed parameters, the deposition inputs (past, current, and future), and the target variable values to which the model is calibrated all contain uncertainties. The multiple optimization procedure that was implemented for calibrating the model allows estimation of the effects of these uncertainties on simulated values from the calibrated model.

The procedure consists of multiple calibrations of each site using random values of the fixed parameters drawn from the observed range of values, and random values of deposition from the range of atmospheric model estimates. Each of the multiple calibrations begin with 1) a random selection of values of fixed parameters and deposition, and 2) a random selection of the starting values of the adjustable parameters. The adjustable parameters are then optimized to achieve a minimum error fit to the target variables. This procedure is repeated ten times for each site. The final calibrated model is represented by the ensemble of parameter values of all of the successful calibrations. To provide an estimate of the uncertainty (or reliability) of a simulated response to a given scenario, all of the ensemble parameter sets are run using the scenario. For any year in the scenario, the largest and smallest values of a simulated variable define the upper and lower confidence bounds for that site's response for the scenario under consideration. Applied for all variables and all years of the scenario, this procedure results in a band of simulated values through time that encompasses the likely response of the site for any point in the scenario. The distributions of these uncertainty estimates for each landscape unit can be regionalized to provide overall estimates of uncertainty for a scenario.

The variations between predicted and observed chemistry (Figure VII-3) may reflect the uncertainty in model structure and performance more accurately than do the results of multiple calibrations. Natural systems respond to processes and rates that are only partially captured by the model formulation. In addition, there is uncertainty associated with the measured values. Thus, it is not surprising that there is some divergence between simulated and observed streamwater ANC over the period of overlap (Figure VII-3). Nevertheless, the simulations are clearly representative of the overall pattern of response.

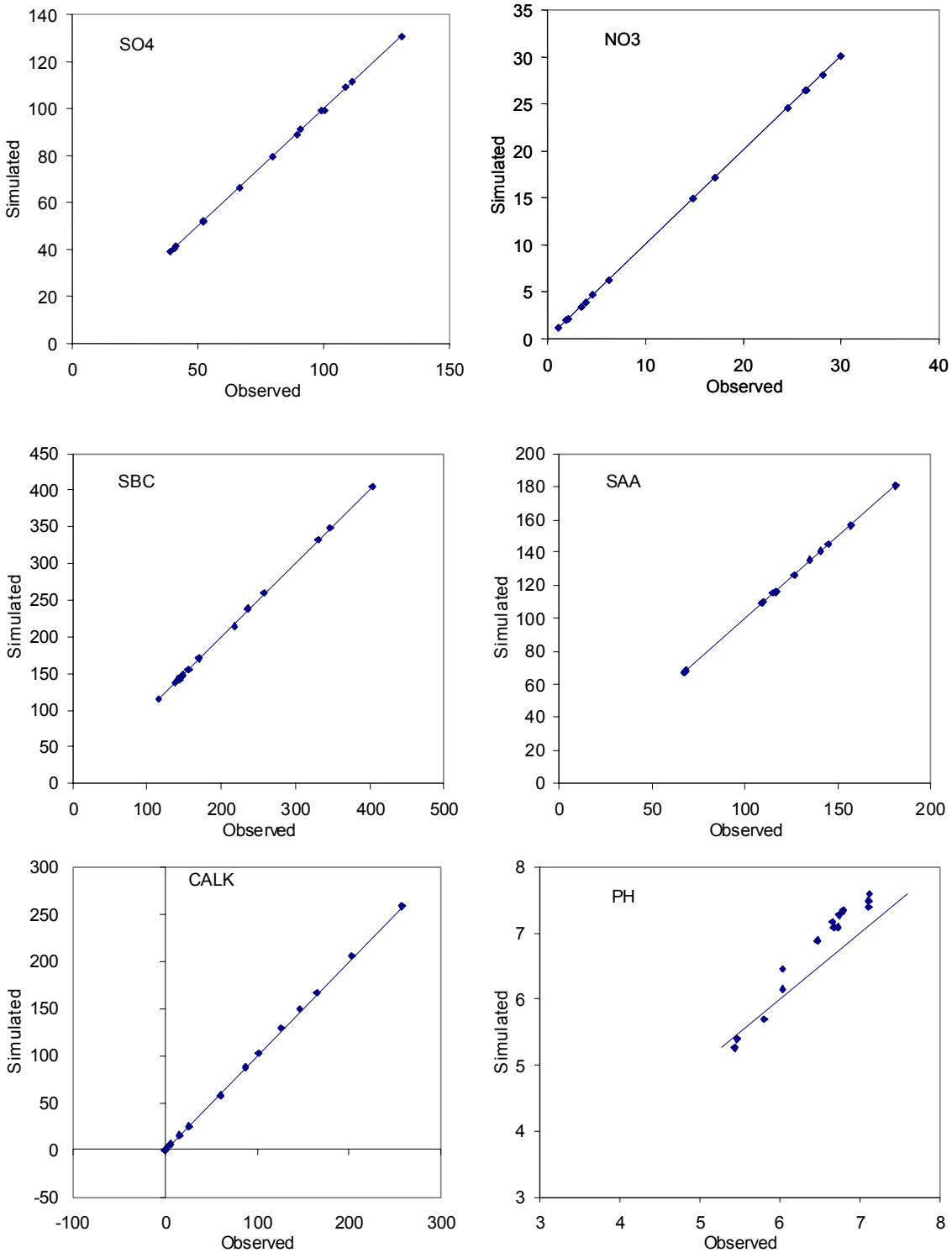

Figure VII-1. Calibration results for the MAGIC model, expressed as predicted versus observed values in the calibration year for sulfate, nitrate, sum of base cations (SBC), sum of mineral acid anions (SAA), calculated ANC (CALK), and pH. Equality lines (1:1) are added for reference.

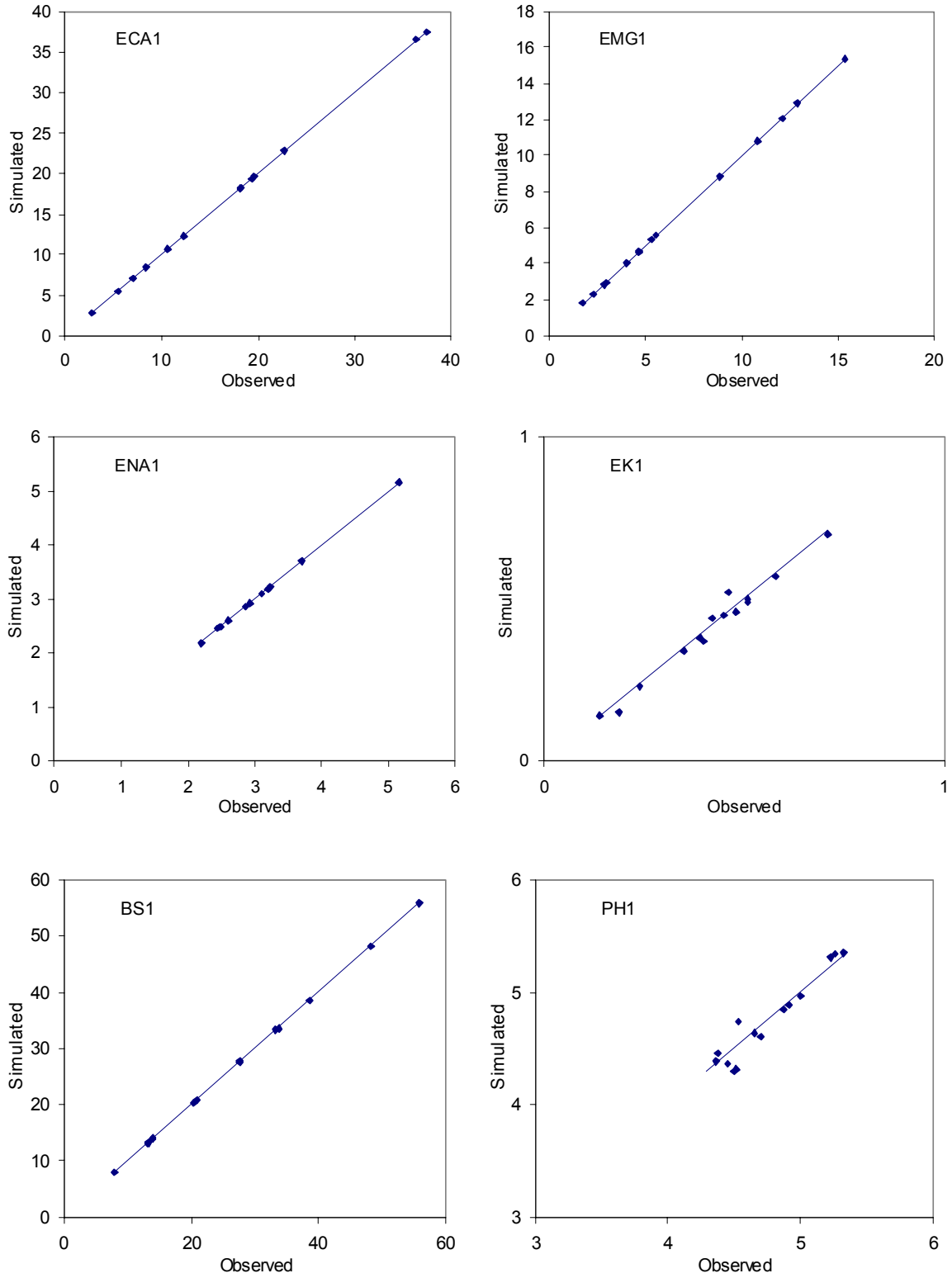

Figure VII-2. Simulated versus observed soils characteristics for modeled watersheds in SHEN, expressed as exchangeable Ca, Mg, Na, and K; base saturation; and soil pH. Equality lines (1:1) are added for reference.

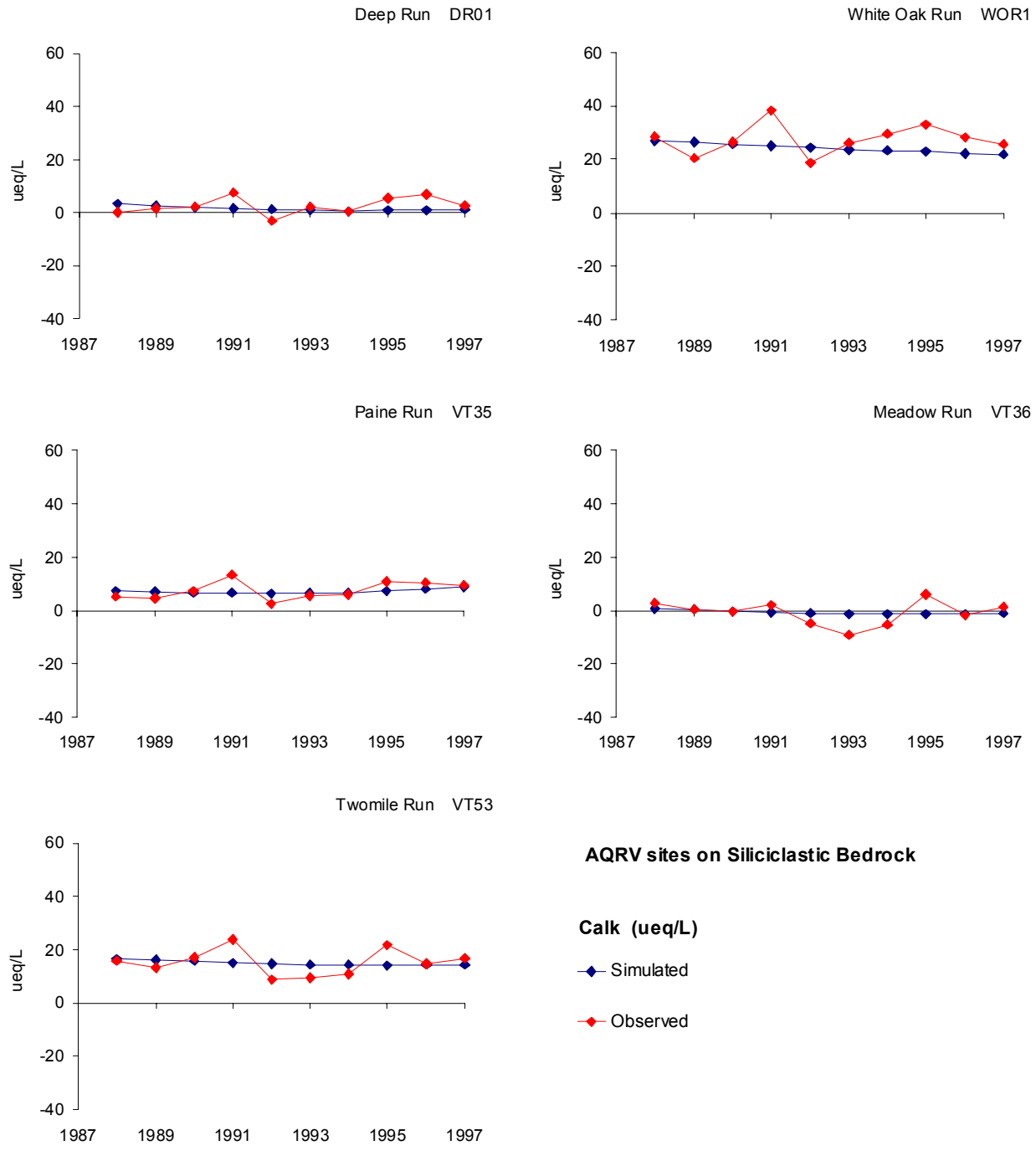

Figure VII-3a. Simulated versus observed ANC over a ten year period for modeling sites on siliciclastic bedrock. The calibration period for these sites was 1988-1992 (5 year average).

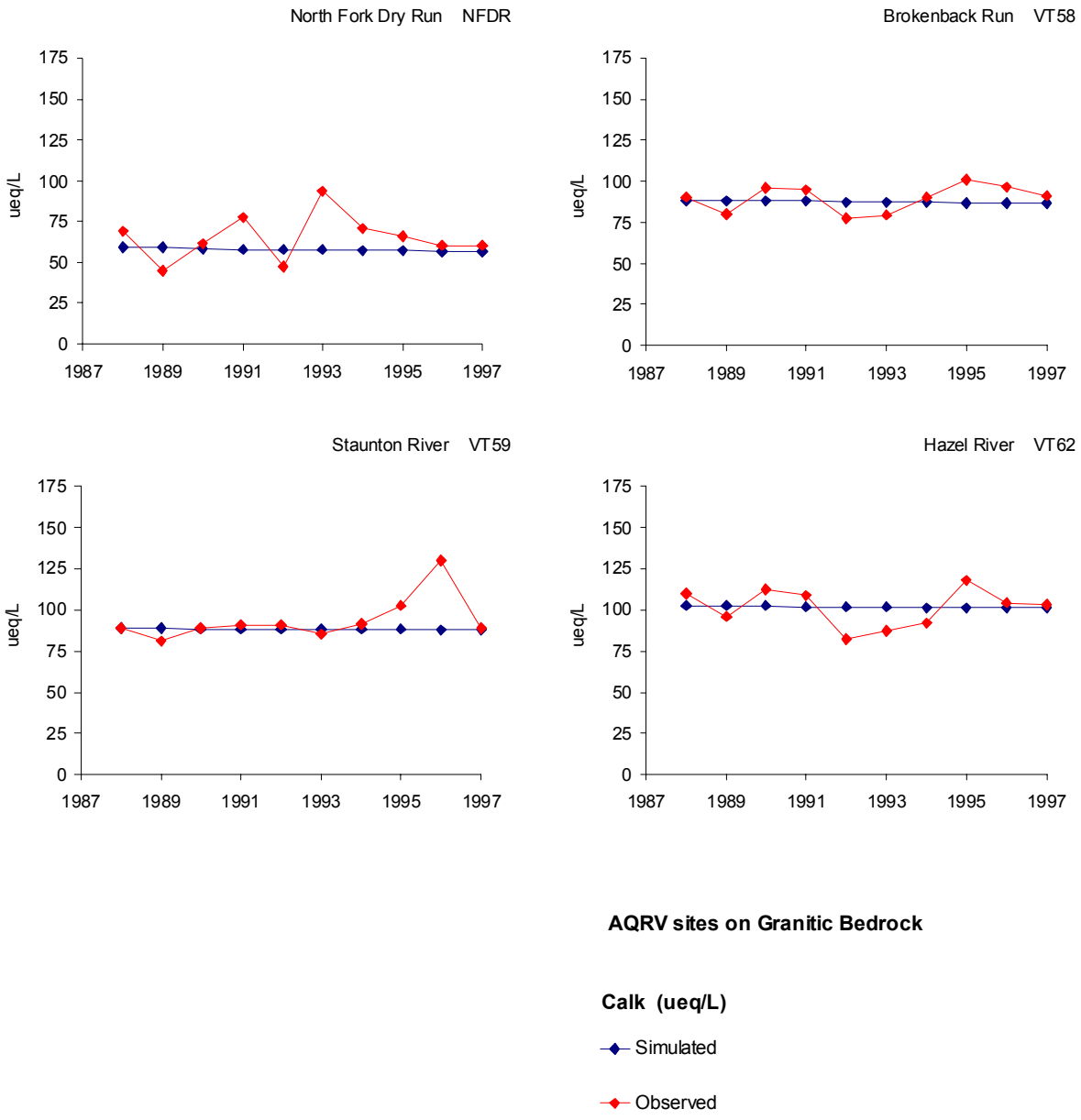

Figure VII-3b. Simulated versus observed ANC over a ten year period for modeling sites on granitic bedrock. The calibration period for these sites was 1988-1992 (5 year average).

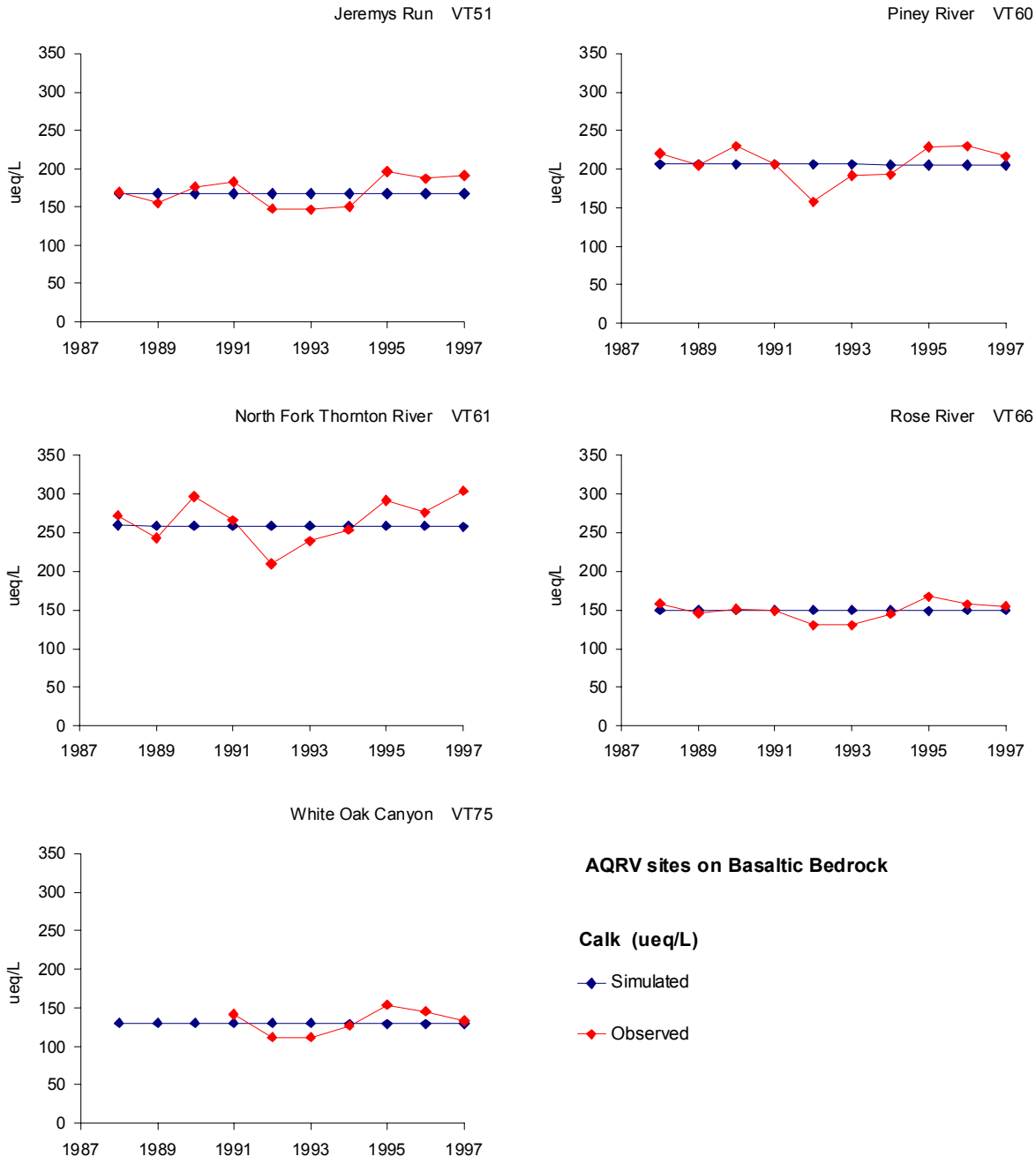

Figure VII-3c. Simulated versus observed ANC over a ten year period for modeling sites on basaltic bedrock. The calibration period for these sites was 1988-1992 (5 year average).

c. Aquatic Modeling Results

MAGIC was successfully calibrated to all modeled watersheds. Results of predicted versus observed chemistry in the calibration year are shown for all modeled sites in Figures VII-1 and VII-2. Agreement was very good for all variables, with the possible exception of pH. The MAGIC model calculates pH using a number of constituents, including the charge-balance ANC and the concentrations of dissolved organic carbon (DOC) and aluminum (Al). Values for DOC and/or Al were missing from some of the model site databases. This introduced additional uncertainty into the estimates of pH for the calibration year.

Demonstrated agreement between predicted and observed streamwater chemistry during the calibration period, as shown in Figures VII-1 and VII-2, does not necessarily demonstrate, however, that the model structure and fundamental assumptions are sufficiently accurate and representative of major watershed processes to yield correct simulations of future conditions. The MAGIC model has been confirmed in several studies that have examined model performance in comparison with independent estimates or measurements of chemical change (c.f., Cosby et al. 1995, 1996; Sullivan et al. 1996) and has been found to be reliable.

A further check on the success of the calibration procedure can be made by comparing yearly time series of simulated values with the observed values at each site for the period of observed data (1988-1997, Figure VII-3). While the model misses some of the observed year-to-year variability, the general agreement with the 10 years of observed data is good at each site. The model was calibrated to the average of the first five years of the observed data. The second five years of data at each site were not used in the calibration procedure.

Future streamwater chemistry was simulated for each site throughout the period 1990 to 2100, based on the scenario of continued constant deposition at 1990 levels and the four emissions control scenarios described in Section IV. Hindcast simulation results are shown in Figure VII-4, suggesting substantial acidification of the modeling sites that occur on siliciclastic bedrock (Figure VII-4a). Among the modeling sites on granitic bedrock, North Fork Dry Run showed evidence of moderate historic acidification, whereas other modeling sites on granitic bedrock and all of the sites on basaltic bedrock showed little historic acidification (Figure VII-4b,c). The inferred pre-industrial ANC of all of the siliciclastic sites and of North Fork Dry Run ranged between about 60 and 90 μeq/L, whereas other sites were inferred to have had pre-industrial ANC near or above 100 μeq/L.

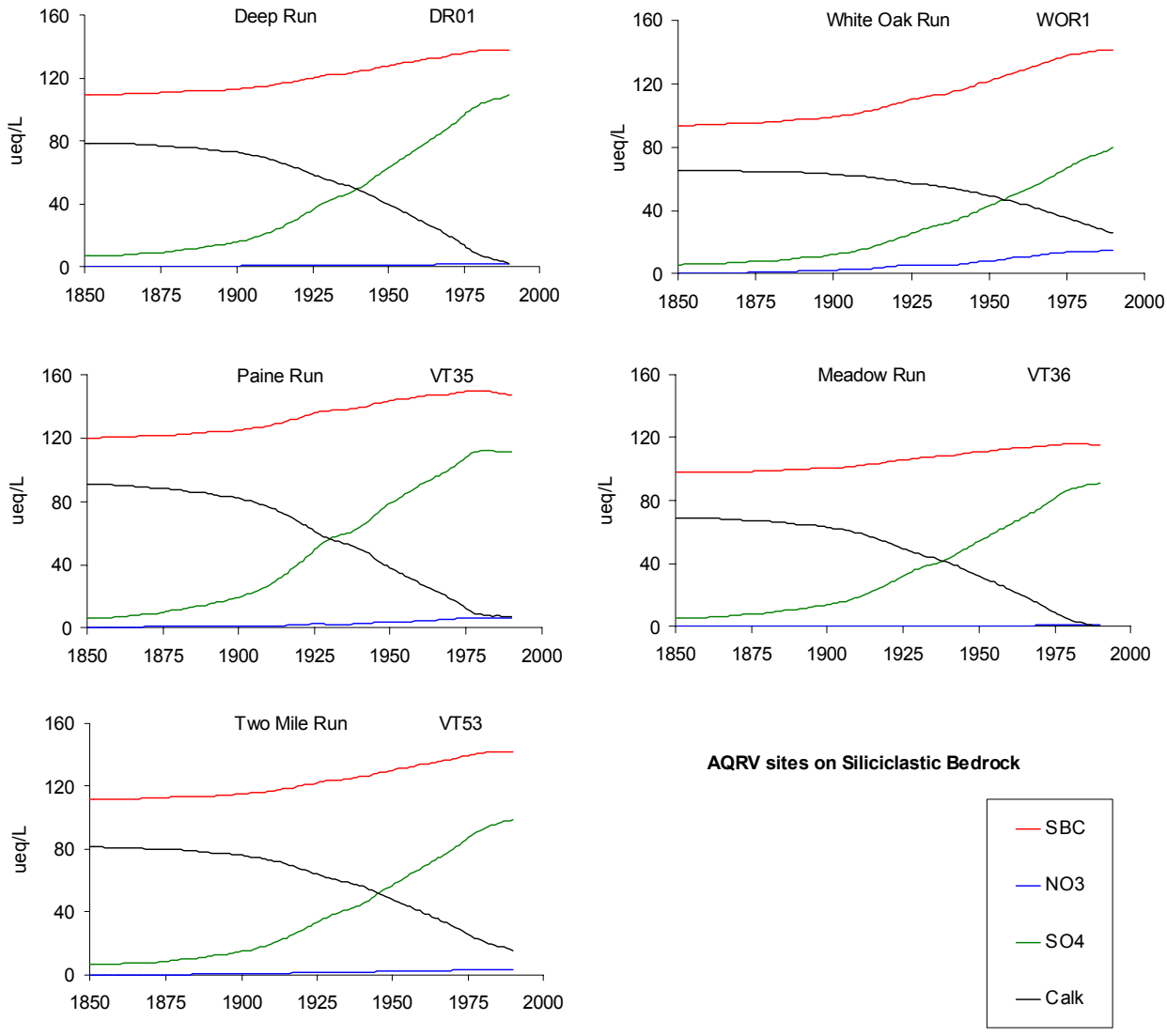

Figure VII-4a. MAGIC hindcast projections for modeled sites on siliciclastic bedrock.

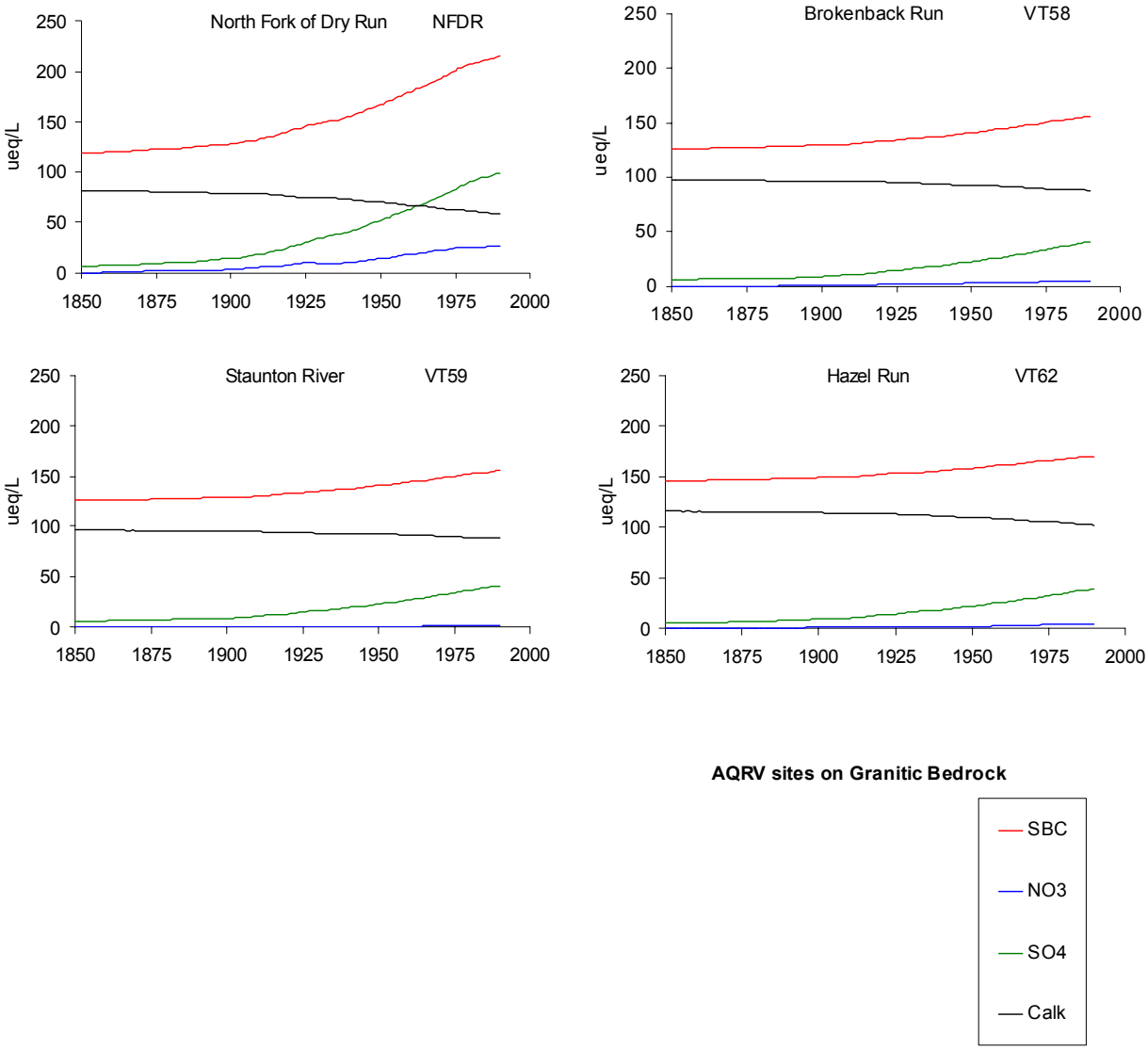

Figure VII-4b. MAGIC hindcast projections for modeled sites on granitic bedrock.

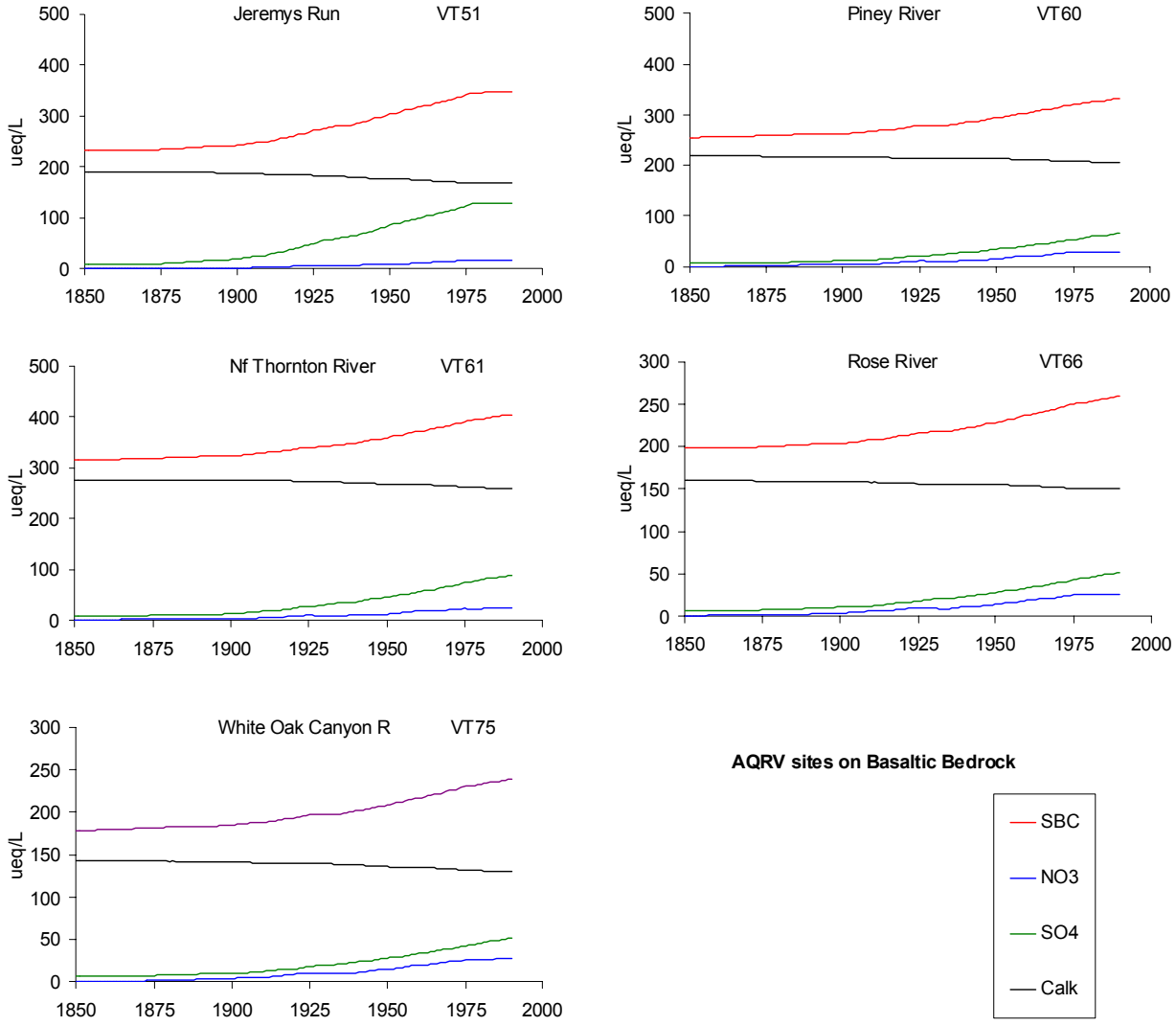

Figure VII-4c. MAGIC hindcast projections for modeled sites on basaltic bedrock.

Projected future concentrations of SO_4^{2-}, nitrate (NO_3^-), sum of base cations, and ANC are presented in Figures VII-5 through VII-8 and Table VII-8 for each of the modeled sites and scenarios. Projected pH values are summarized in Table VII-9 for each site and for each scenario. Sulfate concentrations in streamwater were projected to increase at all sites under the scenario of continued constant deposition. Under the four emissions control scenarios, streamwater SO_4^{2-} concentrations were projected to decrease at all of the sites on siliciclastic bedrock, but results were mixed for the various scenarios applied to sites on granitic and basaltic bedrock. The most stringent emissions control strategy (Scenario 4) resulted in substantial (> 25 μeq/L) projected decreases in streamwater SO_4^{2-} concentrations (Figure VII-5).

Changes in streamwater NO_3^- concentration in response to the scenarios were either negligible or were projected decreases in concentration that were less than about 12 μeq/L (Figure VII-6). Changes in streamwater base cation concentrations were projected to be smallest for the siliciclastic sites, which generally have the lowest base cation concentrations currently, and did not differ substantially among simulations. Base cation leaching was projected to be largest under continued constant deposition and progressively smaller with increasingly stringent emissions control scenarios (Figure VII-7). Projected changes in base cation concentrations were largest for the basaltic sites.

The combined effects of modeled changes in SO_4^{2-} and base cations resulted in projected future changes in streamwater ANC that ranged from less than 10 μeq/L for some siliciclastic sites under Scenarios 1 and 2 to projected ANC increases of more than 40 μeq/L at Deep Run and Paine Run for Scenarios 3 and 4 (Figure VII-8). All siliciclastic sites were projected to become acidic (ANC $\leq$ 0) by the year 2050 under continued deposition at 1990 levels. White Oak Run was projected to nearly become acidic under Scenarios 1 and 2 by 2100, but other sites on siliciclastic bedrock were projected to increase ANC in the future under all emissions control scenarios. In contrast, the majority of the sites on granitic and basaltic bedrock showed projected decreases in ANC under most of the scenarios, largely in response to changes in S adsorption on soils in response to continued S deposition.

We expect that episodic ANC depressions will be superimposed on these projected future chronic ANC values. We lack an approach to rigorously quantify the extent of episodic changes in ANC that would occur in the future, but we expect that such episodic ANC variability would be similar to current episodic behavior. In general, typical episodic ANC depressions of streams

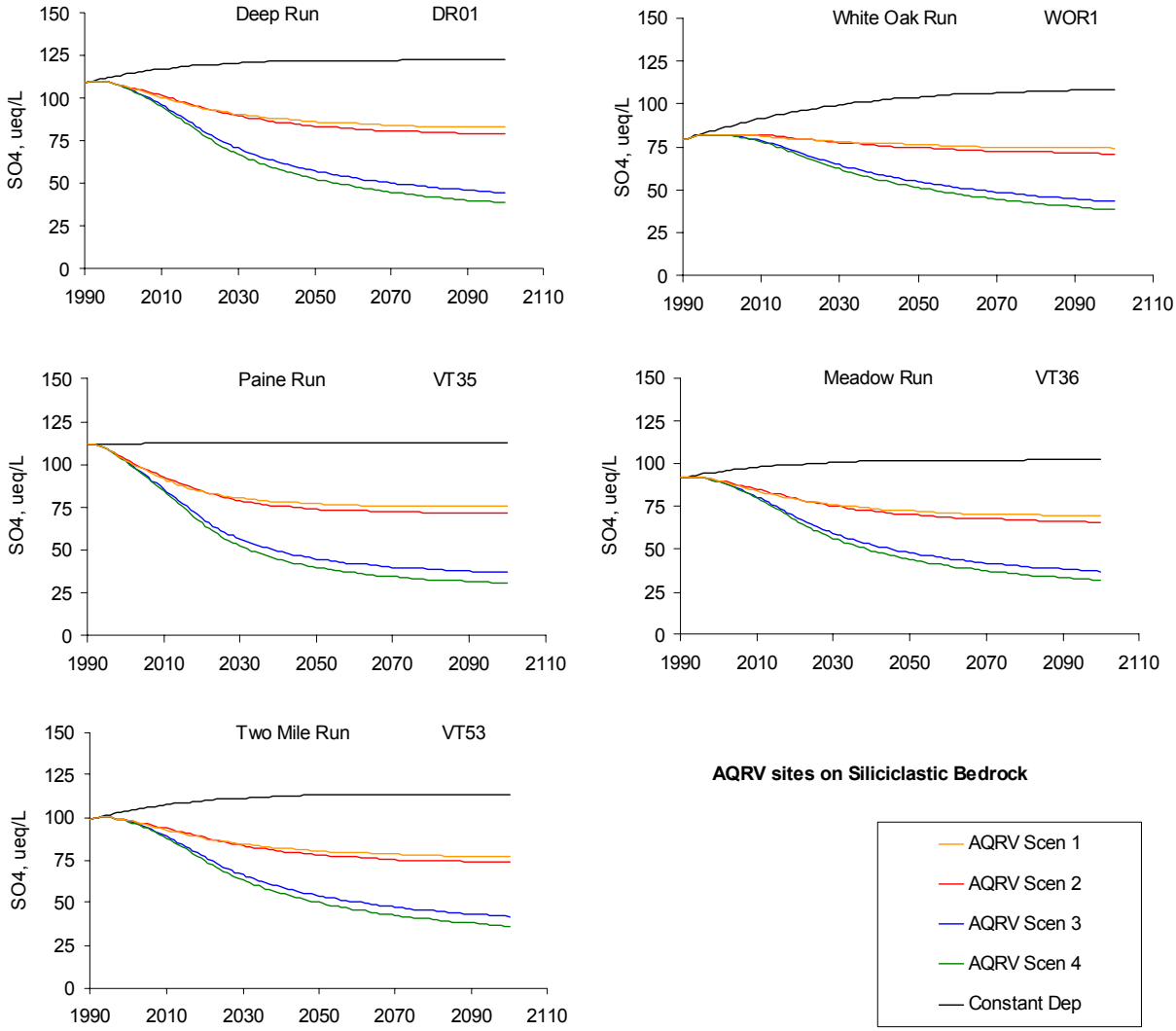

Figure VII-5a. MAGIC model projections of streamwater sulfate under the scenario of constant deposition at 1990 levels and the four emissions control scenarios described in Section IV for modeled sites on siliciclastic bedrock.

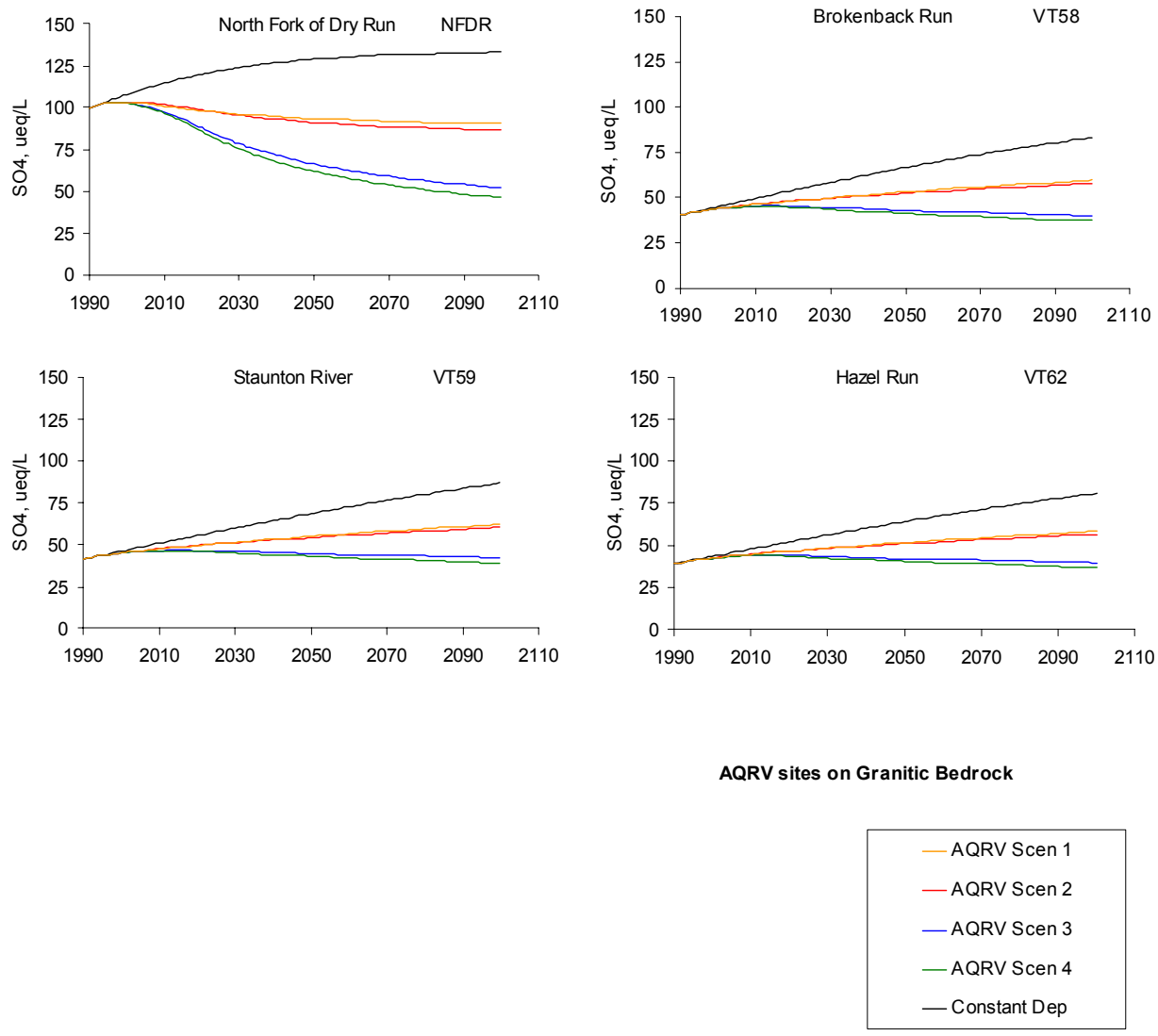

Figure VII-5b. MAGIC model projections of streamwater sulfate under the scenario of constant deposition at 1990 levels and the four emissions control scenarios described in Section IV for modeled sites on granitic bedrock.

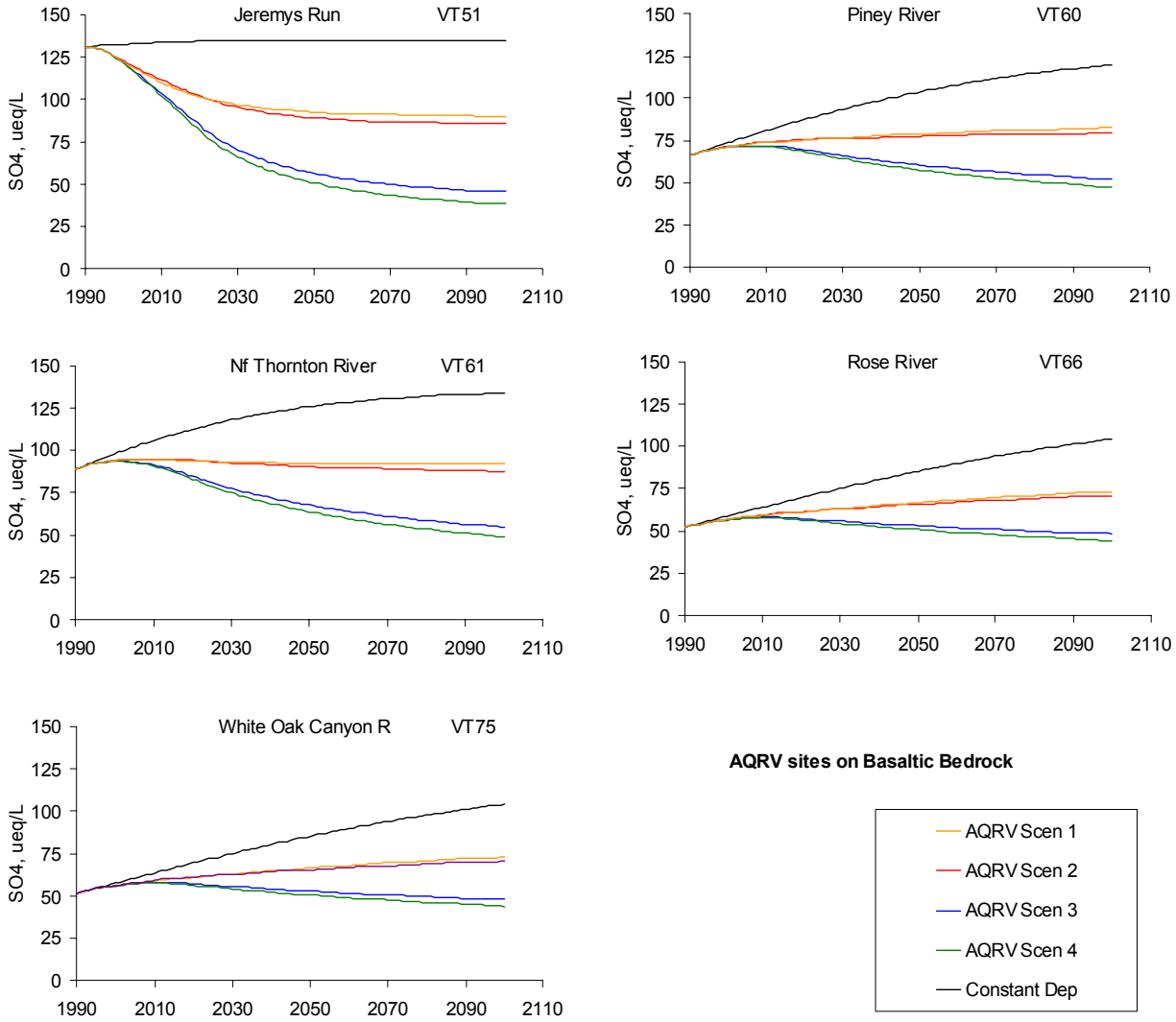

Figure VII-5c. MAGIC model projections of streamwater sulfate under the scenario of constant deposition at 1990 levels and the four emissions control scenarios described in Section IV for modeled sites on basaltic bedrock.

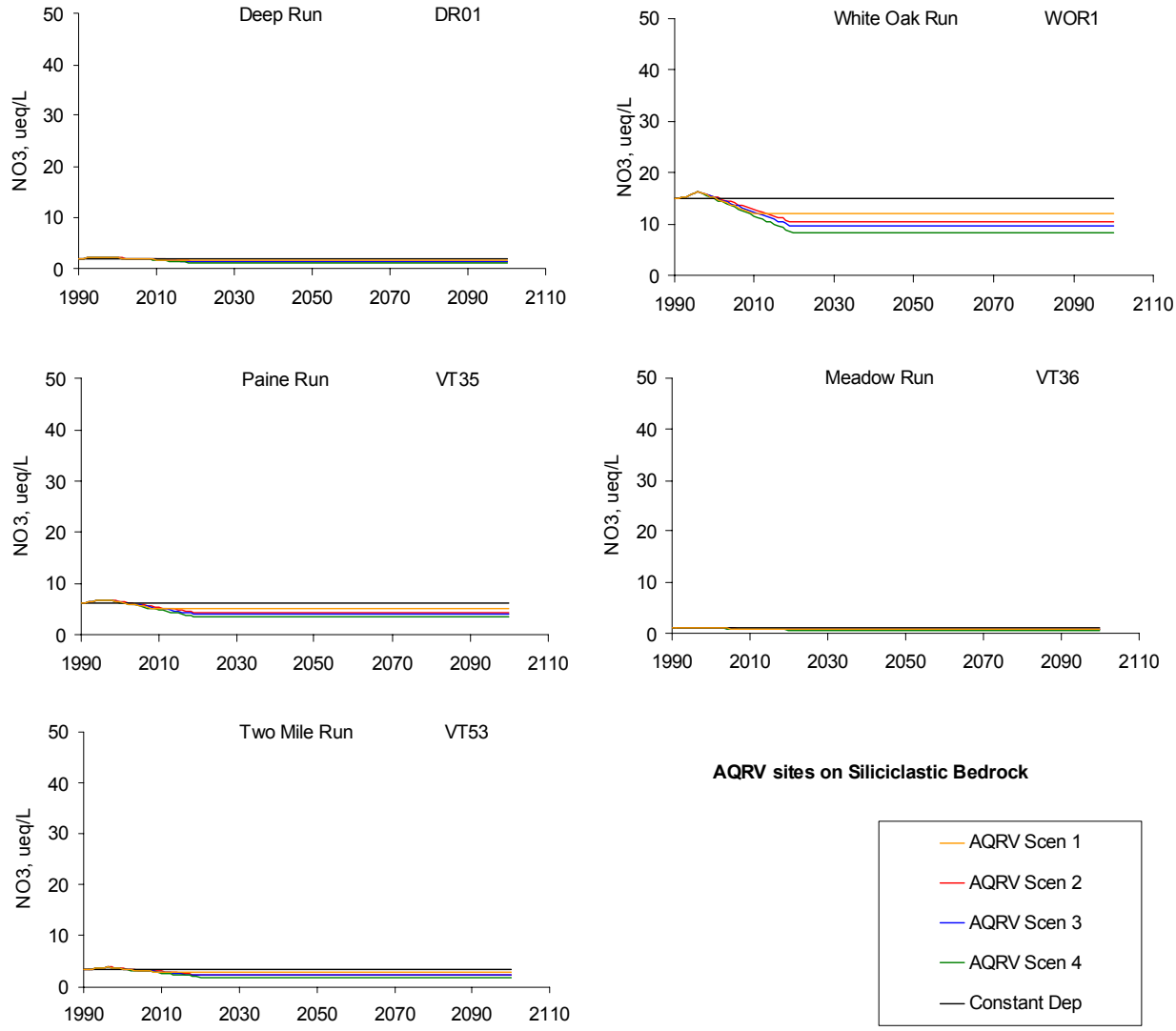

Figure VII-6a. MAGIC model projections of streamwater nitrate under the scenario of constant deposition at 1990 levels and the four emissions control scenarios described in Section IV for modeled sites on siliciclastic bedrock.

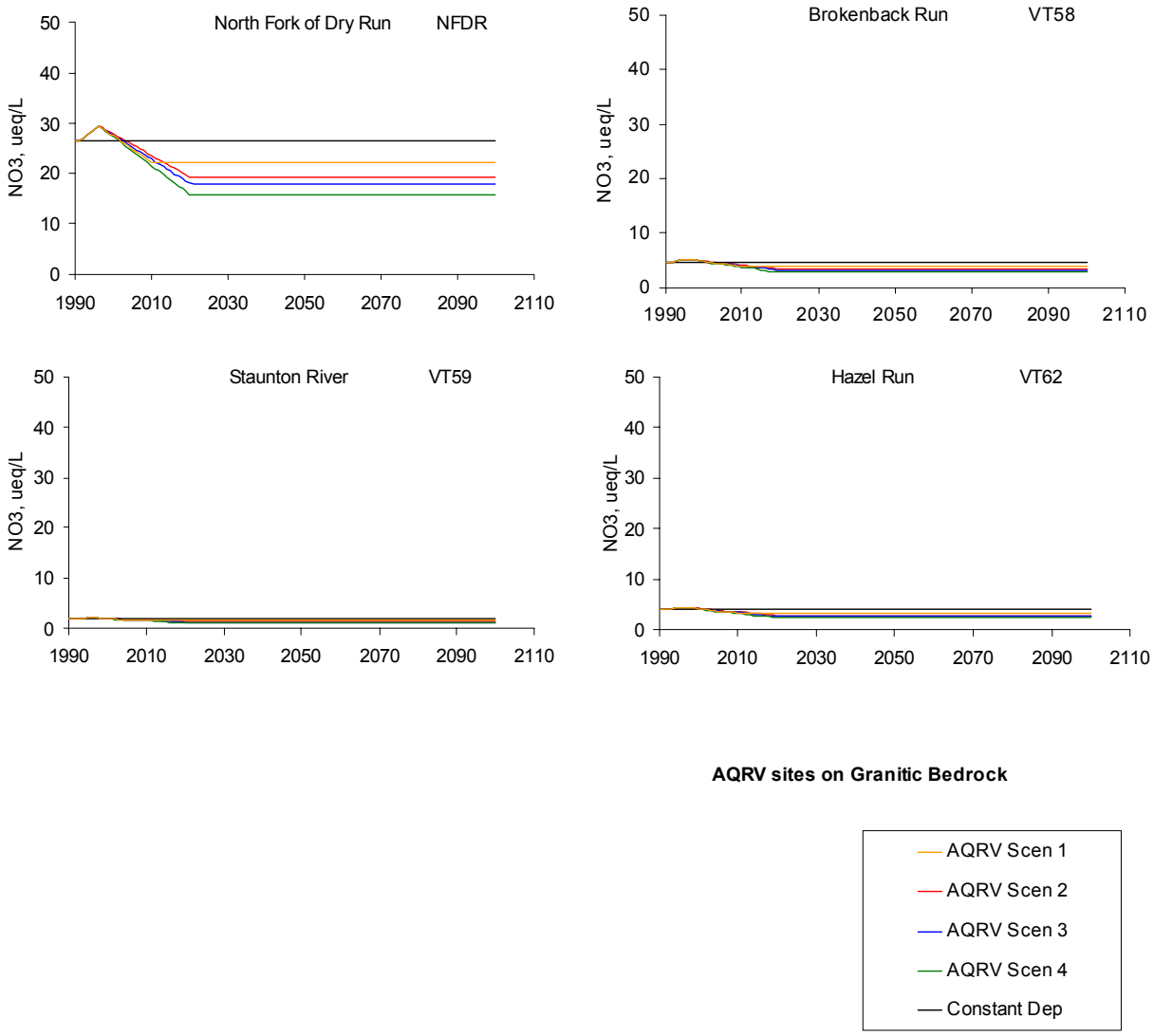

Figure VII-6b. MAGIC model projections of streamwater nitrate under the scenario of constant deposition at 1990 levels and the four emissions control scenarios described in Section IV for modeled sites on granitic bedrock.

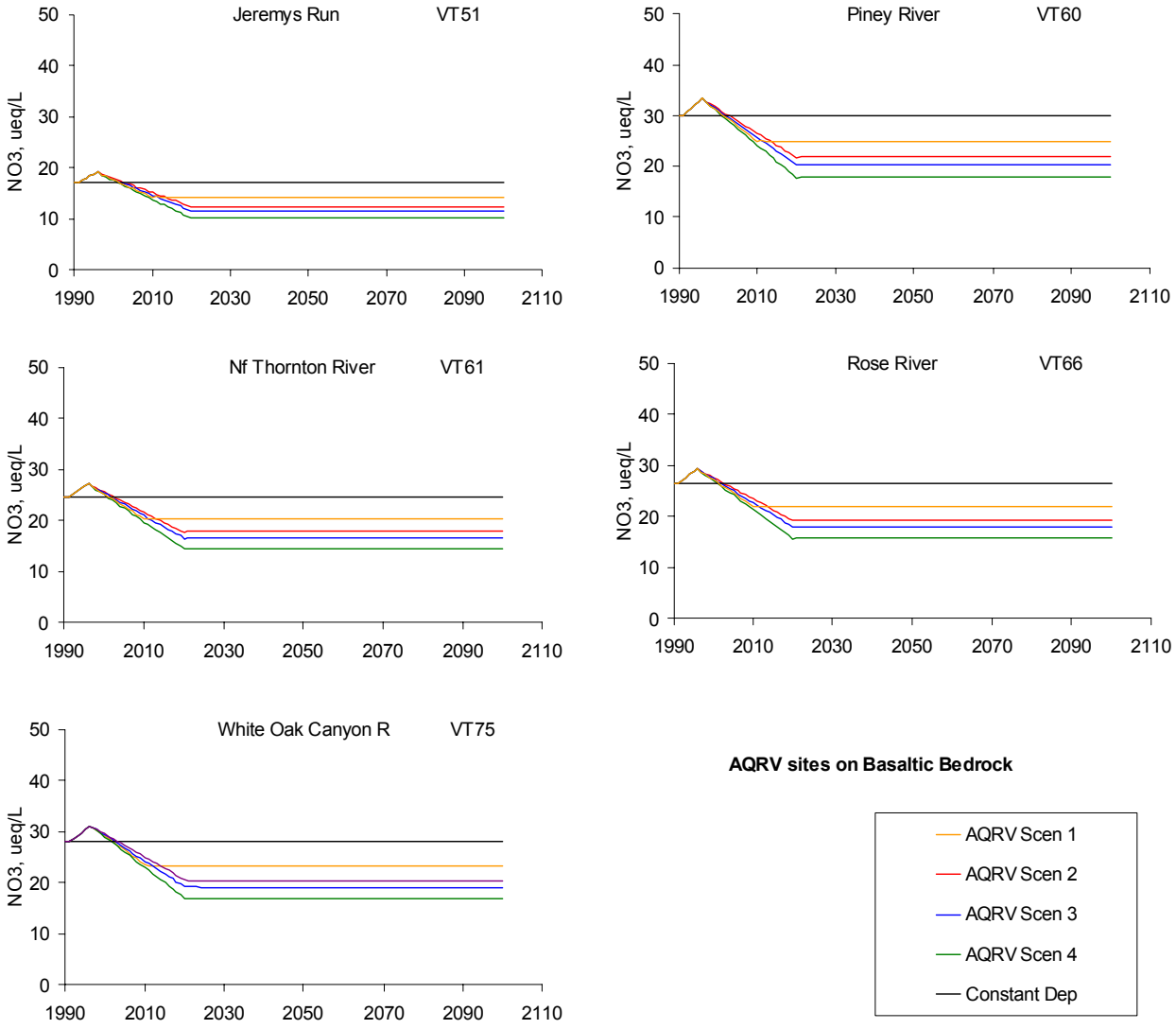

Figure VII-6c. MAGIC model projections of streamwater nitrate under the scenario of constant deposition at 1990 levels and the four emissions control scenarios described in Section IV for modeled sites on basaltic bedrock.

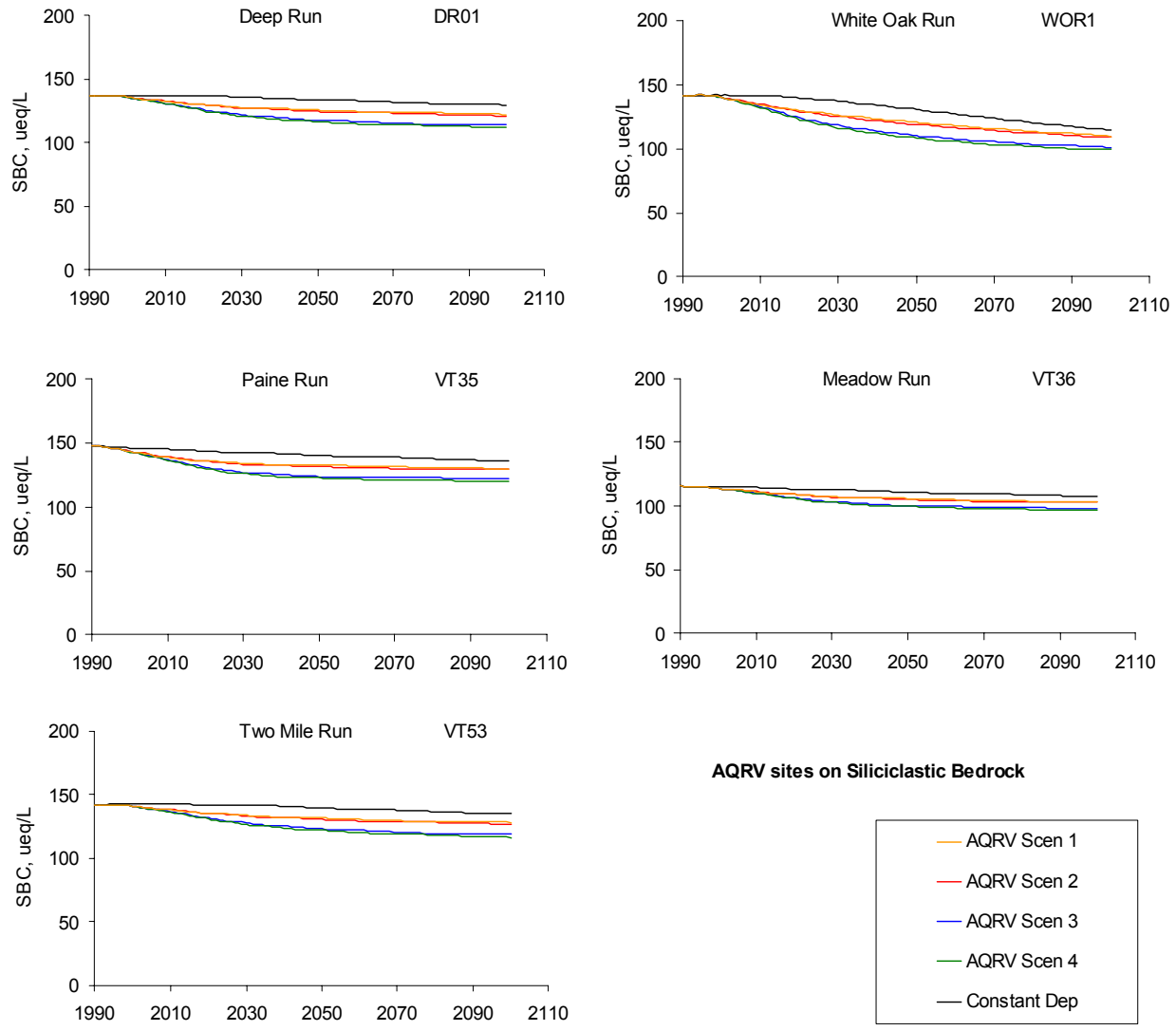

Figure VII-7a. MAGIC model projections of streamwater sum of base cations (SBC) under the scenario of constant deposition at 1990 levels and the four emissions control scenarios described in Section IV for modeled sites on siliciclastic bedrock.

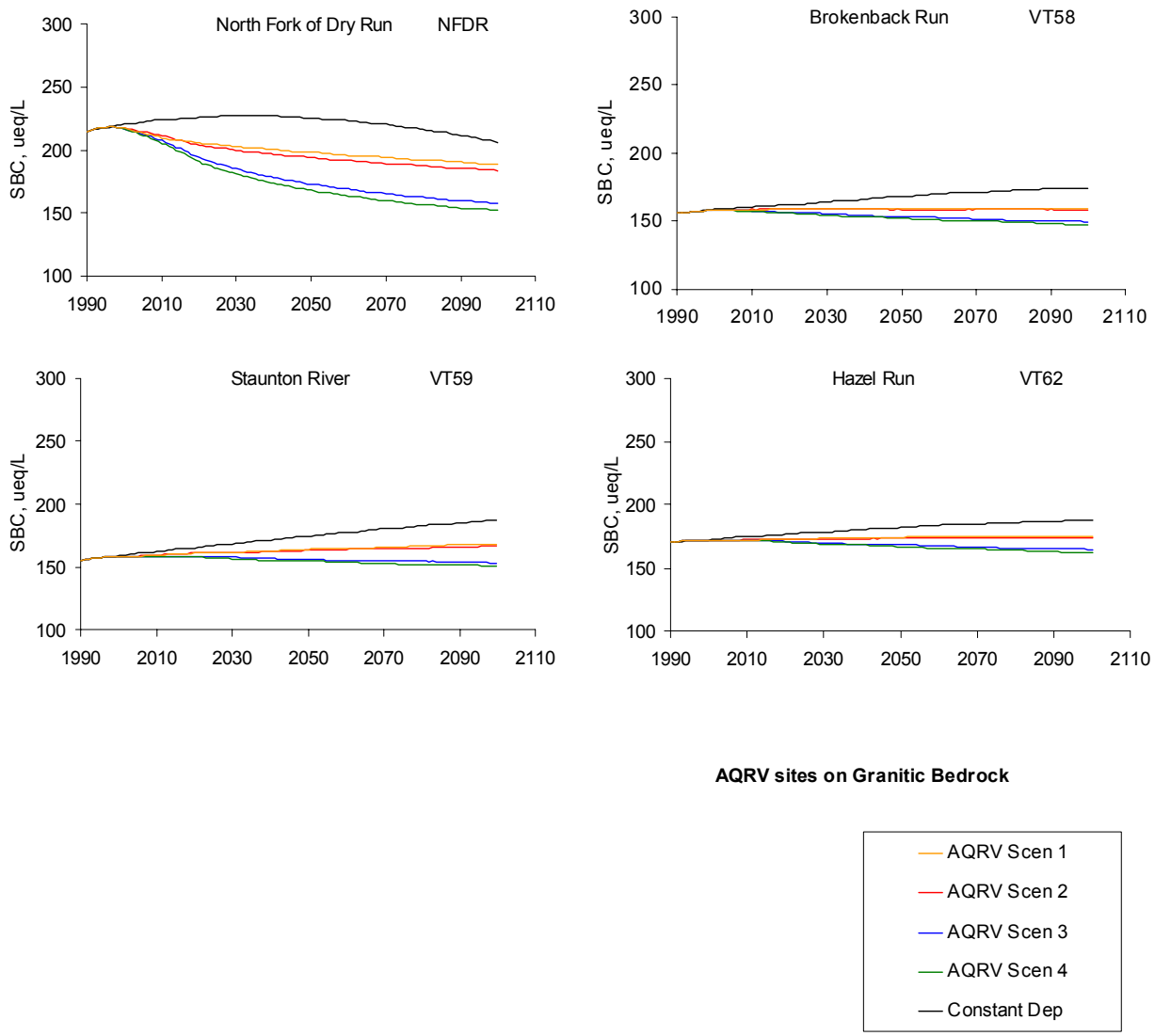

Figure VII-7b. MAGIC model projections of streamwater sum of base cations (SBC) under the scenario of constant deposition at 1990 levels and the four emissions control scenarios described in Section IV for modeled sites on granitic bedrock.

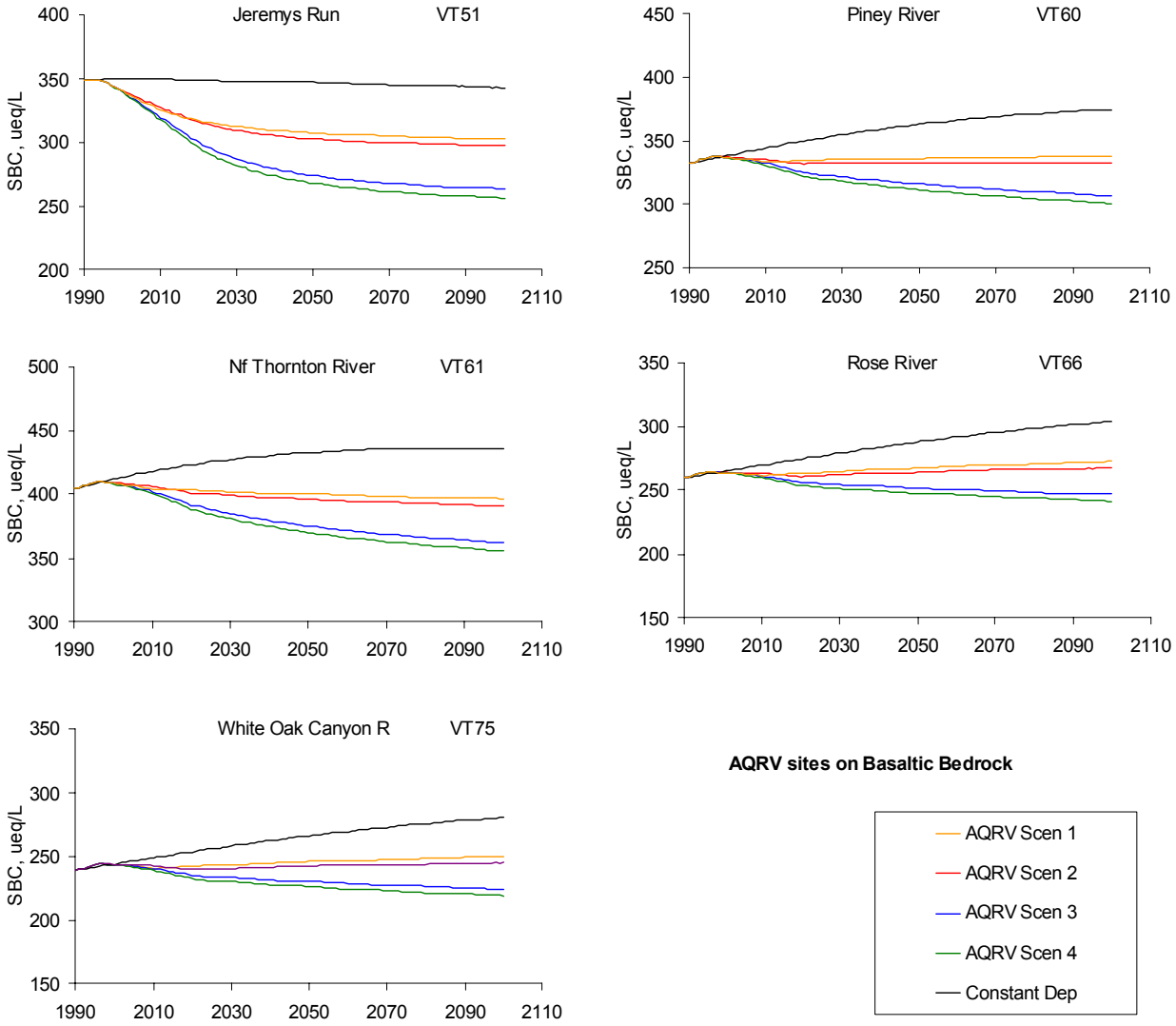

Figure VII-7c. MAGIC model projections of streamwater sum of base cations (SBC) under the scenario of constant deposition at 1990 levels and the four emissions control scenarios described in Section IV for modeled sites on basaltic bedrock.

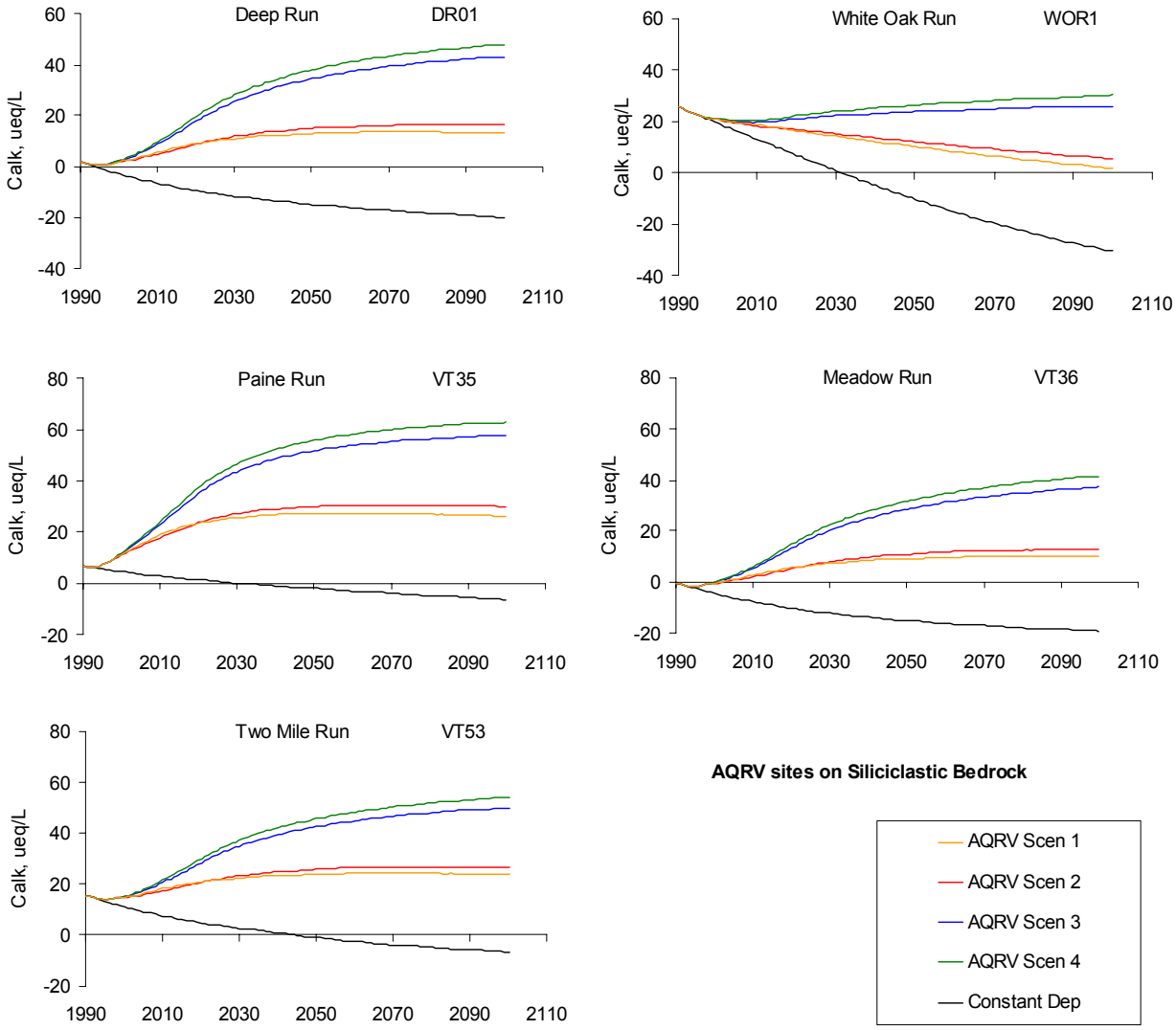

Figure VII-8a. MAGIC model projections of streamwater ANC under the scenario of constant deposition at 1990 levels and the four emissions control scenarios described in Section IV for modeled sites on siliciclastic bedrock. See model estimates of pre-industrial ANC in Table VII-8.

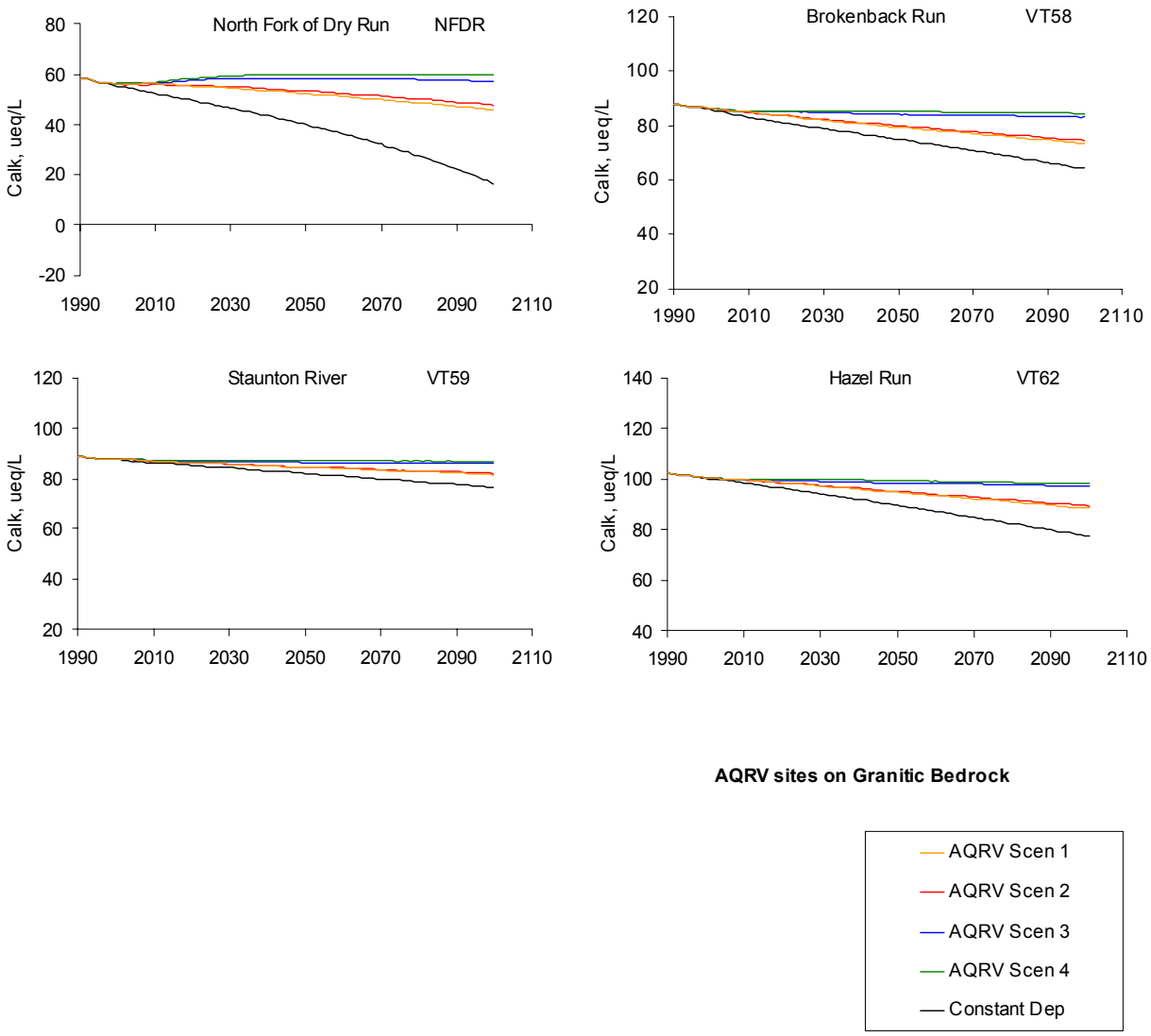

Figure VII-8b. MAGIC model projections of streamwater ANC under the scenario of constant deposition at 1990 levels and the four emissions control scenarios described in Section IV for modeled sites on granitic bedrock. See model estimates of pre-industrial ANC in Table VII-8.

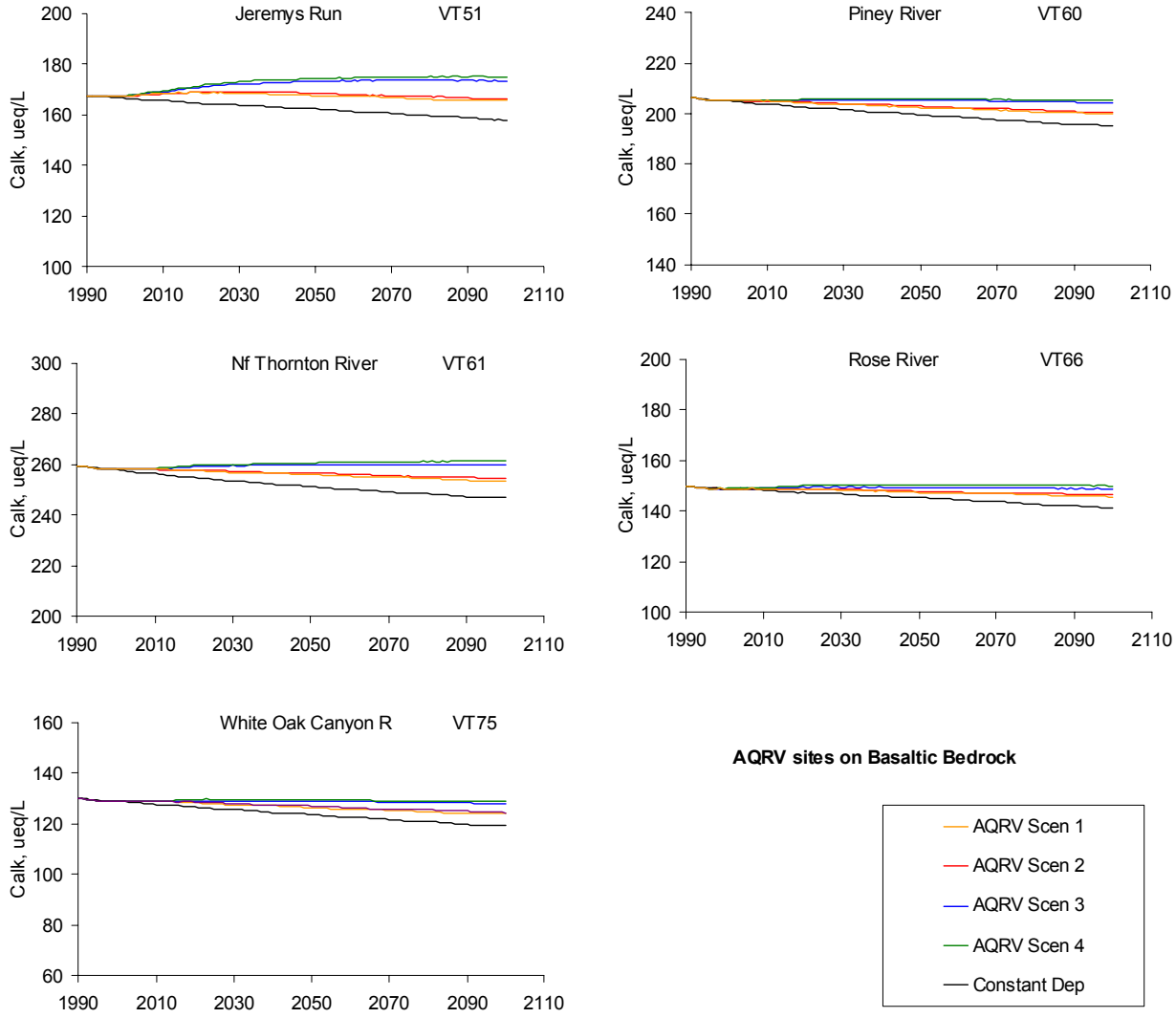

Figure VII-8c. MAGIC model projections of streamwater ANC under the scenario of constant deposition at 1990 levels and the four emissions control scenarios described in Section IV for modeled sites on basaltic bedrock. See model estimates of pre-industrial ANC in Table VII-8.

Table VII-8. ANC (ueq/L) in streams within SHEN derived from MAGIC simulations for the past (in response to historical deposition), the present, and for selected years in the future (in response to simulated constant deposition at 1990 levels and the four emissions control scenarios).

Site[a]	Scenario	Past	Year					
			1990	2000	2010	2020	2040	2100
Sites on Siliciclastic Bedrock								
DR01	Constant	78.5	2.1	-2.9	-6.6	-9.5	-13.3	-19.9
	1	78.5	2.1	2.0	5.8	9.1	12.4	13.2
	2	78.5	2.1	1.9	5.0	8.9	13.9	16.5
	3	78.5	2.1	2.3	8.9	18.0	30.9	43.2
	4	78.5	2.1	2.4	9.6	19.7	33.9	47.9
VT35 (PAIN)	Constant	90.7	6.8	4.5	2.8	1.4	-1.0	-6.3
	1	90.7	6.8	11.5	19.2	23.7	27.0	26.6
	2	90.7	6.8	11.3	18.1	24.0	29.4	30.3
	3	90.7	6.8	12.0	23.2	35.4	48.9	58.0
	4	90.7	6.8	12.1	24.3	37.6	52.4	63.2
VT36	Constant	69.0	-0.2	-4.5	-7.6	-10.1	-13.7	-19.0
	1	69.0	-0.2	-0.2	2.9	5.7	8.6	10.3
	2	69.0	-0.2	-0.3	2.2	5.4	9.9	13.1
	3	69.0	-0.2	0.0	5.6	13.5	25.1	37.4
	4	69.0	-0.2	0.1	6.2	15.0	27.8	41.6
VT53	Constant	81.1	15.7	11.1	7.5	4.8	0.8	-6.6
	1	81.1	15.7	14.9	18.3	20.9	23.5	24.0
	2	81.1	15.7	14.9	17.6	20.9	25.0	27.0
	3	81.1	15.7	15.2	20.8	28.6	39.6	50.0
	4	81.1	15.7	15.3	21.5	30.1	42.2	54.1
WOR1	Constant	65.5	25.6	19.4	13.2	7.0	-4.8	-30.5
	1	65.5	25.6	21.2	19.3	17.0	12.8	2.7
	2	65.5	25.6	21.1	18.8	17.6	14.4	6.6
	3	65.5	25.6	21.3	20.3	21.7	23.7	26.9
	4	65.5	25.6	21.3	20.7	22.7	25.7	30.7
Sites on Granitic Bedrock								
NFDR	Constant	81.6	58.5	55.3	52.3	49.5	43.3	16.5
	1	81.6	58.5	56.5	56.5	55.7	53.7	46.4
	2	81.6	58.5	56.5	56.1	56.0	54.6	48.5
	3	81.6	58.5	56.6	56.9	58.0	58.8	57.8
	4	81.6	58.5	56.7	57.2	58.6	59.8	60.0
VT58	Constant	97.6	87.7	85.8	83.0	80.8	76.9	64.1
	1	97.6	87.7	86.2	85.1	83.6	80.8	73.6
	2	97.6	87.7	86.3	84.9	83.8	81.1	74.6
	3	97.6	87.7	86.3	85.4	85.1	84.6	83.2
	4	97.6	87.7	86.3	85.5	85.5	85.2	84.5

Table VII-8. Continued.

Site[a]	Scenario	Past	Year					
			1990	2000	2010	2020	2040	2100
VT59 (STAN)	Constant	96.0	88.7	87.4	86.2	85.2	83.1	76.6
	1	96.0	88.7	87.7	86.9	86.2	85.1	81.7
	2	96.0	88.7	87.7	86.8	86.2	85.1	82.0
	3	96.0	88.7	87.8	87.1	86.9	86.6	86.0
	4	96.0	88.7	87.7	87.2	87.1	87.1	86.8
VT62	Constant	115.6	102.4	100.3	98.4	96.3	91.8	77.4
	1	115.6	102.4	100.7	99.7	98.6	96.0	88.6
	2	115.6	102.4	100.6	99.6	98.7	96.4	89.6
	3	115.6	102.4	100.7	99.9	99.5	98.9	97.3
	4	115.6	102.4	100.7	100.0	99.8	99.5	98.3
Sites on Basaltic Bedrock								
VT51	Constant	191.0	167.7	166.6	165.5	164.6	163.1	157.9
	1	191.0	167.7	167.7	168.6	168.9	168.3	165.5
	2	191.0	167.7	167.7	168.5	168.9	169.0	166.4
	3	191.0	167.7	167.8	169.3	171.3	173.2	173.6
	4	191.0	167.7	168.0	169.7	171.7	174.0	175.1
VT60 (PINE)	Constant	218.3	206.3	204.9	203.6	202.5	200.4	194.9
	1	218.3	206.3	205.3	205.1	204.4	203.2	200.0
	2	218.3	206.3	205.3	205.0	204.9	203.7	200.8
	3	218.3	206.3	205.4	205.3	205.7	205.6	204.8
	4	218.3	206.3	205.3	205.5	206.1	206.2	205.6
VT61	Constant	276.9	259.4	257.8	256.2	254.7	252.3	246.7
	1	276.9	259.4	258.4	258.3	257.7	256.7	253.6
	2	276.9	259.4	258.3	258.0	258.0	257.2	254.7
	3	276.9	259.4	258.5	258.6	259.3	259.8	260.1
	4	276.9	259.4	258.5	258.8	259.7	260.5	261.3
VT66	Constant	159.4	149.8	148.9	148.1	147.4	145.9	141.1
	1	159.4	149.8	149.2	149.2	148.7	148.0	145.9
	2	159.4	149.8	149.2	149.0	149.1	148.4	146.6
	3	159.4	149.8	149.2	149.3	149.7	149.7	149.3
	4	159.4	149.8	149.2	149.3	150.2	150.3	150.0
VT75	Constant	143.0	130.1	128.9	127.8	126.7	124.6	119.1
	1	143.0	130.1	129.2	129.2	128.6	127.4	124.2
	2	143.0	130.1	129.2	129.0	129.0	127.9	125.0
	3	143.0	130.1	129.2	129.3	129.6	129.3	128.5
	4	143.0	130.1	129.3	129.4	130.0	129.8	129.3

[a] For stream names, see Table VI-2.

Table VII-9. pH in streams within SHEN derived from MAGIC simulations for the past (in response to historical emissions), the present, and for selected years in the future (in response to simulated constant deposition at 1990 levels and the four emissions control scenarios).

Site	Scenario	Past	Year					
			1990	2000	2010	2020	2040	2100
Sites on Siliciclastic Bedrock								
DR01	Constant	7.1	5.4	5.1	5.0	4.9	4.9	4.8
	1	7.1	5.4	5.4	5.6	5.8	6.0	6.1
	2	7.1	5.4	5.4	5.6	5.8	6.1	6.2
	3	7.1	5.4	5.4	5.8	6.2	6.6	6.8
	4	7.1	5.4	5.4	5.9	6.3	6.6	6.8
VT35 (PAIN)	Constant	7.1	5.7	5.6	5.4	5.4	5.2	5.0
	1	7.1	5.7	6.0	6.3	6.4	6.5	6.5
	2	7.1	5.7	6.0	6.2	6.4	6.5	6.6
	3	7.1	5.7	6.0	6.4	6.6	6.8	6.9
	4	7.1	5.7	6.0	6.4	6.7	6.8	6.9
VT36	Constant	7.0	5.3	5.1	5.0	4.9	4.9	4.8
	1	7.0	5.3	5.3	5.5	5.6	5.8	5.9
	2	7.0	5.3	5.3	5.4	5.6	5.9	6.0
	3	7.0	5.3	5.3	5.6	6.1	6.4	6.7
	4	7.0	5.3	5.3	5.7	6.1	6.5	6.7
VT53	Constant	7.1	6.2	5.9	5.7	5.6	5.3	5.0
	1	7.1	6.2	6.1	6.3	6.3	6.4	6.4
	2	7.1	6.2	6.1	6.2	6.3	6.4	6.5
	3	7.1	6.2	6.1	6.3	6.5	6.7	6.8
	4	7.1	6.2	6.1	6.4	6.6	6.7	6.9
WOR1	Constant	7.0	6.5	6.3	6.1	5.7	5.1	4.7
	1	7.0	6.5	6.3	6.3	6.2	6.0	5.4
	2	7.0	6.5	6.3	6.3	6.2	6.1	5.7
	3	7.0	6.5	6.3	6.3	6.4	6.4	6.5
	4	7.0	6.5	6.3	6.3	6.4	6.5	6.6
Sites on Granitic Bedrock								
NFDR	Constant	7.1	6.9	6.9	6.8	6.8	6.7	6.2
	1	7.1	6.9	6.9	6.9	6.9	6.9	6.8
	2	7.1	6.9	6.9	6.9	6.9	6.9	6.8
	3	7.1	6.9	6.9	6.9	6.9	6.9	6.9
	4	7.1	6.9	6.9	6.9	6.9	6.9	6.9
VT58	Constant	7.2	7.1	7.1	7.1	7.1	7.0	6.9
	1	7.2	7.1	7.1	7.1	7.1	7.1	7.0
	2	7.2	7.1	7.1	7.1	7.1	7.1	7.0
	3	7.2	7.1	7.1	7.1	7.1	7.1	7.1
	4	7.2	7.1	7.1	7.1	7.1	7.1	7.1

Table VII-9. Continued.

Site	Scenario	Past	Year					
			1990	2000	2010	2020	2040	2100
VT59 (STAN)	Constant	7.1	7.1	7.1	7.1	7.1	7.1	7.0
	1	7.1	7.1	7.1	7.1	7.1	7.1	7.1
	2	7.1	7.1	7.1	7.1	7.1	7.1	7.1
	3	7.1	7.1	7.1	7.1	7.1	7.1	7.1
	4	7.1	7.1	7.1	7.1	7.1	7.1	7.1
VT62	Constant	7.2	7.2	7.2	7.2	7.1	7.1	7.0
	1	7.2	7.2	7.2	7.2	7.2	7.1	7.1
	2	7.2	7.2	7.2	7.2	7.2	7.1	7.1
	3	7.2	7.2	7.2	7.2	7.2	7.2	7.2
	4	7.2	7.2	7.2	7.2	7.2	7.2	7.2
Sites on Basaltic Bedrock								
VT51	Constant	7.5	7.4	7.4	7.4	7.4	7.4	7.4
	1	7.5	7.4	7.4	7.4	7.4	7.4	7.4
	2	7.5	7.4	7.4	7.4	7.4	7.4	7.4
	3	7.5	7.4	7.4	7.4	7.4	7.4	7.4
	4	7.5	7.4	7.4	7.4	7.4	7.4	7.4
VT60 (PINE)	Constant	7.5	7.5	7.5	7.5	7.5	7.5	7.5
	1	7.5	7.5	7.5	7.5	7.5	7.5	7.5
	2	7.5	7.5	7.5	7.5	7.5	7.5	7.5
	3	7.5	7.5	7.5	7.5	7.5	7.5	7.5
	4	7.5	7.5	7.5	7.5	7.5	7.5	7.5
VT61	Constant	7.6	7.6	7.6	7.6	7.6	7.6	7.6
	1	7.6	7.6	7.6	7.6	7.6	7.6	7.6
	2	7.6	7.6	7.6	7.6	7.6	7.6	7.6
	3	7.6	7.6	7.6	7.6	7.6	7.6	7.6
	4	7.6	7.6	7.6	7.6	7.6	7.6	7.6
VT66	Constant	7.4	7.4	7.3	7.3	7.3	7.3	7.3
	1	7.4	7.4	7.3	7.3	7.3	7.3	7.3
	2	7.4	7.4	7.3	7.3	7.3	7.3	7.3
	3	7.4	7.4	7.3	7.3	7.4	7.4	7.3
	4	7.4	7.4	7.3	7.3	7.4	7.4	7.4
VT75	Constant	7.3	7.3	7.3	7.3	7.3	7.3	7.2
	1	7.3	7.3	7.3	7.3	7.3	7.3	7.3
	2	7.3	7.3	7.3	7.3	7.3	7.3	7.3
	3	7.3	7.3	7.3	7.3	7.3	7.3	7.3
	4	7.3	7.3	7.3	7.3	7.3	7.3	7.3

[a] For stream names, see Table VI-2.

of the siliciclastic type within SHEN would be expected to be in the range of about 5 to 10 µeq/L, such as have been observed for Paine Run, White Oak Run, and Deep Run (Figure VI-18). In contrast, streams on granitic and basaltic bedrock are expected to continue to exhibit

somewhat larger episodic ANC depressions, such as the 20 to 30 μeq/L depressions found for Staunton River and North Fork Dry Run, and the greater than 40 μeq/L depressions found for Piney River (Figure VI-18). Such episodes are most likely to be accompanied by adverse biological effects in streams in which episodic ANC falls near or below zero.

d. Implications for Aquatic Biota

The projected changes in streamwater ANC and pH in response to future (or past) deposition that were summarized in the last section can be used to project expected changes in fish communities in SHEN streams. There are four measures of biological response that can be estimated and that provide information about the community, population and individual responses of fish in SHEN streams. The projected changes in stream ANC (Table VII-8) can be used to estimate: 1) the number of species expected in each stream (using the relationship between ANC and species richness described in Figure VI-16); and 2) the status of the brook trout fishery in each stream (using the relationship between ANC categories and brook trout responses described in Table VI-9). In addition, the projected changes in streamwater pH (Table VII-9) can be used to estimate: 3) the expected condition factor of the more acid-sensitive blacknose dace in each stream (using the relationship between pH and condition factor described in Figure VI-17); and 4) the expected presence or absence of nine different species of fish in each stream (using the data in Table VI-8 which describe upper and lower pH thresholds for loss of each species).

Each of these four measures of biological response was separately estimated for each of the 14 SHEN streams modeled by MAGIC (Table VI-4). In addition, each of the biological responses in each of the streams was estimated for each of the four future emissions controls scenarios discussed in Sections IV and V, as well as for the baseline case of no future change in deposition from the 1990 levels. Future biological responses are presented in tabular form for a number of years for each scenario, and are presented graphically and discussed for the year 2040.

As a means of assessing the relative importance and robustness of the projected future biological changes, each measure of biological response was also calculated for present and past conditions in each stream. The observed present conditions were compared to estimated present conditions as a measure of the precision and accuracy of the biological projections. This was

done by coupling the output of the geochemical model to the various empirical biological response models. The estimated past conditions provide a benchmark for assessing the efficacy of the future emissions control scenarios. We evaluated the extent to which fish communities, populations, or individuals in the streams might be expected to improve or to return to pre-acidification conditions in response to a given future deposition scenario.

Species Richness

A direct outcome of fish population loss as a result of acidification is a decline in species richness (the total number of species in a stream). This appears to be a highly predictable outcome of regional acidification, although the pattern and rate of species loss varies from region to region (see discussion in Section VI). A statistically robust relationship between the ANC of streamwater and fish species richness was found in SHEN as part of the Fish in Sensitive Habitats (FISH) project (Bulger et al. 1999). The numbers of fish species were compared among 13 SHEN streams spanning a range of ANC conditions. There was a highly significant ($p<0.0001$) relationship between stream ANC (during the seven-year period of record) and fish species richness among the 13 streams, such that the streams having the lowest ANC hosted the fewest species (Figure VI-16).

The linear relationship derived from the data in Figure VI-16 was used with the predicted streamwater ANC values (Table VII-8) to provide estimates of the expected number of fish species in each of the modeled streams for the past, present and future chemical conditions simulated for each stream with MAGIC. The coupled geochemical and biological model predictions were evaluated by comparing the predicted species richness in each of the 13 streams with the observed number of species that occur in each stream (Table II-1). The agreement between predicted and observed species numbers was good (Figure VII-9), with a root mean squared error (RMSE) in predicted number of species across the 13 streams of 1.2 species. The average error was 0.3 species, indicating that the coupled models are unbiased in their predictions. Model reconstructions of past species richness in the streams (Figure VII-10) suggested that historical loss of species has been greatest in the siliciclastic streams. The average number of species lost on the three bedrock types were estimated as: 1.6 species on siliciclastic bedrock; 0.4 species on granitic bedrock; and 0.4 species on basaltic bedrock. In the case of the siliciclastic streams, the projected past changes were much larger than the average error and RMSE of the coupled models, suggesting that the projections are reasonably robust.

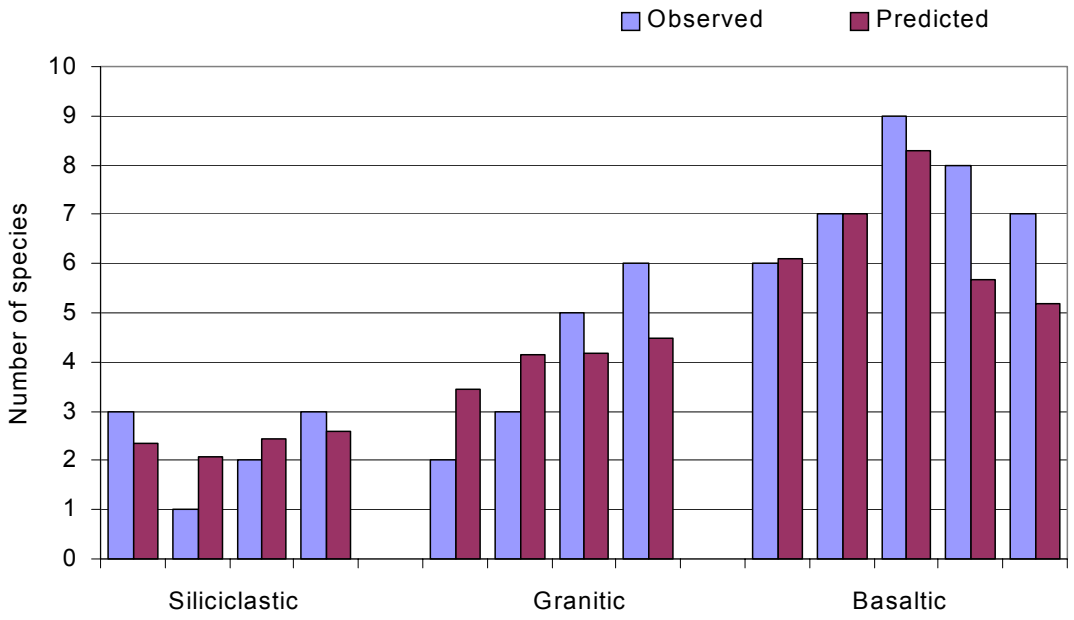

Figure VII-9. Predicted and observed number of fish species in 13 SHEN streams for the year 2000.

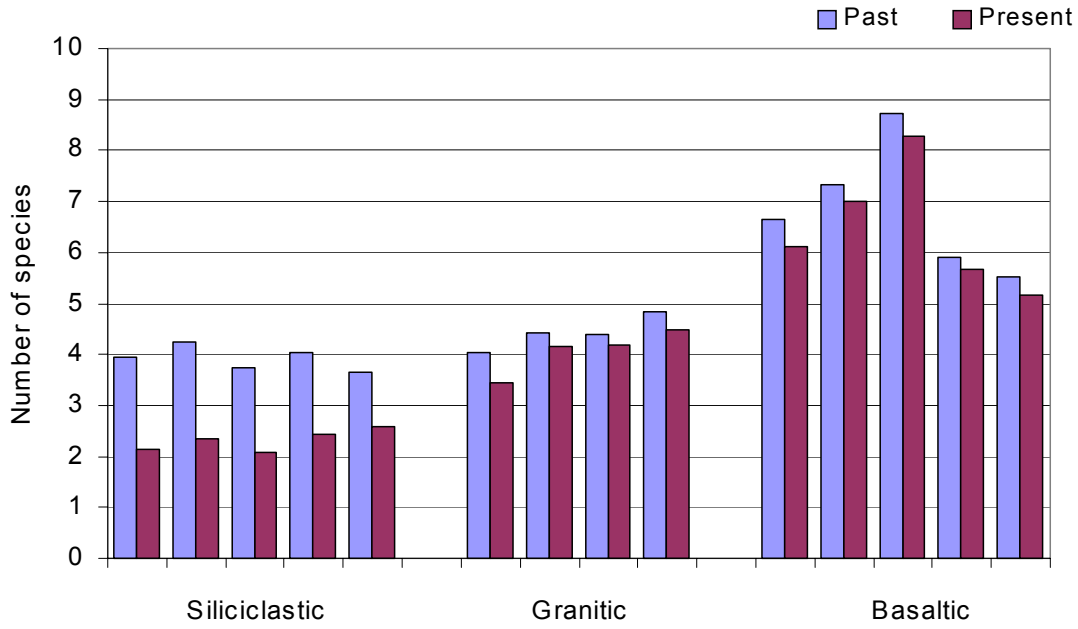

Figure VII-10. Projected number of fish species in 14 SHEN streams for past and present conditions.

The coupled geochemical and biological models were also used to predict expected changes in future numbers of species in each of the streams for selected years in each of the future deposition scenarios (Table VII-10). For all except the constant future deposition scenario, the models suggested that species richness will increase in the future, and that increases in species richness will be greatest in siliciclastic streams (Figure VII-11). The projected recovery of species richness, however, would not return these streams to their estimated past conditions (Figure VII-10) under any of the scenarios considered.

Table VII-10. Projected number of fish species in streams within SHEN estimated from simulations for the past in response to historical deposition and for the future in response to simulated constant deposition at 1990 levels and the four emissions control scenarios.

		Year						
Site[a]	**Scenario**	**Past**	**1990**	**2000**	**2010**	**2020**	**2040**	**2100**
Sites on Siliciclastic Bedrock								
DR01	Constant	4.0	2.1	2.0	1.9	1.8	1.8	1.6
	1	4.0	2.1	2.1	2.2	2.3	2.4	2.4
	2	4.0	2.1	2.1	2.2	2.3	2.4	2.5
	3	4.0	2.1	2.1	2.3	2.5	2.8	3.1
	4	4.0	2.1	2.1	2.3	2.5	2.9	3.2
VT35 (PAIN)	Constant	4.3	2.2	2.2	2.1	2.1	2.1	1.9
	1	4.3	2.2	2.4	2.5	2.6	2.7	2.7
	2	4.3	2.2	2.3	2.5	2.7	2.8	2.8
	3	4.3	2.2	2.4	2.6	2.9	3.2	3.5
	4	4.3	2.2	2.4	2.7	3.0	3.3	3.6
VT36	Constant	3.7	2.1	2.0	1.9	1.8	1.7	1.6
	1	3.7	2.1	2.1	2.1	2.2	2.3	2.3
	2	3.7	2.1	2.1	2.1	2.2	2.3	2.4
	3	3.7	2.1	2.1	2.2	2.4	2.7	3.0
	4	3.7	2.1	2.1	2.2	2.4	2.7	3.1
VT53	Constant	4.0	2.5	2.3	2.3	2.2	2.1	1.9
	1	4.0	2.5	2.4	2.5	2.6	2.6	2.7
	2	4.0	2.5	2.4	2.5	2.6	2.7	2.7
	3	4.0	2.5	2.4	2.6	2.8	3.0	3.3
	4	4.0	2.5	2.4	2.6	2.8	3.1	3.4
WOR1	Constant	3.6	2.7	2.5	2.4	2.2	2.0	1.3
	1	3.6	2.7	2.6	2.5	2.5	2.4	2.1
	2	3.6	2.7	2.6	2.5	2.5	2.4	2.2
	3	3.6	2.7	2.6	2.6	2.6	2.6	2.7
	4	3.6	2.7	2.6	2.6	2.6	2.7	2.8
Sites on Granitic Bedrock								
NFDR	Constant	4.0	3.5	3.4	3.3	3.3	3.1	2.5
	1	4.0	3.5	3.4	3.4	3.4	3.4	3.2
	2	4.0	3.5	3.4	3.4	3.4	3.4	3.2
	3	4.0	3.5	3.4	3.4	3.5	3.5	3.5
	4	4.0	3.5	3.4	3.4	3.5	3.5	3.5

Table VII-10. Continued.

Site	Scenario	Year						
		Past	**1990**	**2000**	**2010**	**2020**	**2040**	**2100**
VT58	Constant	4.4	4.2	4.1	4.1	4.0	3.9	3.6
	1	4.4	4.2	4.1	4.1	4.1	4.0	3.8
	2	4.4	4.2	4.1	4.1	4.1	4.0	3.9
	3	4.4	4.2	4.1	4.1	4.1	4.1	4.1
	4	4.4	4.2	4.1	4.1	4.1	4.1	4.1
VT59 (STAN)	Constant	4.4	4.2	4.2	4.1	4.1	4.1	3.9
	1	4.4	4.2	4.2	4.2	4.1	4.1	4.0
	2	4.4	4.2	4.2	4.2	4.1	4.1	4.0
	3	4.4	4.2	4.2	4.2	4.2	4.2	4.1
	4	4.4	4.2	4.2	4.2	4.2	4.2	4.2
VT62	Constant	4.8	4.5	4.5	4.4	4.4	4.3	3.9
	1	4.8	4.5	4.5	4.5	4.4	4.4	4.2
	2	4.8	4.5	4.5	4.5	4.4	4.4	4.2
	3	4.8	4.5	4.5	4.5	4.5	4.4	4.4
	4	4.8	4.5	4.5	4.5	4.5	4.5	4.4
Sites on Basaltic Bedrock								
VT51	Constant	6.7	6.1	6.1	6.0	6.0	6.0	5.9
	1	6.7	6.1	6.1	6.1	6.1	6.1	6.0
	2	6.7	6.1	6.1	6.1	6.1	6.1	6.1
	3	6.7	6.1	6.1	6.1	6.2	6.2	6.2
	4	6.7	6.1	6.1	6.1	6.2	6.3	6.3
VT60 (PINE)	Constant	7.3	7.0	7.0	7.0	6.9	6.9	6.8
	1	7.3	7.0	7.0	7.0	7.0	7.0	6.9
	2	7.3	7.0	7.0	7.0	7.0	7.0	6.9
	3	7.3	7.0	7.0	7.0	7.0	7.0	7.0
	4	7.3	7.0	7.0	7.0	7.0	7.0	7.0
VT61	Constant	8.7	8.3	8.3	8.2	8.2	8.1	8.0
	1	8.7	8.3	8.3	8.3	8.3	8.2	8.2
	2	8.7	8.3	8.3	8.3	8.3	8.2	8.2
	3	8.7	8.3	8.3	8.3	8.3	8.3	8.3
	4	8.7	8.3	8.3	8.3	8.3	8.3	8.3
VT66	Constant	5.9	5.7	5.7	5.6	5.6	5.6	5.5
	1	5.9	5.7	5.7	5.7	5.6	5.6	5.6
	2	5.9	5.7	5.7	5.7	5.7	5.6	5.6
	3	5.9	5.7	5.7	5.7	5.7	5.7	5.7
	4	5.9	5.7	5.7	5.7	5.7	5.7	5.7
VT75	Constant	5.5	5.2	5.2	5.1	5.1	5.1	4.9
	1	5.5	5.2	5.2	5.2	5.2	5.1	5.1
	2	5.5	5.2	5.2	5.2	5.2	5.1	5.1
	3	5.5	5.2	5.2	5.2	5.2	5.2	5.2
	4	5.5	5.2	5.2	5.2	5.2	5.2	5.2

[a] For stream names, see Table VI-2.

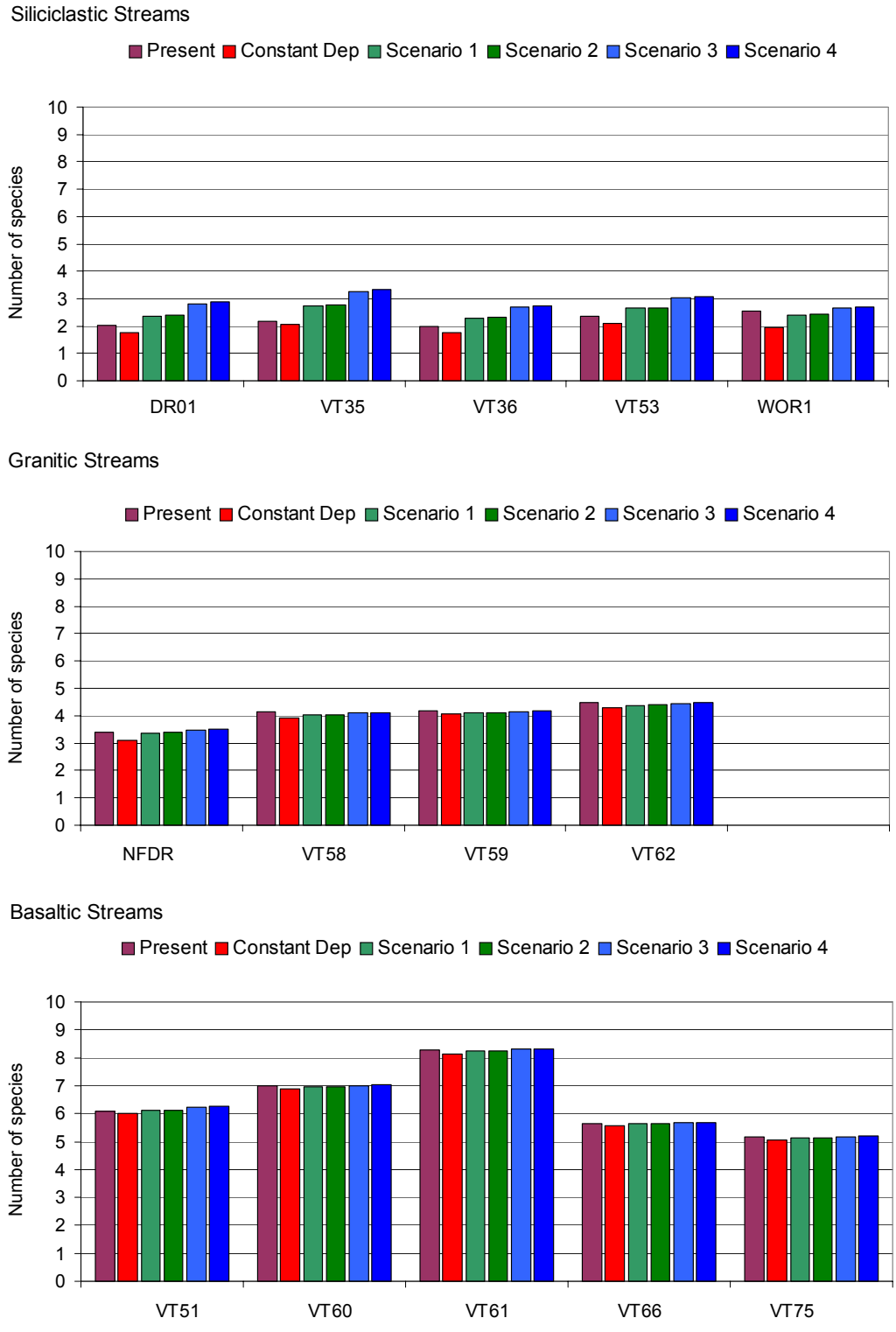

Figure VII-11. Projected number of fish species in 14 SHEN streams for the year 2040 in response to simulated constant deposition at 1990 levels and the four emissions control scenarios.

Brook Trout Status

ANC categories for brook trout response to acidification have been established for forested headwater catchments in western Virginia (Bulger et al., 2000; see Table VI-9). The ANC classes and brook trout status categories defined in Table VI-9 were used with the projected streamwater ANC values from Table VII-8 to provide estimates of the expected brook trout status in each of the modeled streams for the simulated past, present and future chemical conditions. The coupled geochemical and biological model projections were evaluated by comparing the observed brook trout status with the predicted brook trout status in each of the 13 streams, calculated from observed ANC values (Table VII-6). The agreement among categories was exact (Figure VII-12). As a further check, Table II-1 indicates that all modeled streams actually have brook trout present. The coupled models (and the observed ANC data) predicted that only one of the streams is currently unsuitable for brook trout, but the simulated ANC for that stream was only -1 ueq/L (observed = -2 ueq/L), just below the threshold for the unsuitable category.

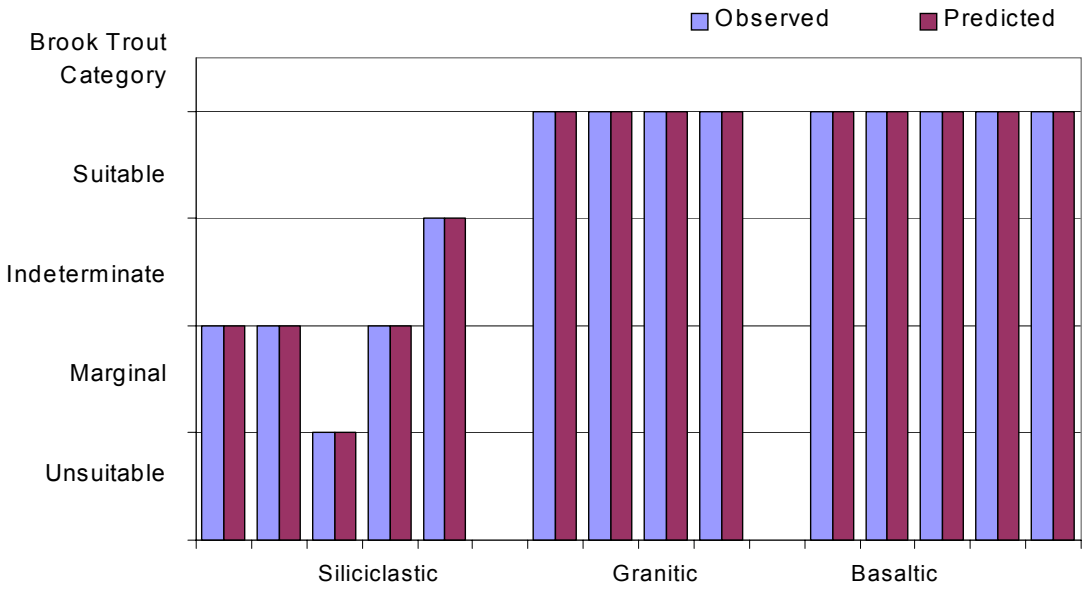

Figure VII-12. Predicted and observed brook trout categories in 14 SHEN streams for 1988-1992.

Model reconstructions of past brook trout status in the streams (Figure VII-13) suggested that all of the streams were suitable for brook trout in the past. The brook trout status has declined most in the siliciclastic streams. The brook trout status of streams draining granitic and basaltic catchments has not changed historically, even though the model suggests that these streams have lost ANC (Table VII-8).

The coupled geochemical and biological models were also used to predict the expected changes in brook trout status in each of the streams for selected years in each of the future deposition scenarios (Table VII-11). For all except the constant future deposition scenario, the models suggested that brook trout status will improve in all siliciclastic streams (Figure VII-14). The basaltic and granitic streams all showed increased ANC (Table VII-8) but no change in brook trout status because they are all already in the highest category (Figure VII-14).

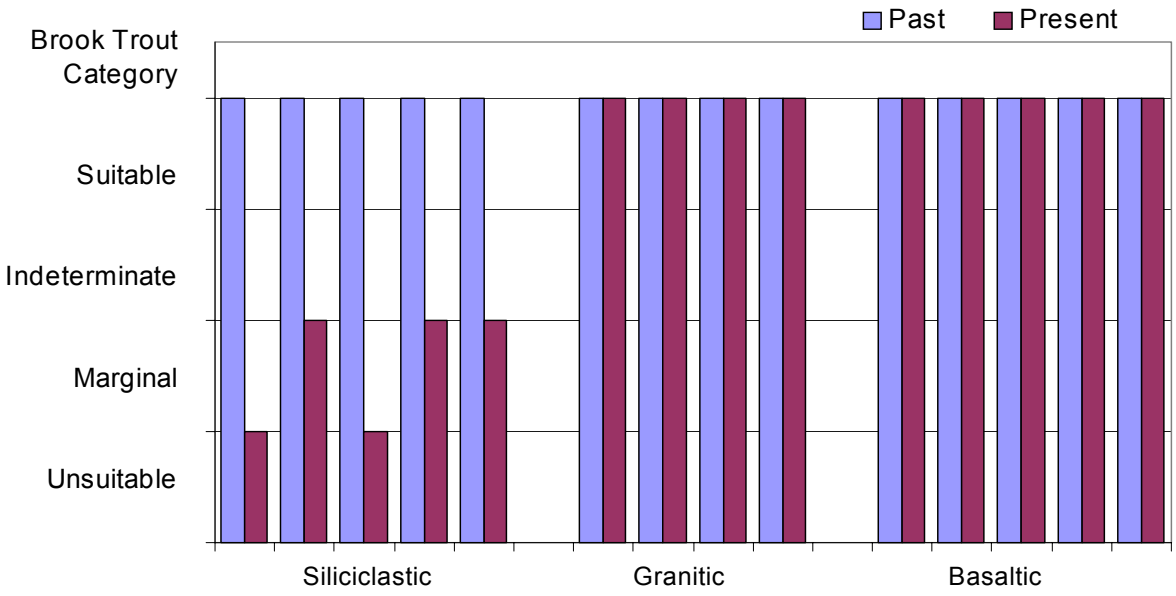

Figure VII-13. Projected brook trout categories in 14 SHEN streams for past and present (2000) conditions.

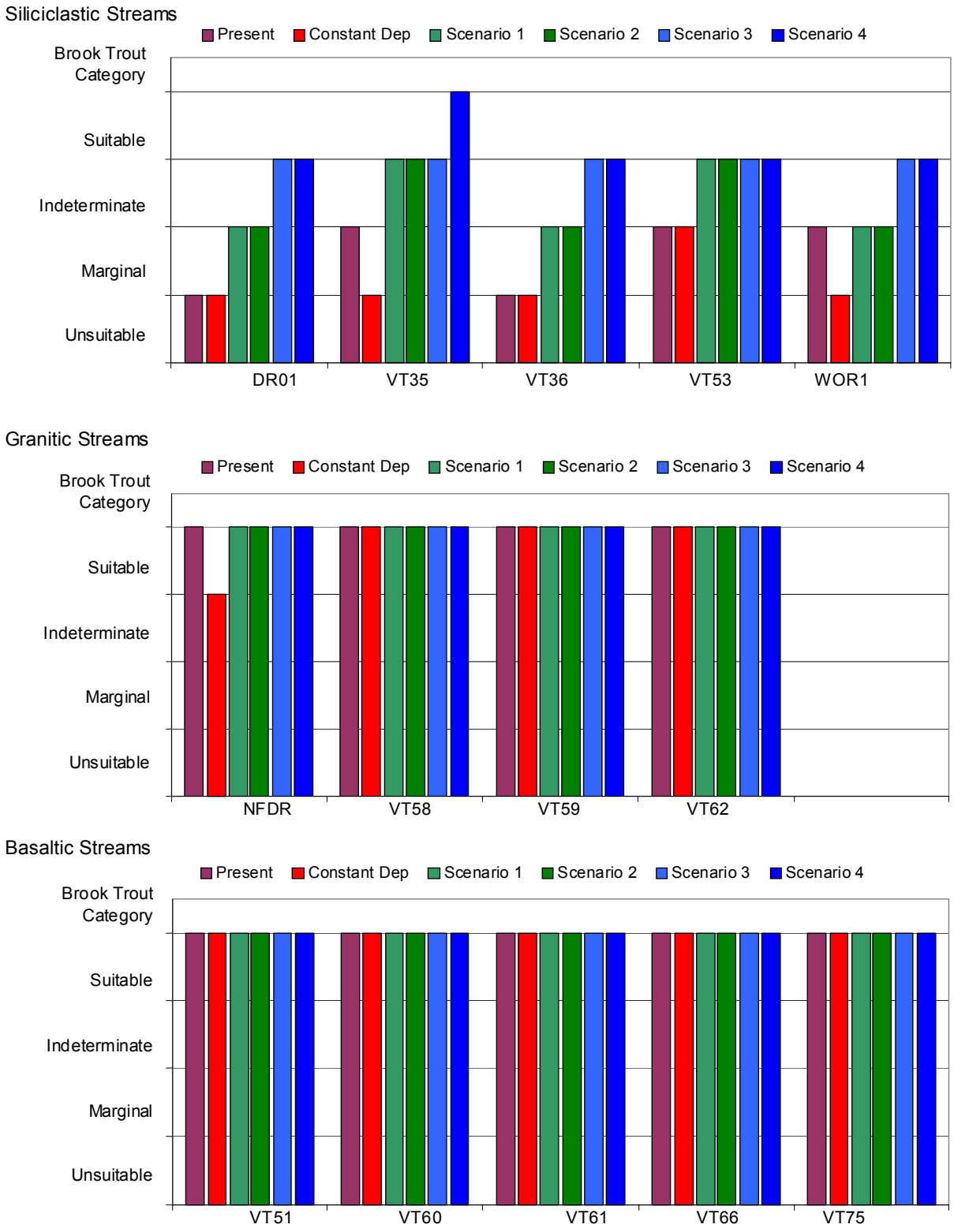

Figure VII-14. Projected brook trout categories in 14 SHEN streams for the year 2040 in response to simulated constant deposition at 1990 levels and the four emissions control scenarios.

Table VII-11. Projected brook trout categories in streams within SHEN estimated from simulations for the past in response to historical deposition and for the future in response to simulated constant deposition at 1990 levels and the four emissions control scenarios.

		Year						
Site[a]	**Scenario**	**Past**	**1990**	**2000**	**2010**	**2020**	**2040**	**2100**
Sites on Siliciclastic Bedrock								
DR01	Constant	Suitable	Marginal	Unsuitable	Unsuitable	Unsuitable	Unsuitable	Unsuitable
	1	Suitable	Marginal	Marginal	Marginal	Marginal	Marginal	Marginal
	2	Suitable	Marginal	Marginal	Marginal	Marginal	Marginal	Marginal
	3	Suitable	Marginal	Marginal	Marginal	Marginal	Indeterm	Indeterm
	4	Suitable	Marginal	Marginal	Marginal	Marginal	Indeterm	Indeterm
VT35 (PAIN)	Constant	Suitable	Marginal	Marginal	Marginal	Marginal	Unsuitable	Unsuitable
	1	Suitable	Marginal	Marginal	Marginal	Indeterm	Indeterm	Indeterm
	2	Suitable	Marginal	Marginal	Marginal	Indeterm	Indeterm	Indeterm
	3	Suitable	Marginal	Marginal	Indeterm	Indeterm	Indeterm	Suitable
	4	Suitable	Marginal	Marginal	Indeterm	Indeterm	Suitable	Suitable
VT36	Constant	Suitable	Unsuitable	Unsuitable	Unsuitable	Unsuitable	Unsuitable	Unsuitable
	1	Suitable	Unsuitable	Unsuitable	Marginal	Marginal	Marginal	Marginal
	2	Suitable	Unsuitable	Unsuitable	Marginal	Marginal	Marginal	Marginal
	3	Suitable	Unsuitable	Marginal	Marginal	Marginal	Indeterm	Indeterm
	4	Suitable	Unsuitable	Marginal	Marginal	Marginal	Indeterm	Indeterm
VT53	Constant	Suitable	Marginal	Marginal	Marginal	Marginal	Marginal	Unsuitable
	1	Suitable	Marginal	Marginal	Marginal	Indeterm	Indeterm	Indeterm
	2	Suitable	Marginal	Marginal	Marginal	Indeterm	Indeterm	Indeterm
	3	Suitable	Marginal	Marginal	Indeterm	Indeterm	Indeterm	Suitable
	4	Suitable	Marginal	Marginal	Indeterm	Indeterm	Indeterm	Suitable
WOR1	Constant	Suitable	Indeterm	Marginal	Marginal	Marginal	Unsuitable	Unsuitable
	1	Suitable	Indeterm	Indeterm	Marginal	Marginal	Marginal	Marginal
	2	Suitable	Indeterm	Indeterm	Marginal	Marginal	Marginal	Marginal
	3	Suitable	Indeterm	Indeterm	Indeterm	Indeterm	Indeterm	Indeterm
	4	Suitable	Indeterm	Indeterm	Indeterm	Indeterm	Indeterm	Indeterm
Sites on Granitic Bedrock								
NFDR	Constant	Suitable	Suitable	Suitable	Suitable	Indeterm	Indeterm	Marginal
	1	Suitable	Suitable	Suitable	Suitable	Suitable	Suitable	Indeterm
	2	Suitable	Suitable	Suitable	Suitable	Suitable	Suitable	Indeterm
	3	Suitable	Suitable	Suitable	Suitable	Suitable	Suitable	Suitable
	4	Suitable	Suitable	Suitable	Suitable	Suitable	Suitable	Suitable
VT58	Constant	Suitable	Suitable	Suitable	Suitable	Suitable	Suitable	Suitable
	1	Suitable	Suitable	Suitable	Suitable	Suitable	Suitable	Suitable
	2	Suitable	Suitable	Suitable	Suitable	Suitable	Suitable	Suitable
	3	Suitable	Suitable	Suitable	Suitable	Suitable	Suitable	Suitable
	4	Suitable	Suitable	Suitable	Suitable	Suitable	Suitable	Suitable
VT59 (STAN)	Constant	Suitable	Suitable	Suitable	Suitable	Suitable	Suitable	Suitable
	1	Suitable	Suitable	Suitable	Suitable	Suitable	Suitable	Suitable
	2	Suitable	Suitable	Suitable	Suitable	Suitable	Suitable	Suitable
	3	Suitable	Suitable	Suitable	Suitable	Suitable	Suitable	Suitable
	4	Suitable	Suitable	Suitable	Suitable	Suitable	Suitable	Suitable
VT62	Constant	Suitable	Suitable	Suitable	Suitable	Suitable	Suitable	Suitable
	1	Suitable	Suitable	Suitable	Suitable	Suitable	Suitable	Suitable
	2	Suitable	Suitable	Suitable	Suitable	Suitable	Suitable	Suitable
	3	Suitable	Suitable	Suitable	Suitable	Suitable	Suitable	Suitable
	4	Suitable	Suitable	Suitable	Suitable	Suitable	Suitable	Suitable

Table VII-11. Continued.

Site	Scenario	Year						
		Past	**1990**	**2000**	**2010**	**2020**	**2040**	**2100**
Sites on Basaltic Bedrock								
VT51	Constant	Suitable	Suitable	Suitable	Suitable	Suitable	Suitable	Suitable
	1	Suitable	Suitable	Suitable	Suitable	Suitable	Suitable	Suitable
	2	Suitable	Suitable	Suitable	Suitable	Suitable	Suitable	Suitable
	3	Suitable	Suitable	Suitable	Suitable	Suitable	Suitable	Suitable
	4	Suitable	Suitable	Suitable	Suitable	Suitable	Suitable	Suitable
VT60 (PINE)	Constant	Suitable	Suitable	Suitable	Suitable	Suitable	Suitable	Suitable
	1	Suitable	Suitable	Suitable	Suitable	Suitable	Suitable	Suitable
	2	Suitable	Suitable	Suitable	Suitable	Suitable	Suitable	Suitable
	3	Suitable	Suitable	Suitable	Suitable	Suitable	Suitable	Suitable
	4	Suitable	Suitable	Suitable	Suitable	Suitable	Suitable	Suitable
VT61	Constant	Suitable	Suitable	Suitable	Suitable	Suitable	Suitable	Suitable
	1	Suitable	Suitable	Suitable	Suitable	Suitable	Suitable	Suitable
	2	Suitable	Suitable	Suitable	Suitable	Suitable	Suitable	Suitable
	3	Suitable	Suitable	Suitable	Suitable	Suitable	Suitable	Suitable
	4	Suitable	Suitable	Suitable	Suitable	Suitable	Suitable	Suitable
VT66	Constant	Suitable	Suitable	Suitable	Suitable	Suitable	Suitable	Suitable
	1	Suitable	Suitable	Suitable	Suitable	Suitable	Suitable	Suitable
	2	Suitable	Suitable	Suitable	Suitable	Suitable	Suitable	Suitable
	3	Suitable	Suitable	Suitable	Suitable	Suitable	Suitable	Suitable
	4	Suitable	Suitable	Suitable	Suitable	Suitable	Suitable	Suitable
VT75	Constant	Suitable	Suitable	Suitable	Suitable	Suitable	Suitable	Suitable
	1	Suitable	Suitable	Suitable	Suitable	Suitable	Suitable	Suitable
	2	Suitable	Suitable	Suitable	Suitable	Suitable	Suitable	Suitable
	3	Suitable	Suitable	Suitable	Suitable	Suitable	Suitable	Suitable
	4	Suitable	Suitable	Suitable	Suitable	Suitable	Suitable	Suitable

[a] For stream names, see Table VI-2.

Blacknose Dace Condition Factor

As a measure of the non-lethal effects of acidification, Bulger et al. (1999) compared condition factor (a measure of robustness of individual fish) in populations of blacknose dace in 11 streams within SHEN spanning a range of pH/ANC conditions. They found (see Figure VI-17) a highly significant relationship between mean stream pH and condition factor in blacknose dace. The results of the condition factor comparisons among the 11 streams indicated that the mean length-adjusted condition factor of fish from the stream with the lowest ANC (and pH) was about 20% lower than that of the fish in best condition. Bulger et al. (1999) concluded that this lower condition factor was attributable to acid stress in the blacknose dace population of that stream, and more generally, that the range of condition factor for blacknose dace among the SHEN streams was a result of the range of observed streamwater pH.

The linear relationship derived from the data in Figure VI-17 was used with the predicted streamwater pH values (Table VII-9) to provide estimates of the expected condition factor of blacknose dace in each of the modeled streams for the past, present and future conditions simulated for the streams. The coupled geochemical and biological model projections were evaluated by comparing the predicted condition factor in each of the 13 streams with the presence or absence of blacknose dace in each stream (Table II-1) for the year 2000. There were no direct measurements of condition factor in the streams in 2000, so no direct evaluation could be made. The indirect comparison (Figure VII-15), however, showed that the stream with the lowest predicted condition factor for the year 2000 (condition factor < 8.0) did not support a population of blacknose dace. This suggests that the predicted condition factor may be a useful index of acid stress effects on blacknose dace populations in SHEN.

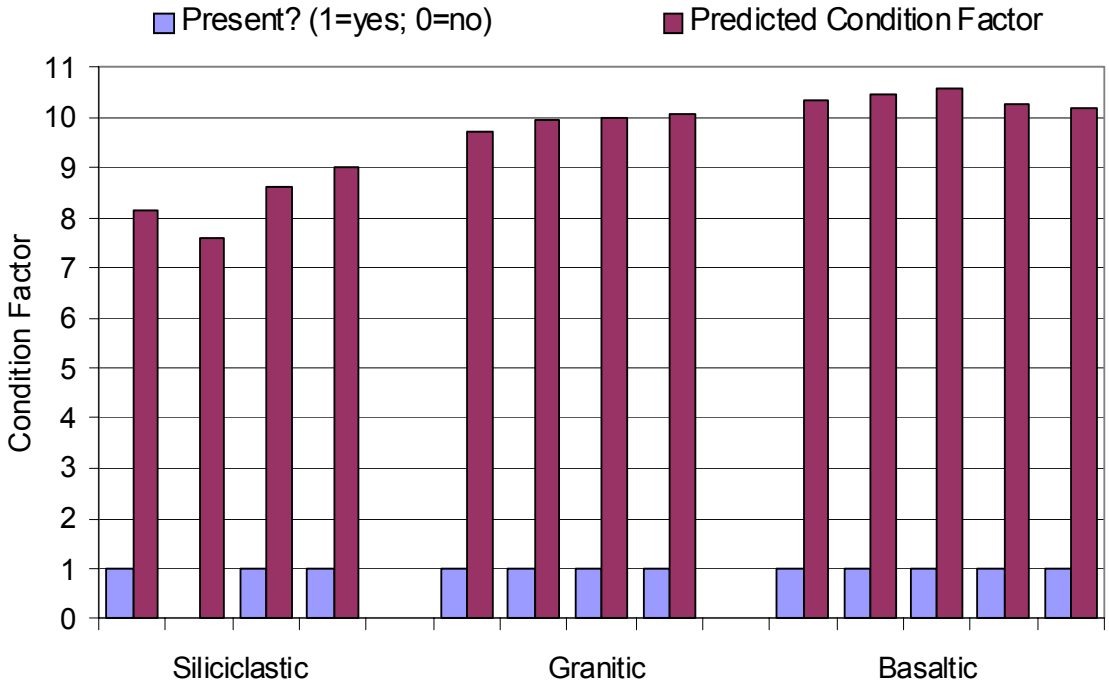

Figure VII-15. Projected condition factor for blacknose dace and observed presence/absence of blacknose dace in 13 SHEN streams for the year 2000.

Model reconstructions of past condition factor for blacknose dace in the streams (Figure VII-16) suggested that loss of condition factor (added acid stress) in blacknose dace populations has been greatest in the siliciclastic streams. Predictions of the expected changes in condition factor for blacknose dace in each of the streams for selected years in each of the future deposition scenarios (Table VII-12) showed that recovery of condition factor (reduction of acid stress) is expected in the siliciclastic streams for all future scenarios except constant deposition. The degree of recovery is greatest for Scenarios 3 and 4 (Figure VII-17).

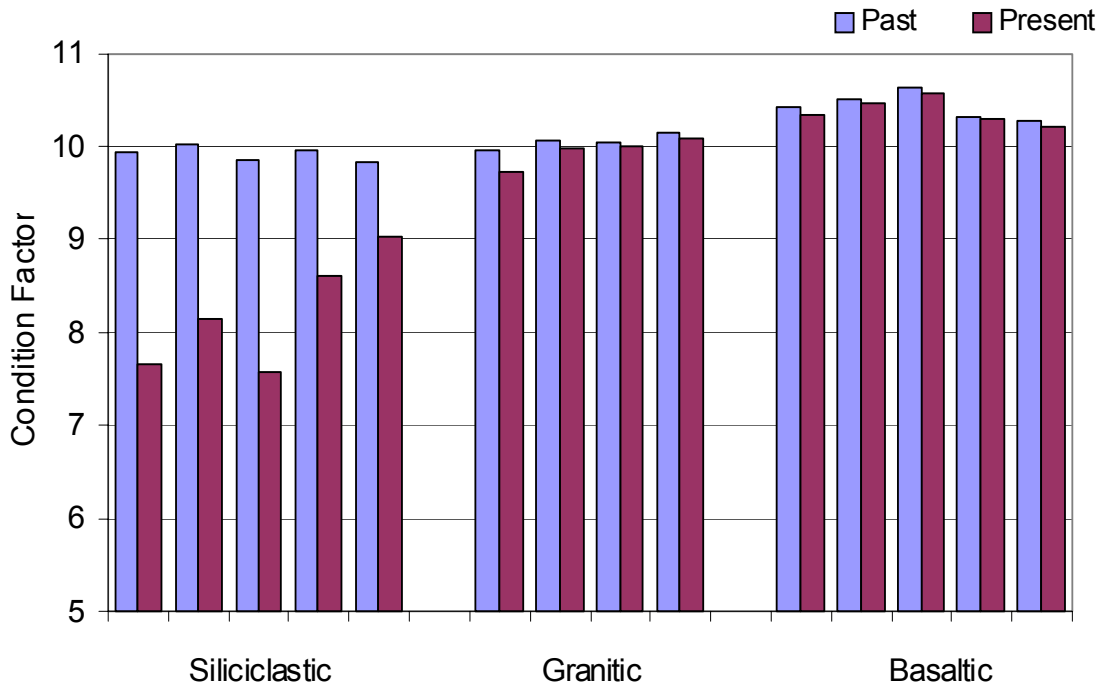

Figure VII-16. Projected condition factor for blacknose dace in 14 SHEN streams for past and present conditions.

Table VII-12. Projected condition factor for blacknose dace in streams within SHEN estimated from simulations for the past in response to historical deposition and for the future in response to simulated constant deposition at 1990 levels and the four emissions control scenarios.

		Year						
Site[a]	**Scenario**	**Past**	**1990**	**2000**	**2010**	**2020**	**2040**	**2100**
Sites on Siliciclastic Bedrock								
DR01	Constant	9.9	8.0	7.7	7.5	7.4	7.3	7.2
	1	9.9	8.0	8.0	8.3	8.5	8.7	8.7
	2	9.9	8.0	8.0	8.2	8.5	8.8	8.9
	3	9.9	8.0	8.0	8.5	9.0	9.4	9.6
	4	9.9	8.0	8.0	8.5	9.0	9.4	9.6
VT35 (PAIN)	Constant	10.0	8.3	8.1	8.0	7.9	7.8	7.5
	1	10.0	8.3	8.6	9.0	9.2	9.3	9.2
	2	10.0	8.3	8.6	9.0	9.2	9.3	9.3
	3	10.0	8.3	8.7	9.1	9.4	9.7	9.8
	4	10.0	8.3	8.7	9.2	9.5	9.7	9.8
VT36	Constant	9.9	7.8	7.6	7.5	7.4	7.3	7.2
	1	9.9	7.8	7.8	8.0	8.2	8.5	8.6
	2	9.9	7.8	7.8	8.0	8.2	8.5	8.7
	3	9.9	7.8	7.8	8.2	8.8	9.2	9.5
	4	9.9	7.8	7.8	8.3	8.8	9.3	9.6
VT53	Constant	9.9	8.9	8.6	8.4	8.2	7.9	7.5
	1	9.9	8.9	8.8	9.0	9.1	9.2	9.2
	2	9.9	8.9	8.8	8.9	9.1	9.2	9.3
	3	9.9	8.9	8.8	9.1	9.3	9.5	9.7
	4	9.9	8.9	8.9	9.1	9.3	9.6	9.7
WOR1	Constant	9.8	9.2	9.0	8.7	8.3	7.6	7.1
	1	9.8	9.2	9.1	9.0	8.9	8.7	8.0
	2	9.8	9.2	9.1	9.0	8.9	8.8	8.3
	3	9.8	9.2	9.1	9.1	9.1	9.2	9.3
	4	9.8	9.2	9.1	9.1	9.1	9.2	9.4
Sites on Granitic Bedrock								
NFDR	Constant	10.0	9.8	9.7	9.7	9.7	9.6	8.9
	1	10.0	9.8	9.7	9.7	9.7	9.7	9.6
	2	10.0	9.8	9.7	9.7	9.7	9.7	9.6
	3	10.0	9.8	9.7	9.7	9.7	9.8	9.7
	4	10.0	9.8	9.7	9.7	9.8	9.8	9.8
VT58	Constant	10.1	10.0	10.0	10.0	9.9	9.9	9.8
	1	10.1	10.0	10.0	10.0	10.0	9.9	9.9
	2	10.1	10.0	10.0	10.0	10.0	9.9	9.9
	3	10.1	10.0	10.0	10.0	10.0	10.0	10.0

Table VII-12. Continued.

Site	Scenario	Year						
		Past	**1990**	**2000**	**2010**	**2020**	**2040**	**2100**
	4	10.1	10.0	10.0	10.0	10.0	10.0	10.0
VT59 (STAN)	Constant	10.0	10.0	10.0	10.0	10.0	10.0	9.9
	1	10.0	10.0	10.0	10.0	10.0	10.0	9.9
	2	10.0	10.0	10.0	10.0	10.0	10.0	10.0
	3	10.0	10.0	10.0	10.0	10.0	10.0	10.0
	4	10.0	10.0	10.0	10.0	10.0	10.0	10.0
VT62	Constant	10.2	10.1	10.1	10.1	10.0	10.0	9.9
	1	10.2	10.1	10.1	10.1	10.1	10.0	10.0
	2	10.2	10.1	10.1	10.1	10.1	10.0	10.0
	3	10.2	10.1	10.1	10.1	10.1	10.1	10.1
	4	10.2	10.1	10.1	10.1	10.1	10.1	10.1
Sites on Basaltic Bedrock								
VT51	Constant	10.4	10.3	10.3	10.3	10.3	10.3	10.3
	1	10.4	10.3	10.3	10.4	10.4	10.4	10.3
	2	10.4	10.3	10.3	10.4	10.4	10.4	10.3
	3	10.4	10.3	10.3	10.4	10.4	10.4	10.4
	4	10.4	10.3	10.3	10.4	10.4	10.4	10.4
VT60 (PINE)	Constant	10.5	10.5	10.5	10.5	10.5	10.4	10.4
	1	10.5	10.5	10.5	10.5	10.5	10.5	10.4
	2	10.5	10.5	10.5	10.5	10.5	10.5	10.5
	3	10.5	10.5	10.5	10.5	10.5	10.5	10.5
	4	10.5	10.5	10.5	10.5	10.5	10.5	10.5
VT61	Constant	10.6	10.6	10.6	10.6	10.6	10.6	10.6
	1	10.6	10.6	10.6	10.6	10.6	10.6	10.6
	2	10.6	10.6	10.6	10.6	10.6	10.6	10.6
	3	10.6	10.6	10.6	10.6	10.6	10.6	10.6
	4	10.6	10.6	10.6	10.6	10.6	10.6	10.6
VT66	Constant	10.3	10.3	10.3	10.3	10.3	10.3	10.3
	1	10.3	10.3	10.3	10.3	10.3	10.3	10.3
	2	10.3	10.3	10.3	10.3	10.3	10.3	10.3
	3	10.3	10.3	10.3	10.3	10.3	10.3	10.3
	4	10.3	10.3	10.3	10.3	10.3	10.3	10.3
VT75	Constant	10.3	10.2	10.2	10.2	10.2	10.2	10.2
	1	10.3	10.2	10.2	10.2	10.2	10.2	10.2
	2	10.3	10.2	10.2	10.2	10.2	10.2	10.2
	3	10.3	10.2	10.2	10.2	10.2	10.2	10.2
	4	10.3	10.2	10.2	10.2	10.2	10.2	10.2

[a] For stream names, see Table VI-2.

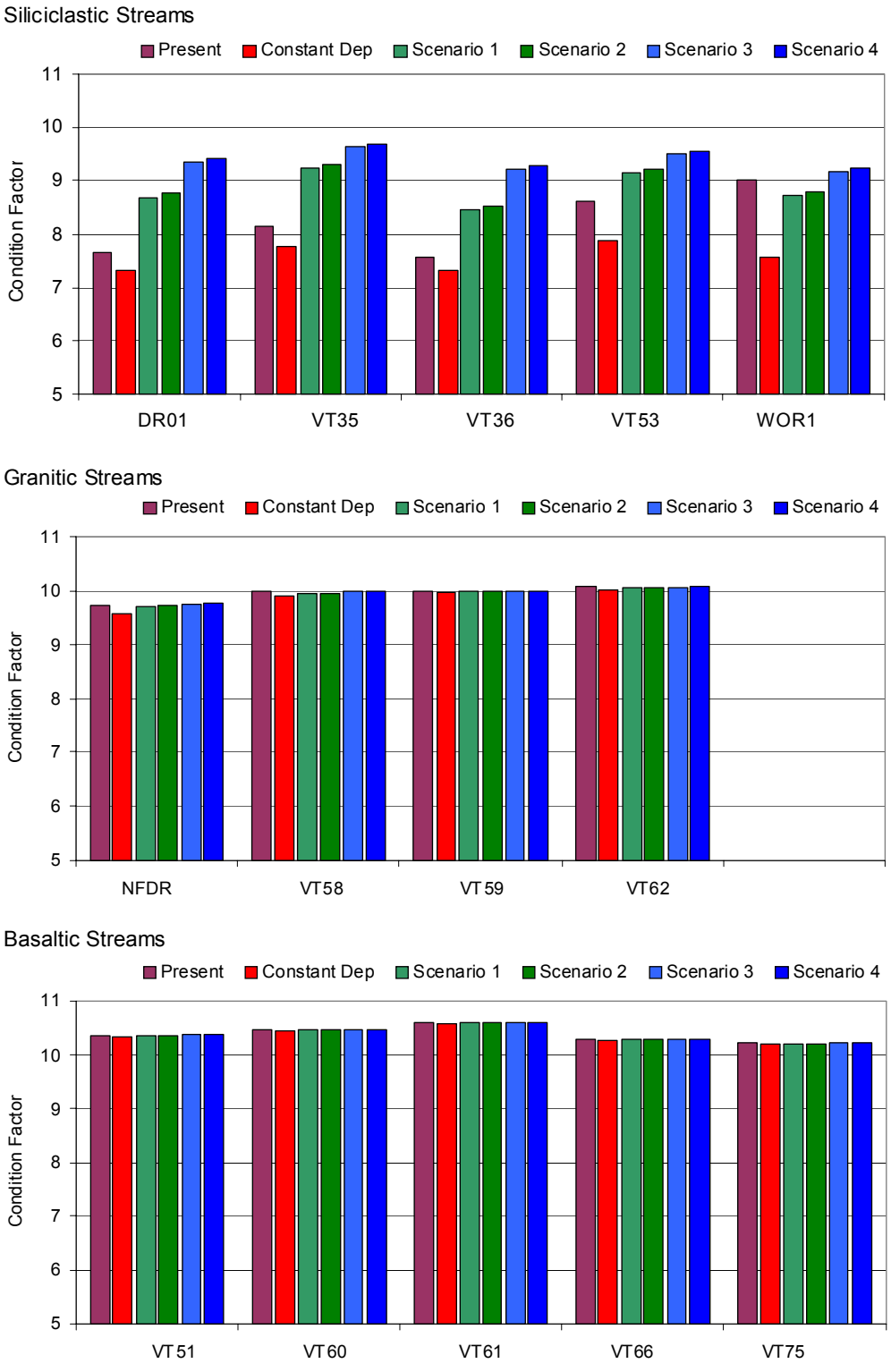

Figure VII-17. Projected condition factor for blacknose dace in 14 SHEN streams for the year 2040 in response to simulated constant deposition at 1990 levels and the four emissions control scenarios.

Species Presence/Absence

Although there are known differences in acid sensitivity among fish species, experimentally determined acid sensitivities are available for only a minority of freshwater fish species. For example, of 28 species of fish commonly found in SHEN, the critical pH range is known for only nine (see Table VI-8 and associated discussion). Critical pH can be defined as the threshold for significant adverse effects on fish populations. In general, there is no single pH threshold for a given species. Table VI-8 reports a range of pH values which represent the various investigators' estimates of uncertainty of this critical pH for any species. The range of response within species depends in part on differences in sensitivity among life stages, and on different exposure concentrations of calcium (Ca^{2+}) and Al. These ranges of critical pH can be used to predict the potential presence or absence of these species in a stream, given the streamwater pH.

In this section, we combine the pH ranges presented in Table VI-8 with predicted streamwater pH values (Table VII-9) to provide estimates of the expected presence or absence of nine fish species in each of the modeled streams for the past, present and future conditions simulated for the streams. The projections presented here concerning presence/absence ignore whether or not other habitat factors are suitable (temperature, food sources, etc.). As such, these projections are useful *only* as an *index*. This index allows the question to be asked "If other habitat factors are suitable, would the acid/base status of the streamwater (pH) be suitable for the presence of this species of fish in this stream?" When calculating the presence/absence, the range of critical pH values in Table VI-8 was explicitly considered by establishing three categories of prediction: 1) *suitable conditions* mean that the predicted pH was above the upper pH threshold for that species; 2) *marginal conditions* mean that predicted pH was between the upper and lower thresholds; and 3) *unsuitable conditions* for a species means that the predicted pH was below the lower threshold of the pH range.

The coupled geochemical and biological model projections were evaluated by comparing the predicted presence/absence of each species with observed presence/absence data (Table II-1). As can be seen (Figure VII-18), for the species considered in these predictions only four of the nine species actually appear in any the 14 modeled streams, regardless of the predicted pH. This re-emphasizes the use of this metric of biological response as an *index* of potential biological suitability for these streams. Lack of observed presence of many of the species may be due to inadequacy of habitat variables other than pH.

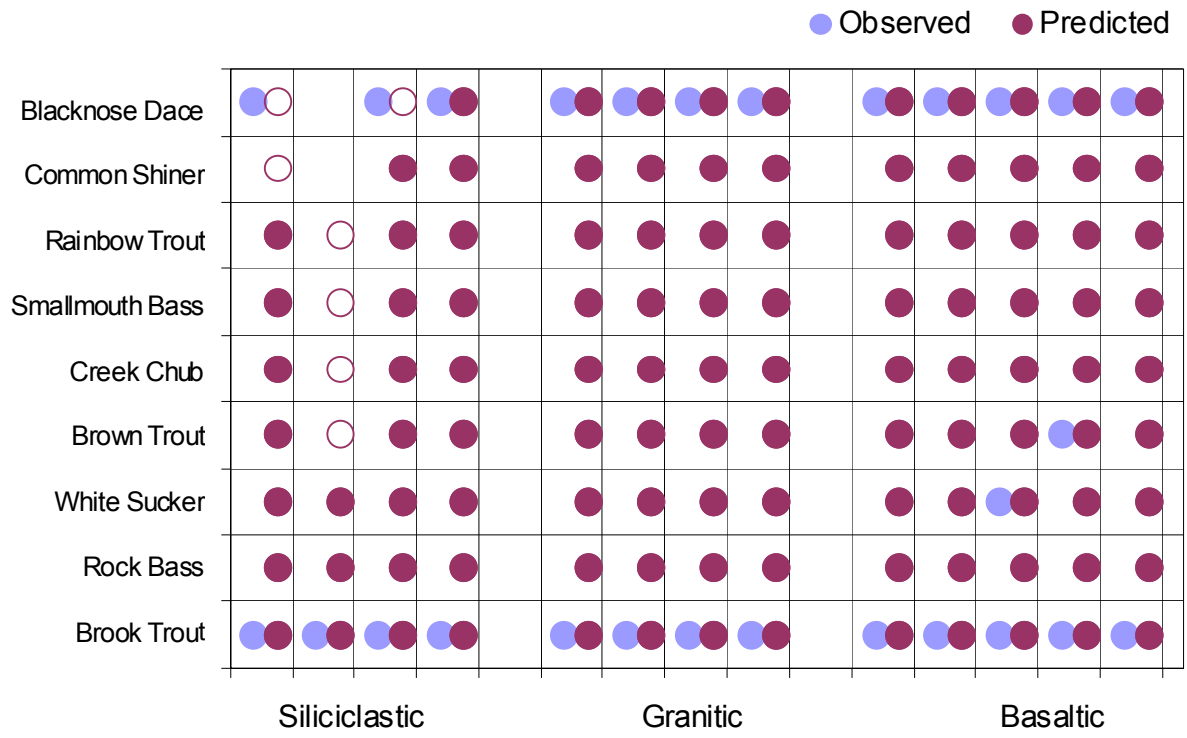

Figure VII-18. Projected suitability of streamwater pH for, and observed presence/absence of, nine fish species in 13 SHEN streams for the year 2000. For the projections (right side of each column), solid symbols indicate that streamwater pH is suitable; open symbols indicate that streamwater pH is marginal; no symbol indicates that streamwater pH is unsuitable. For the observations (left side of each column), presence is indicated by a solid symbol and absence is indicated by no symbol.

Model reconstructions of the past for these nine species (Figure VII-19) suggested that past streamwater pH should have produced suitable conditions for all species in all streams, and the decrease in suitability (both in terms of number of streams and number of species) has been greatest in the siliciclastic streams. Projections of the expected future presence/absence of the nine species in each of the streams for a selected year in each of the future deposition scenarios (Figure VII-20) showed that recovery of marginal or suitable conditions for all nine species in all streams is expected for all future scenarios except constant deposition.

Discussion of Biological Modeling Results

In order to make the projections described above of likely past and future responses of aquatic biota to changing deposition in SHEN, the geochemical model MAGIC was coupled

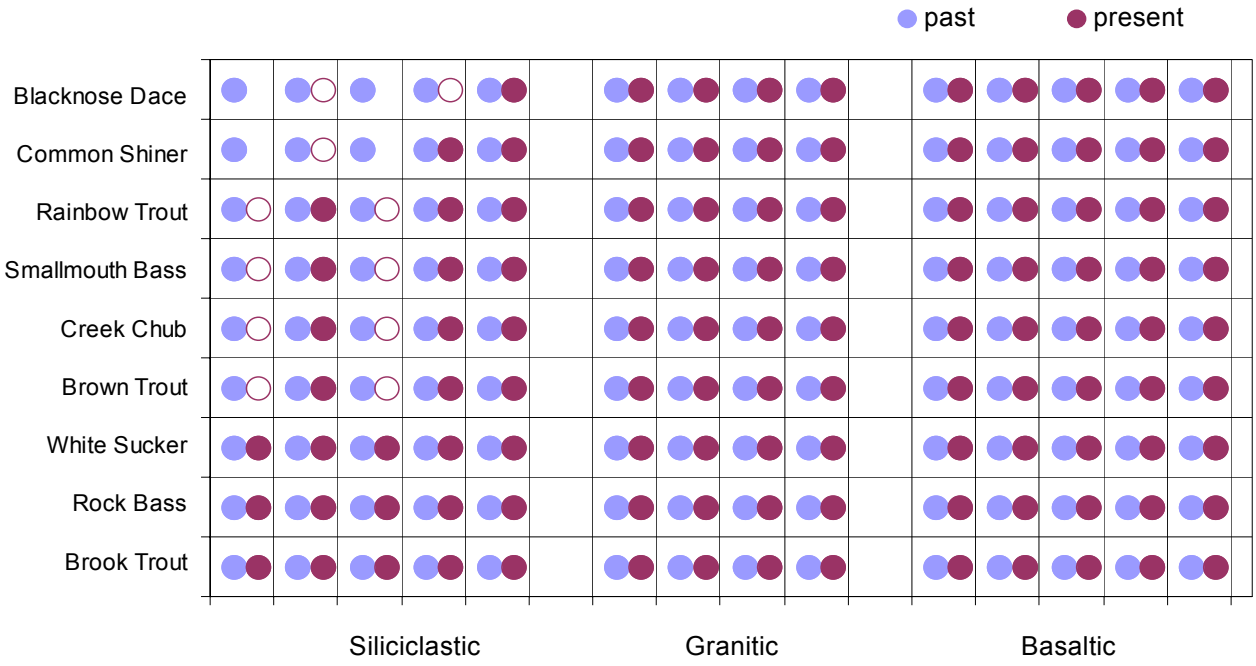

Figure VII-19. Projected suitability of streamwater pH for nine fish species in 14 SHEN streams for past (left side of column) and present (right side of column) conditions. Solid symbols indicate that streamwater pH is suitable; open symbols indicate that streamwater pH is marginal; no symbol indicates that streamwater pH is unsuitable.

with several empirical relationships which link biological response to water quality. The coupling of these models is straightforward from a procedural point of view. The interpretation and utility of the results, however, require consideration of a number of points that arise because of the different nature of the models that were coupled.

Unlike MAGIC which is a process-based model, the biological effects estimates are based on observed empirical relationships rooted in correlation and expressed as linear relationships. Correlation does not necessarily imply causality, but an observed pattern of co-variation between variables does provide a quantitative context for extrapolation. In this case, the projections being made do not require extrapolation beyond the observed ranges of observations, and therefore the projections are statistically robust. To the extent that the observed empirical relationships used in the coupled models do in fact reflect the effects of acid stress on aquatic biota, the projections are also biologically robust.

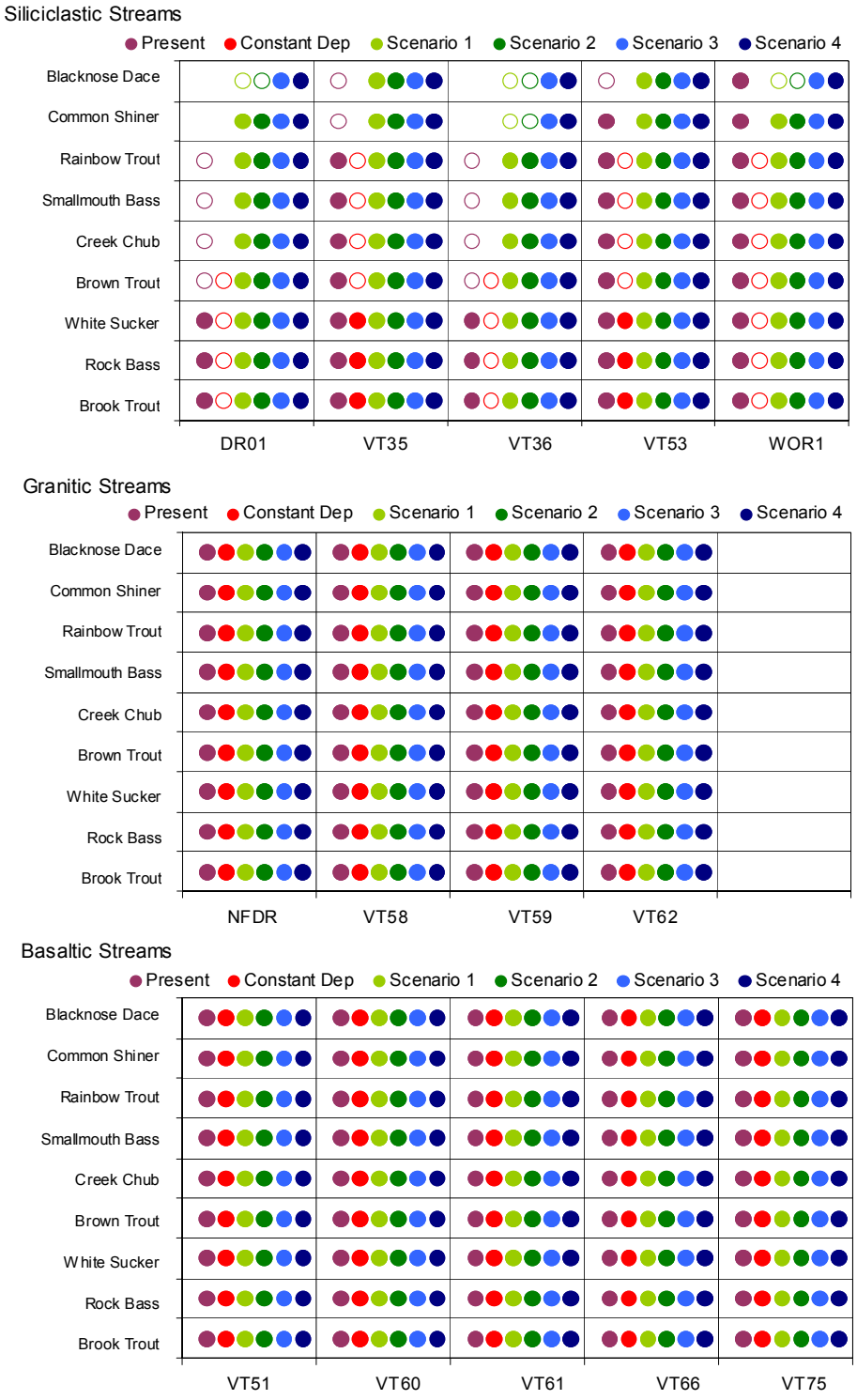

Figure VII-20. Projected suitability of streamwater pH for nine fish species in 14 SHEN streams for the year 2040 in response to simulated constant deposition at 1990 levels and the four emissions control scenarios. Solid symbols indicate that streamwater pH is suitable; open symbols indicate that streamwater pH is marginal; no symbol indicates that streamwater pH is unsuitable.

Besides the distinction between process-based and empirical models, the geochemical and biological response models differ in another way. MAGIC is a dynamic model and explicitly predicts the time-course of changing water quality. The empirical relationships used for the biological response models, however, are static. These relationships reflect a point in time (when the observations were made) and provide no information concerning the *dynamics* of biological response. That is, the empirical models predict a new biological status for a new water chemistry, but give no indication of the time required to achieve the biological status once the water quality change has occurred.

There are thus two considerations that must be kept in mind when interpreting the biological responses predicted in this section: the causality of the relationship between water quality and response, and the dynamics of biological response. With respect to the issue of causality, acidification is a disturbance, and disturbance always lowers species richness. Loss of species usually lowers productivity and stability of ecosystems. Fish biodiversity loss is a predictable and proven consequence of acidification, and there are abundant examples of this in North America and Europe (c.f., Bulger et al. 2000). Continued fish biodiversity loss is not sustainable, and carries significant ecological and economic costs.

With respect to the dynamics of biological recovery, there is no theoretical basis on which to predict the paths of biological recovery. At some scale, each stream or river is unique. The null hypothesis is that recovery will proceed in the same fashion as acidification, only backwards. Thus, for example, the last species lost (the most acid tolerant) would be the first to return. However, time lags are expected because of species recolonization times, which differ widely among species and among streams.

Stream macroinvertebrate communities are often dominated by immature life stages of flying insects, such as mayflies, dragonflies, and stoneflies. Such species have rather rapid colonization times, such that a functional stream macroinvertebrate community may return in about three years. However, fish community recovery is expected to be quite variable, depending on sources of colonists. In streams, fish could be introduced as soon as the water quality becomes suitable and/or the macroinvertebrate community becomes established. In streams which had simple fish communities in the past, a fish community might become rapidly established with species introductions, or might take many decades for complex communities

without species introductions. In SHEN, recolonization would be expected to be relatively rapid because of the interconnectivity of all of the rivers, which provides a ready supply of colonists.

e. Prognosis for Recovery of Aquatic Ecosystems

Background

As described above, available data, model projections, and the weight of scientific evidence suggest that air pollution and acidic deposition have caused environmental degradation of surface waters, forests, and visibility in SHEN. Recent emissions control efforts have focused on attempts to reduce air pollution and deposition sufficiently to permit ecosystem recovery, if not to pre-industrial levels, at least to levels that might allow some reduction in ecological damage. Key questions now facing scientists and policy-makers have to do with the degree in space and in time to which S, N, and volatile organic carbon emissions will need to be reduced in order to allow ecosystem recovery to proceed and to prevent further damage (c.f., Jenkins et al. 1998). A substantial body of scientific literature exists on this topic with respect to aquatic effects, and modeling approaches are available with which to specify the needed emissions reductions.

Public policy measures to reduce emissions should be based on an understanding of dose/response relationships which reflect the tolerance of natural ecosystems to various inputs of atmospheric pollutants. This need has given rise to the concepts of critical levels of pollutants and critical loads of deposition (e.g., Bull 1991, 1992), as well as interest in establishing and refining standards for ambient air pollution and acid deposition. A critical level or load can be defined as a quantitative estimate of an exposure (concentration or loading) to one or more pollutants below which significant harmful effects on specified sensitive elements of the environment do not occur according to present knowledge (e.g. Nilsson 1986, Gundersen 1992). Although such an approach to establishing a standard is intuitively satisfying, the assignment of a standard or critical load is difficult because a variety of natural processes and anthropogenic activities affect the status of sensitive resources, in addition to air pollution and atmospheric deposition of S and N. Furthermore, the pollutant concentrations or deposition loadings that may be required to protect *the most sensitive* elements of an ecosystem may be difficult to quantify.

The basic concept of critical load is relatively simple: the threshold concentration of pollutants at which harmful effects on sensitive receptors begin to occur. Implementation of the concept is, however, not at all simple or straight-forward. For example, the acid-base chemistry of surface waters typically exhibits substantial intra- and interannual variability. Seasonal variability in the concentration of key chemical parameters often varies by more than the amount of acidification that might occur in the future in response to acidic deposition. Such variability makes quantification of acidification and recovery responses difficult, and also complicates attempts to evaluate sensitivity to acidification based on "index" or annual average chemistry, as is typically collected in stream surveys.

Technical information required by the U.S. EPA for assessing the feasibility of adopting one or more acid deposition standards for the protection of aquatic resources was summarized by Sullivan and Eilers (1994), Van Sickle and Church (1995), and Church and Van Sickle (1999). Quantitative model-based analyses were conducted for areas of the United States intensively studied in EPA's model forecasting program, the Direct Delayed Response Project (DDRP, Church et al. 1989). The MAGIC model (Cosby et al. 1985a,b) was used to project changes in surface water chemistry for a range of S and N deposition scenarios, assuming a range of N retention efficiencies (Van Sickle and Church 1995). Subsequently, a report was prepared for Congress on the feasibility of adopting one or more acid deposition standards (U.S. EPA 1995). The report concluded that establishment of such standards for S and N deposition in the United States was technically feasible, but that two critical areas of uncertainty advised against the setting of national standards at that time. First, policy decisions regarding appropriate or desired goals for protecting sensitive systems were needed, especially with respect to the level of protection desired and the costs and benefits of such protection. Second, key scientific unknowns, particularly regarding watershed processes that govern N dynamics, limited the ability to recommend specific standards for N deposition at that time (EPA 1995a, Sullivan 2000).

Federal agencies have made progress regarding policy decisions on protection of sensitive systems; however decisions for some resources and locations are still needed. The more scientific data that is made available for Federal land managers to base these types of decisions on, the more robust the decisions are likely to be in the future.

Prior to and since publication of EPA's Acid Deposition Standards Feasibility Report (U.S. EPA 1995), considerable research has been conducted on the topics of N dynamics and the effects of atmospheric N deposition (c.f., Sullivan 1993, Emmett et al. 1997, Jenkins et al. 1997, Cosby et al. 1997, Aber et al. 1997, 1998). A variety of dynamic models are now available with which to estimate critical loads for N at the watershed scale. Nitrogen dynamics have recently been added to the MAGIC model (Cosby et al. 2001; see also Appendix F), thus allowing MAGIC to be used for assessment of critical loads for either S or N or a combination of the two.

The forest soils in SHEN currently retain virtually all atmospheric N except during and subsequent to insect infestation. A preliminary modeling study of a representative catchment in SHEN using the PnET model (Aber and Federer 1992, Aber et al. 1997) found that both the forests and the forest soils in SHEN are very actively aggrading N (Fievet 2001). The model output suggested that, at current levels of N deposition and barring pest outbreaks or substantial land use changes, more than 100 years will elapse before the forest ecosystem becomes "saturated" with N to the point that significant N losses in streamwater will occur. This result is similar to that found for aggrading temperate hardwood forests elsewhere (Aber et al. 1998). In the SHEN forests, the current levels of atmospheric N deposition are below threshold values commonly associated with forest N saturation (Sullivan, 2000). Also, the forests within the park are regenerating as a consequence of large-scale disturbances prior to the formation of the park, and therefore have relatively high N demand. For these reasons, the critical load of N deposition (at least with respect to N leaching and acidification) is not as important a consideration for this park as is the critical load of S deposition at the present time. Of course, this could change if N deposition dramatically increased in the future.

The adoption of acid deposition standards or thresholds for the protection of surface water quality from potential adverse effects of S and N deposition is a multifaceted problem. It requires that S and N be treated separately as potentially-acidifying agents. Appropriate criteria must be selected as being indicative of damaged water quality, for example ANC or pH. Once a criterion has been selected, a critical value must be estimated, below which the criterion should not fall. For example, if the selected criterion is surface water ANC, one could specify that ANC should not fall below, or should recover to, 0, 20, or 50 μeq/L in response to acidic deposition (e.g., Kämäri et al. 1992). Selection of critical values for ANC or pH is confounded by the existence of streams that are acidic or very low in pH or ANC due entirely to natural factors,

irrespective of acidic deposition (Sullivan 1990). In particular, low contributions of base cations in solution, due to low weathering rates and/or minimal contact between drainage waters and mineral soils, and high concentrations of organic acids contribute to naturally low pH and ANC in surface waters. Other factors also can be important in some cases, including watershed sources of S (Sullivan 2000).

Acid deposition standards or thresholds might be selected on the basis of protecting aquatic systems from either chronic or episodic acidification. Thus, selection of appropriate acidic deposition standards or thresholds involves consideration of a matrix of factors. Specification of numerical values for the protection of sensitive resources against adverse impacts associated with S and/or N deposition is dependent on a host of both scientific and policy decisions. These include, for example:

- scientific determination of the extent to which water chemistry will change in its acid-base character in response to various deposition loading rates (chemical dose-response relationship),
- scientific estimation of the biological responses associated with given changes in water chemistry (biological dose-response relationship),
- policy determination of the percent of sensitive resources within a given region that one wishes to protect against adverse changes, and
- policy determination of what biological changes must be protected against (Sullivan 2000).

It is now fairly straightforward to estimate the dose-response functions for a given watershed or group of watersheds within a region, although this does entail a moderate level of uncertainty (e.g., Turner et al. 1992, Sullivan and Eilers 1994, van Sickle and Church 1995, Sullivan 2000). Furthermore, there are generally well-accepted criteria for specifying biological response functions, both chronically and episodically (e.g., Section VII.C.1.d., Baker et al. 1990b, Wigington et al. 1993), based on observed empirical relationships and a general knowledge of the magnitude of episodic excursions from measured chronic chemistry and regional hydrology (e.g., Eshleman 1988, Webb et al. 1994).

Critical Loads Analysis for SHEN Streams

The principal objectives of the critical loads work reported here for aquatic ecosystems in SHEN were to determine, using the MAGIC model, threshold levels of sustained atmospheric

deposition of S below which adverse effects to sensitive aquatic receptors in SHEN will not occur, and to evaluate interactions between the critical ANC endpoint value specified and the time period over which the critical load is examined. Critical loads for S deposition were calculated using the MAGIC model for the 14 streams selected in SHEN for modeling, distributed into geological sensitivity classes as follows: 5 each on siliciclastic and basaltic bedrock, and 4 on granitic bedrock.

The MAGIC model was used in an iterative fashion to calculate the S deposition values that would cause the chemistry of each of the modeled streams to either increase or decrease streamwater ANC (depending on the current value) to reach the specified critical levels. For some analyses, the critical ANC levels were set at 0, 20, and 50 μeq/L, the first two of which are believed to approximately correspond with chronic and episodic damage to the relatively acid-tolerant brook trout populations in park streams (Bulger et al. 2000). Other more acid-sensitive species of aquatic biota may be impacted at higher ANC values. In order to conduct this critical loads analysis for S deposition, it was necessary to specify the corresponding levels of N deposition. Nitrogen deposition accounts, however, for only a minor component of the overall acidification response of streams in the park. For this analysis, future N deposition was held constant at 1990 levels (7.6 kg N/ha/yr). It was also necessary to specify the times in the future at which the critical ANC values would be reached. We selected the years 2020, 2040, and 2100. It must be recognized that streamwater chemistry will continue to change in the future for many decades subsequent to stabilization of deposition levels. This is mainly because soils will continue to change in the degree to which they adsorb incoming S and because some watersheds will have become depleted of base cations. The latter process can cause streamwater base cation concentrations and ANC to decrease over time while SO_4^{2-} and NO_3^- concentrations maintain relatively constant levels.

The levels of S deposition that were simulated to cause streamwater ANC to increase or decrease to the three specified critical levels (0, 20, and 50 μeq/L) are listed in Table VII-13 for each of the modeled streams. Estimated critical loads for S deposition ranged from less than zero (ANC objective not attainable) to several hundred kg/ha/yr, depending on the selected site, ANC endpoint, and evaluation year.

It is useful to put the results of this critical loads analysis into the perspective of the population of streams within the park. This cannot be done directly, however, because the

Table VII-13. Estimated critical load (kg/ha/yr) of sulfur[a] to achieve a variety of ANC (μeq/L) endpoints in a variety of future years for modeled streams in SHEN.[b]

Site[d]	Bedrock Class[e]	ANC (μeq/L)		Critical Load to Achieve ANC Value[c]								
				ANC = 0			ANC = 20			ANC = 50		
		1990	Pre-1900	2020	2040	2100	2020	2040	2100	2020	2040	2100
VT36	S	0	69	9	9	9	2	5	6	< 0	< 0	1
DR01	S	2	78	14	13	12	5	8	9	< 0	< 0	3
VT35[f]	S	7	91	16	15	14	11	11	11	1	4	6
VT53	S	16	81	20	17	15	11	12	11	< 0	1	5
WOR1	S	26	66	22	15	10	5	6	6	< 0	< 0	< 0
NFDR	G	60	82	53	33	17	43	26	13	15	10	7
VT58	G	88	98	119	59	29	109	53	25	83	40	18
VT59[f]	G	88	96	164	86	45	154	79	40	127	62	30
VT62	G	102	116	122	60	29	112	55	26	92	44	20
VT75	B	126	143	331	183	78	307	173	76	248	147	69
VT66	B	147	159	155	118	73	143	109	69	127	93	60
VT51	B	166	191	281	151	65	267	145	64	239	134	62
VT60[f]	B	204	218	241	147	72	230	142	70	211	134	67
VT61	B	258	277	502	281	124	487	276	122	459	265	119

[a] Deposition of sulfur in 1990 was about 13 kg/ha/yr
[b] All simulations based on straight-line ramp changes in deposition from 2000 to 2010, followed by constant deposition thereafter.
[c] <0 indicates that the ANC endpoint could not be achieved (no recovery) even if S deposition was reduced to zero.
[d] See Table VI-2 for stream names
[e] Siliciclastic, S; Granitic, G; Basaltic, B
[f] Intensively studied sites are VT35 (PAIN), VT59 (STAN), and VT60 (PINE)

modeled streams were not statistically selected. This can be done indirectly if the range of critical load estimates is relatively narrow within a given ANC class or geologic sensitivity class or if the critical load estimates vary in a predictable way as a function of some aspect of the current streamwater chemistry. Results of the estimated critical load values are summarized by ANC class and by geologic sensitivity class in Table VII-14. None of the granitic or basaltic streams exhibited critical loads values lower than the current S deposition level (13 kg/ha/yr), when evaluated for the year 2100 using ANC criterion values of either 0 or 20 μeq/L.

In marked contrast, all of the modeled siliciclastic streams exhibited critical loads ≤ 11 kg/ha/yr to protect against acidification to ANC ≤ 20 in the year 2100 (Table VII-14). The median modeled siliciclastic stream had a calculated critical load to protect against acidification to ANC ≤ 20 μeq/L that was about 31% lower than the 1990 deposition that was used as the baseline for the modeling analyses (13 kg S/ha/yr).

Table VII-14. Median and range of estimated critical load values for sulfur deposition, by principal geologic sensitivity class within the watershed.

Geologic Sensitivity Class	Number of Modeled Streams in Class (n)	Median (Range) Estimated Critical Load of Sulfur Deposition (kg/ha/yr) for the Year 2100		
		ANC = 0	ANC = 20 μeq/L	ANC = 50 μeq/L
Siliciclastic	5	12 (9-15)	9 (6-11)	3 (<0-6)
Granitic	4	29 (17-45)	26 (13-40)	20 (7-30)
Basaltic	5	73 (65-124)	70 (64-122)	67 (60-119)

The calculated S deposition critical load for streams in SHEN varied as a function of watershed sensitivity (as reflected in geologic sensitivity class, and soils and streamwater characteristics), the selected chemical criterion (critical ANC value), and the future year for which the evaluation was made. All of these criteria are important. For example, the modeled critical S load to protect the 14 modeled streams in SHEN from becoming acidic (ANC=0) in the year 2100 varied from 9 to 124 kg S/ha/yr (Table VII-13). Similarly, for site WOR1 (White Oak Run) in the year 2100, the critical load to protect against ANC=0 was 10 kg S/ha/yr, but this watershed could tolerate only 6 kg S/ha/yr to protect against acidification to ANC of 20 μeq/L within the same time period. The model suggested that it would not be possible to achieve ANC=50 μeq/L at this site by 2100, even if S deposition was reduced to zero. The estimated pre-1900 ANC of this stream was 66 μeq/L, which declined to 26 μeq/L by 1990.

Table VII-15 provides estimates of the percent change in S deposition required from 1990 loads to achieve ANC values of 0, 20, or 50 μeq/L by the years 2020, 2040, and 2100. Of the streams underlain by siliciclastic bedrock, only Meadow Run (VT36) and White Oak Run (WOR1) required decreased deposition to protect against acidification to ANC=0 in any of the projection year endpoints. However, all of the sites underlain by siliciclastic bedrock required reduced deposition in order to protect against acidification to ANC below 20 μeq/L in all three future evaluation years (Table VII-15). The required deposition reductions ranged from 9% (Twomile Run) to 55% (White Oak Run) for the evaluation year 2100. All except one (White Oak Run) of the siliciclastic sites were projected to be able to achieve ANC above 50 μeq/L in 2100, but S deposition would have to be reduced by 55 to 89% to realize that objective.

Table VII-15. Estimated percent change in 1990 sulfur deposition[a] required to produce a variety of ANC (μeq/L) endpoints in a variety of future years for streams in SHEN.[b]

Site[d]	Bedrock Class[e]	ANC (μeq/L)		Percent Change in 1990 Deposition to Achieve ANC Value[c]								
				ANC = 0			ANC = 20			ANC = 50		
		1990	Pre-1900	2020	2040	2100	2020	2040	2100	2020	2040	2100
VT36	S	0	69	-24	-25	-28	-84	-59	-50	< -100	< -100	-89
DR01	S	2	78	8	3	-2	-59	-35	-28	< -100	< -100	-73
VT35[f]	S	7	91	28	17	10	-16	-13	-15	-96	-67	-55
VT53	S	16	81	58	34	20	-14	-7	-9	< -100	-92	-61
WOR1	S	26	66	77	16	-18	-60	-56	-55	< -100	< -100	< -100
NFDR	G	60	82	321	162	33	245	111	7	18	-19	-45
VT59[f]	G	88	96	1210	583	262	1126	526	221	908	397	140
VT58	G	88	98	851	371	130	767	324	103	558	215	45
VT62	G	102	116	868	375	133	795	335	109	633	251	63
VT75	B	126	143	2535	1358	525	2344	1281	505	1880	1071	449
VT66	B	147	159	1138	840	484	1042	767	446	908	640	378
VT51	B	166	191	2136	1102	416	2028	1059	409	1808	970	392
VT60[f]	B	204	218	1821	1074	472	1737	1035	457	1584	965	431
VT61	B	258	277	3904	2140	890	3780	2104	876	3561	2016	851

[a] Current deposition of sulfur is 13 kg/ha/yr
[b] All simulations based on straight-line ramp changes in deposition from 2000 to 2010, followed by constant deposition thereafter.
[c] < 100% indicates that the ANC endpoint could not be achieved (no recovery) even if S deposition was reduced to zero.
[d] See Table VI-2 for stream names
[e] Siliciclastic, S; Granitic, G; Basaltic, B
[f] Intensively studied sites are VT35 (PAIN), VT59 (STAN), and VT60 (PINE)

The relationships between critical load, selection of ANC criterion value, and selection of evaluation year are illustrated in Figures VII-21 and VII-22. Higher critical loads can be tolerated if one only wishes to protect against acidification to the year 2020, as compared with more stringent deposition reductions required to protect systems against acidification for a longer period of time (Figure VII-21). Higher critical loads can be tolerated to prevent acidification to ANC = 0 (chronic acidification) than if one wishes to be more restrictive and prevent acidification to ANC below 20 μeq/L (possible episodic acidification; Figure VII-22).

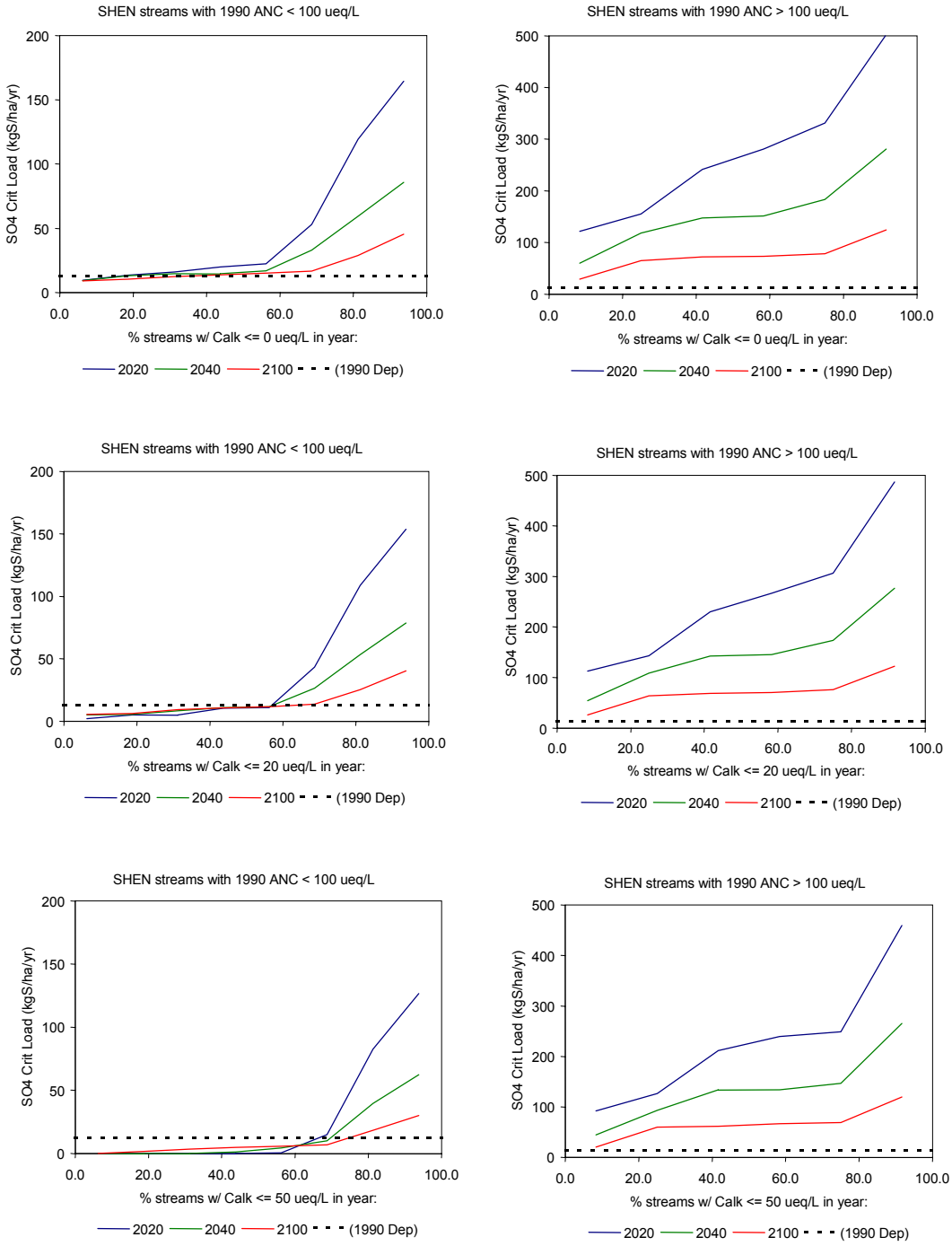

Figure VII-21. Relationship between the simulated sulfur deposition load and the percent of modeled streams in SHEN that have ANC less than or equal to a critical value (0, 20, or 50 µeq/L) in three different future years (2020, 2040, 2100). Deposition in 1990 is indicated as a dotted reference line. For ease of comparison, streams are grouped according to whether 1990 ANC was above or below 100 µeq/L.

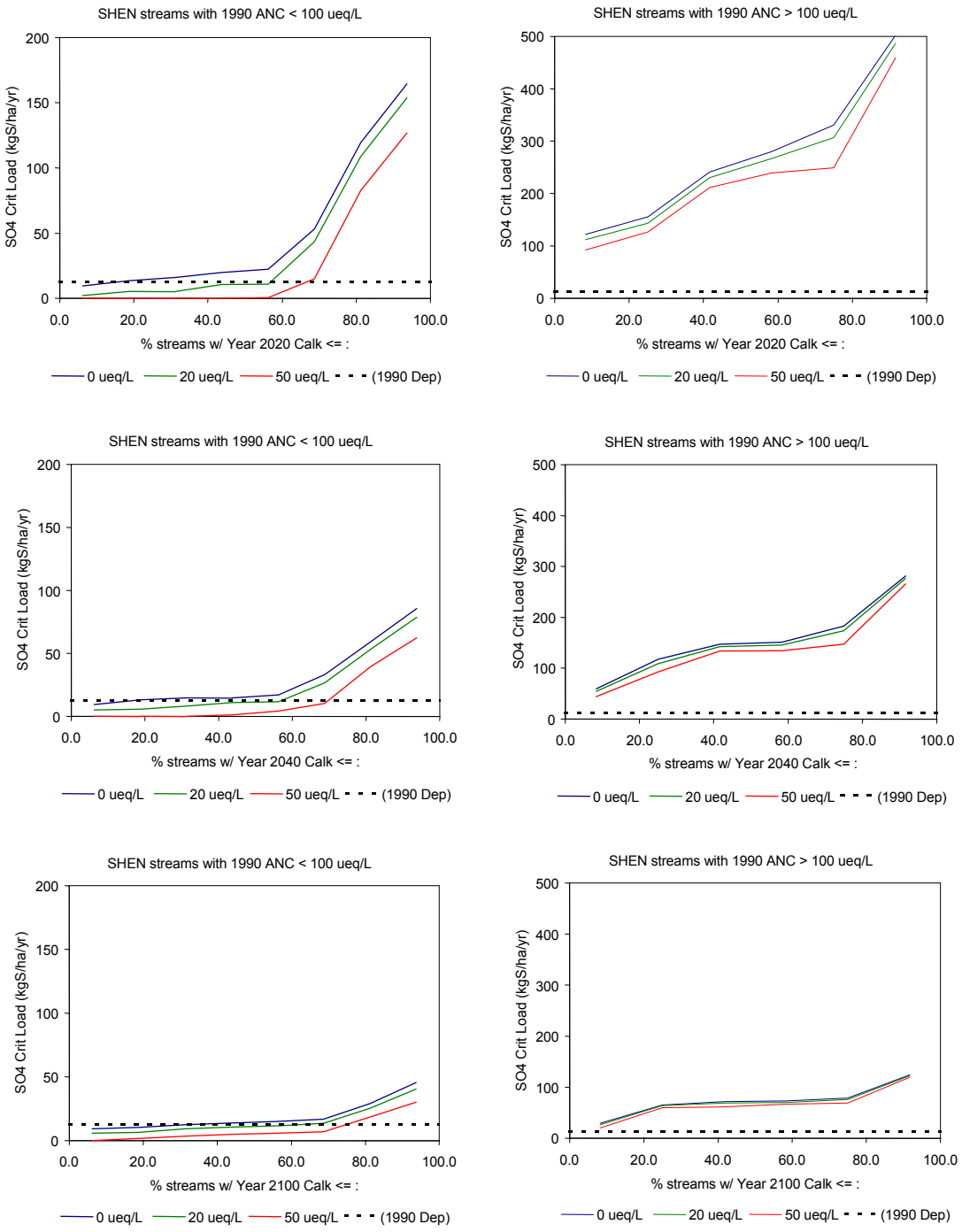

Figure VII-22. Relationship between the simulated sulfur deposition load and the percent of modeled streams in SHEN that have ANC less than or equal to a critical value (0, 20, or 50 µeq/L) in three different future years (2020, 2040, 2100). Deposition in 1990 is indicated as a dotted reference line. For ease of comparison, streams are grouped according to whether 1990 ANC was above or below 100 µeq/L.

The model suggested that it would not be possible to regain streamwater ANC values by the year 2100 that would be similar to pre-industrial ANC, at least for the most acid-sensitive systems, even if S deposition was reduced to zero. For example, of the modeled streams that had ANC < 100 μeq/L in 1990, only one (Staunton River) was projected to reach within 10% of its inferred pre-industrial ANC value anytime between now and 2100, regardless of how much S deposition was reduced.

The data presented in Tables VII-13 and VII-14 and in Figures VII-21 and VII-22, clearly illustrate that how you phrase the critical load question is extremely important. The estimated deposition change required to achieve certain benchmark streamwater chemistry endpoints can be highly variable depending on how and for what time period the endpoint is defined, and on the starting point chemistry of the watersheds that are selected for modeling.

The model estimates of critical loads of S deposition required to prevent streamwater acidification to ANC values below 0, 20, and 50 μeq/L varied consistently as a function of measured ANC in 1990, which in turn was separated into rather distinct groupings according to geologic sensitivity class (Figure VII-23). For example, these model output data suggested, based on the equation given in Figure VII-23, middle panel, that all streams within the park that had 1990 ANC ≤ 20 μeq/L would require critical load values between 2.5 and 14.4 kg S/ha/yr to maintain ANC above 20 μeq/L in the year 2040. Similarly, the model data suggested that a critical load of 7.3 kg S/ha/yr would protect all streams in the park that had positive ANC in 1990 from becoming chronically acidic by 2040; a critical load of 2.5 kg S/ha/yr would allow those same streams to achieve or maintain ANC above 20 μeq/L by 2040; but even with a reduction in S deposition to zero, some of those streams would not achieve or maintain ANC above 50 μeq/L by 2040.

The equations describing the relationships between MAGIC model estimates of S critical load and 1990 streamwater ANC values are given in Table VII-16 for the various ANC endpoints and end years considered. Once the desired ANC endpoint and end year are specified, these equations can be used to estimate the critical load of S deposition that would be required, based on MAGIC model projections, to achieve or maintain those ANC endpoint criteria values for any stream in the park. Note, however, that the model projections suggested that it would not be possible to achieve ANC = 50 μeq/L in any of the end years evaluated for at least some low-ANC streams.

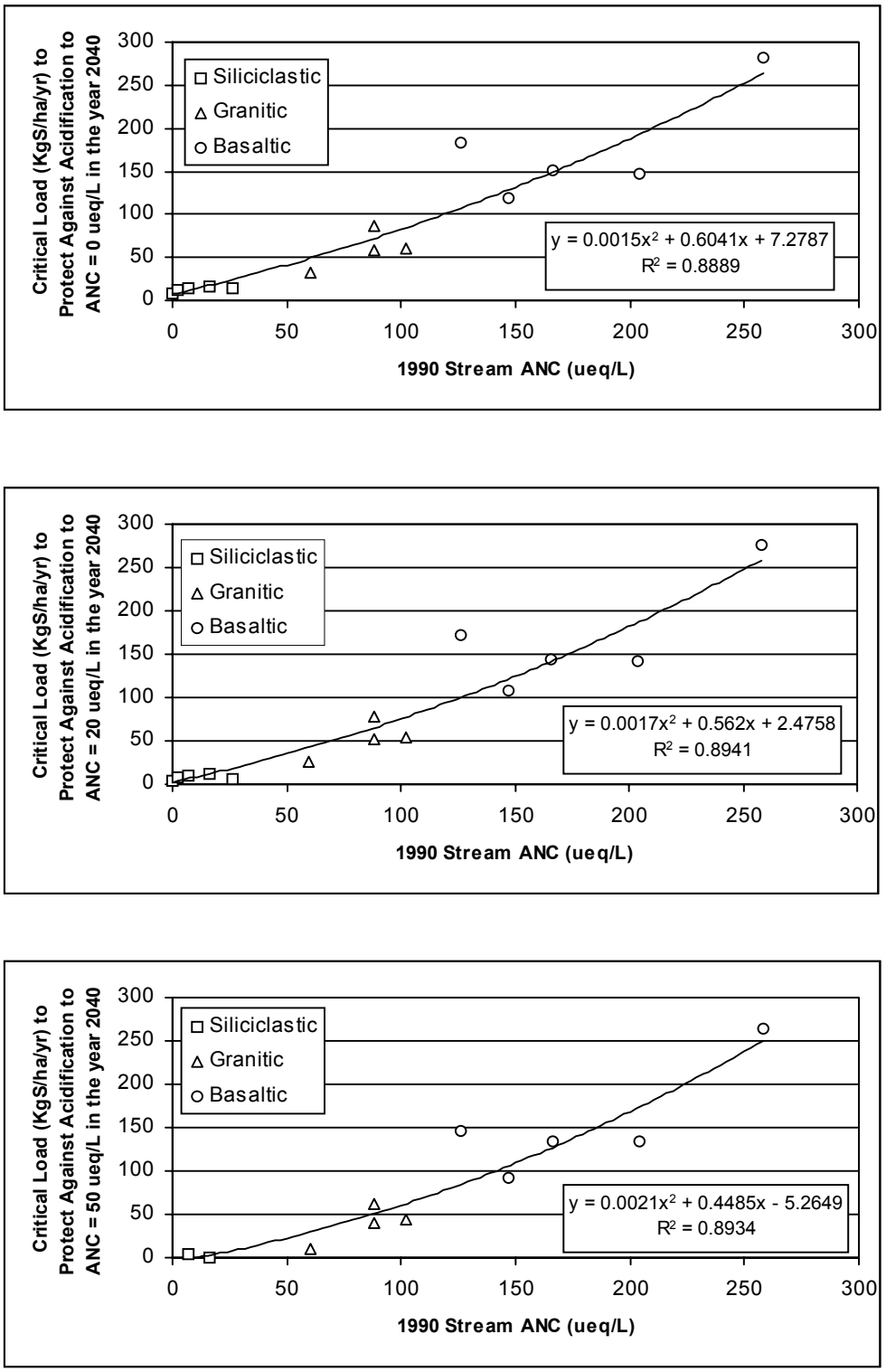

Figure VII-23. Sulfur critical load simulated by the MAGIC model to protect streams in SHEN against acidification to ANC below 0 (top panel), 20 μeq/L (middle panel), and 50 μeq/L (bottom panel) by the year 2040, as a function of 1990 ANC and geologic sensitivity class.

Table VII-16. Regression equations for estimating critical load of sulfur deposition to protect against having ANC below a given threshold in a given endpoint year, based on 14 modeled streams in SHEN.

ANC Threshold	Endpoint Year	Number of Sites (n)[a]	r-squared value	Equation to Estimate Critical Load of Sulfur Deposition (kg S/ha/yr) Given 1990 ANC (μeq/L)
0	2020	14	0.8567	$y = 0.0023x^2 + 1.1588x + 6.2184$
0	2040	14	0.8889	$y = 0.0015x^2 + 0.6041x + 7.2787$
0	2100	14	0.8989	$y = 0.0006x^2 + 0.2698x + 8.6056$
20	2020	14	0.8645	$y = 0.0025x^2 + 1.0949x - 1.9446$
20	2040	14	0.8941	$y = 0.0017x^2 + 0.562x + 2.4758$
20	2100	14	0.9016	$y = 0.0007x^2 + 0.2662x + 5.1181$
50	2020	10	0.9375	$y = 0.0327x^{1.7175}$
50	2040	11	0.8934	$y = 0.0021x^2 + 0.4485x - 5.2649$
50	2100	13	0.9135	$y = 0.0009x^2 + 0.2245x + 0.8005$

[a] For each ANC threshold and endpoint year, MAGIC model results were evaluated for 14 streams. However, output suggested that ANC = 50 μeq/L would not be achieved for some of these streams in some endpoint years even if S deposition was reduced to zero.

We did not attempt to estimate critical loads for N deposition in SHEN. Empirical studies in both Europe and the northeastern United States have suggested that N deposition must be higher than currently occurs at SHEN (7.8 kg N/ha/yr) before forest soils become saturated and begin to chronically leach NO_3^- to surface waters. Dise and Wright (1995) examined watershed and plot-scale input-output budgets for N across Europe and found elevated N leaching at sites that received in excess of about 10 kg/ha/yr of N, about one-fourth higher than the N deposition received at SHEN. Sullivan et al. (1997) found that the observed fall NO_3^- concentration in Adirondack Mountain lakes, New York, could largely be explained by NO_3^- deposition directly to the lake surface without the need for NO_3^- leaching from watershed soils. Those lakes that did show lakewater NO_3^- concentrations higher than would be predicted from direct NO_3^- deposition to the lake surface were generally among the most acid-sensitive of the study lakes (pH 4.7 to 5.3) and received generally high levels of N deposition (~ 10 to 12 kg N/ha/yr, Ollinger et al. 1993). Thus, the finding that watershed soils in SHEN take up essentially 100% of incoming N in the absence of major disturbance seems reasonable under current N deposition. If N deposition increases substantially in the future, then the possibility of N saturation of forest ecosystems in SHEN may become an important concern.

Target Loads

A target load (e.g. Henriksen and Brakke 1988) can be based on political, economic, or temporal considerations, and implies that the environment will be protected to a specified level (i.e. certain degree of allowable damage) and/or over a specified period of time. There has been a rapid acceptance of the concepts of critical and target loads throughout Europe and Canada for use in political negotiations concerning air pollution and development of abatement strategies to mitigate environmental damage (e.g., Posch et al. 1997).

Whereas a critical load is objectively determined, a target load is based on both science and policy. A target load is set on the basis of, in addition to model-based estimates of critical loads, such considerations as:

- desire to protect the ecosystem against chronic critical load exceedance
- temporal components of acidification/recovery processes, so that, for example, resources could be protected only for a specified period of time or allowed to recover within a designated window
- seasonal and episodic variability in water chemistry, and probable associated biological responses
- model, data, and knowledge uncertainty and any desire to err on the side of resource protection.

A target load is subjectively determined, but it is rooted in science and incorporates allowances for uncertainty and ecosystem variability.

Criteria of unacceptable change should be set in relation to known or expected effects on aquatic or terrestrial organisms. For protection of aquatic organisms, the ANC of surface water is most commonly used (Nilsson and Grennfelt 1988, Henriksen and Brakke 1988, Sverdrup et al. 1990). Concentrations below which ANC should not be permitted to fall have been set at 0, 20, and 50 ueq/L for various applications (e.g., Kämäri et al. 1992).

Selection of the best, or most appropriate, target load for protecting and restoring sensitive resources in SHEN is not a scientific issue. Model simulations such as those presented in this report will provide useful information for the decision process, although the final determination must be based on NPS policy judgment.

2. Vegetation

a. Background

The most important known threat from air pollution to vegetation resources in SHEN is the threat of O_3 damage to forest growth and health. Ozone is likely to be a long-term debilitating stress to the park's trees and forests. An O_3 effects modeling analysis was therefore conducted, with the following objectives:

- to use models of tree and forest stand response, individually and linked, to project the current impact of O_3 on the growth of forest trees and stands in SHEN
- to extrapolate the results of the simulations over the spatial extent of the species and stands within the park
- to project the impact of future O_3 scenarios on the growth and development of forest trees and stands in the park.

These simulation results are for O_3 alone, and do not consider interactions of O_3 with insects, diseases, drought, and other potentially exacerbating stresses, or cumulative stresses known to alter responses of trees to ozone.

This simulation analysis was not designed to predict the extent of visible injury to foliage. This type of injury is expected to continue at SHEN unless ambient O_3 levels decrease below current levels. Such visible injury is, however, unlikely to lead to large growth reductions of individual species or stand basal area.

b. Modeling Methods for Ground-level Ozone Effects

Ozone and Meteorology Scenarios for Simulations

Hourly O_3 data from the Big Meadows site were acquired from the Aerometric Information Retrieval System (AIRS) database for 1997-1999 and summarized to determine an average value for SUM06, the 5-month cumulative summation of hourly O_3 concentrations that equaled or exceeded 60 ppb between 8:00 AM and 8:00 PM. Additional hourly exposure regimes were then created for input into TREGRO (Weinstein et al. 1991) to create exposure-response functions relating simulated growth to O_3 exposure and precipitation and to generate growth modifiers for use in ZELIG (Urban 1980, Urban et al. 1991). Two sub-ambient and four above-ambient regimes were generated from hourly O_3 monitoring and are summarized in Tables VII-17 and

VII-18[2]. Table VII-17 provides the three-year exposure metrics, that is, the total exposure provided in the TREGRO simulations. Table VII-18 lists the year-by-year exposure, illustrating the variation between years. The three-year exposure regimes used for TREGRO simulations are illustrated in Figures VII-24 and VII-25. The lowest O_3 exposure (Ozone1) was used as a base for standardization of response.

Although summary metrics are used to characterize exposure regimes, TREGRO uses hourly O_3 concentrations as input data. To create the hourly exposure concentrations for use in TREGRO, a quadratic weighting of hourly O_3 concentrations was used:

$$Oz' = Oz * [1 - (1-f) * Oz / \max(Oz)]$$

where max(Oz) = annual maximum hourly O_3 concentration and f is the scale adjustment of the max(Oz) (Tingey et al. 2001). For example, a 10% reduction of the maximum hourly O_3 concentration corresponds to f=0.9 and a 10% increase of the maximum concentration corresponds to f=1.1.

TREGRO Parameterizations

TREGRO, a physiologically-based model of the growth of individual trees (Weinstein et al. 1991) was used to study the response of large trees to O_3. TREGRO (Version 3.0.0.10)[3] was parameterized for large, mature individuals of 8 species for use in this study: basswood (*Tilia Americana* L.), black cherry (*Prunus serotina* Ehrh.), chestnut oak (*Quercus prinus* L.), red maple (*Acer rubrum* L.), red oak (*Quercus rubra* L.), sugar maple (*Acer saccharaum* L.), white ash (*Fraxinus americana* L.), and yellow poplar (*Liriodendron tulipifera* L.). Parameterizations for black cherry, red maple, red oak, sugar maple, and yellow poplar were available from the Plant Modeling Group at Boyce Thompson Institute, Ithaca, NY. These parameter sets were adjusted slightly so that the simulated growth under Big Meadows meteorological conditions

---

[2] There are many metrics to summarize O_3 exposures, with no clear favorite among the research and regulatory communities of North America and Europe. We chose a 5-month (May-September) 12-hour (8:00 AM - 8:00 PM) SUM06, which is a summation of all hours $\geq$0.06 ppm O_3 during those times. In Tables VII-1 and VII-2, other common metrics are presented as well so that exposures used in these studies may be related to other common measures, as desired, by users of this report.

[3] TREGRO is available from David A. Weinstein (daw5@cornell.edu), Boyce Thompson Institute, Cornell University, Ithaca, NY 14853

Table VII-17. Total three-year daylight (0800-2000) ozone exposure metrics[a] (ppm·hr) calculated from hourly concentrations used for TREGRO simulations.

	SUM 0			SUM 06[b]			W126			AOT 04		
Simulated Ozone Exposure	12 month	5 month	3 month	12 month	5 month	3 month	12 month	5 month	3 month	12 month	5 month	3 month
1	549	265	164	14	36	9	68	41	28	78	52	34
2	567	283	175	90	78	54	86	66	44	92	69	45
3[c]	630	322	199	220	182	123	170	132	87	145	106	69
4	660	340	211	266	214	144	213	164	108	171	123	78
5	719	375	234	369	282	185	302	227	149	225	158	102
6	778	410	255	465	343	221	393	288	188	2798	192	124
7	1,149	630	394	980	611	386	912	590	375	637	411	262

[a] SUM 0 is the sum of all O_3 concentrations; SUM 06 is the sum of all concentrations ≥0.06 ppm; W126 is a sigmoidally weighted summation of all concentrations, and AOT 04 is the sum of all hours after subtracting a threshold of up to 0.04 ppm. All summations are for the 1997-1999 period, from 0800 to 2000 EST, for the entire year (12 month), May-September (5 month), or June-August (3 month). These are summary statistics only—TREGRO uses the actual hourly data (SUM0).

[b] 25 ppm·hr, 3-month, 12-hour SUM06 is the metric recommended by EPA staff as the secondary standard to protect sensitive vegetation in Class I areas

[c] Simulated O_3 exposure #3 represents ambient 1997-1999 exposure at Big Meadows.

Table VII-18. Ozone exposure metrics[a], by year, calculated from hourly concentrations used for TREGRO simulations.

Simulated Ozone Exposure	SUM 0			SUM 06			W126			AOT 4		
	1997	1998	1999	1997	1998	1999	1997	1998	1999	1997	1998	1999
1	177	176	196	14	9	36	19	17	33	22	22	34
2	186	184	196	30	24	36	28	25	33	30	28	34
3[b]	195	217	218	46	96	78	38	70	61	37	56	53
4	204	227	229	63	111	92	50	86	77	44	65	62
5	223	246	250	93	142	134	76	116	110	61	82	82
6	242	266	271	128	168	169	104	146	143	77	100	102
7	358	386	405	303	321	356	305	334	273	188	216	232

[a] SUM 0 is the sum of all O_3 concentrations; SUM 06 is the sum of all concentrations ≥ 0.06 ppm; W126 is a sigmoidally weighted summation of all concentrations, and AOT 04 is the sum of all hours after subtracting a threshold of up to 0.04 ppm. All summations are for the 1997-1999 period, from 0800 to 2000 EST, for the June-August (3 month) period. These are summary statistics only; TREGRO uses the actual hourly data (SUM0).

[b] Simulated O_3 exposure #3 represents ambient 1997-1999 exposure at Big Meadows.

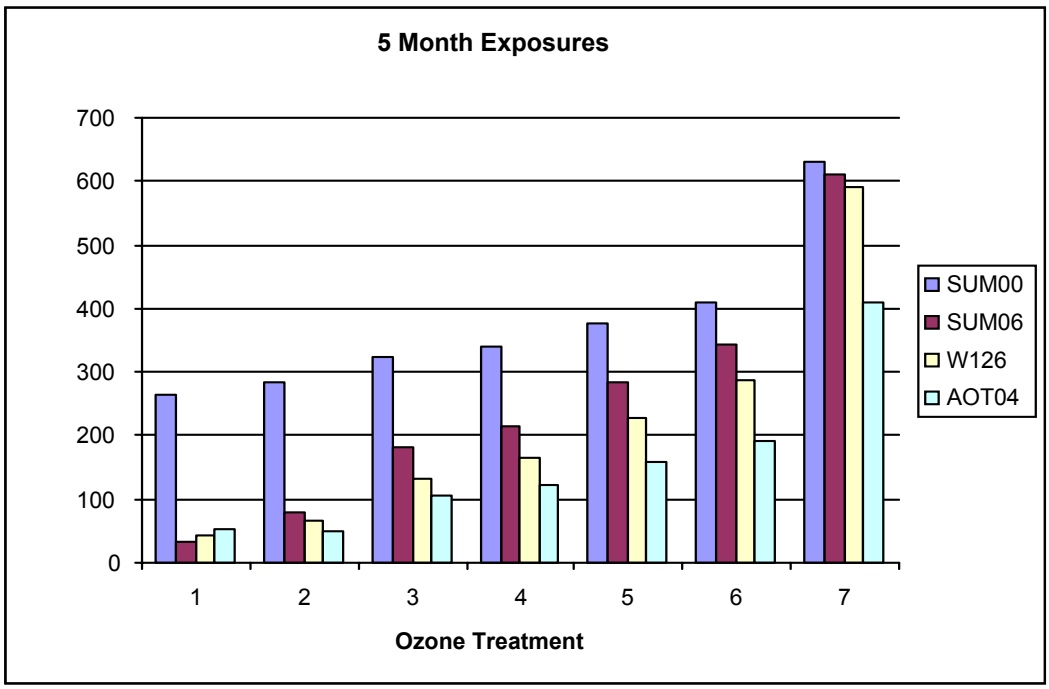

Figure VII-24. Ozone exposures (total for 1997-1999) used in TREGRO simulations. Treatment 3 is the 1997-1999 monitored ambient exposure at Big Meadows.

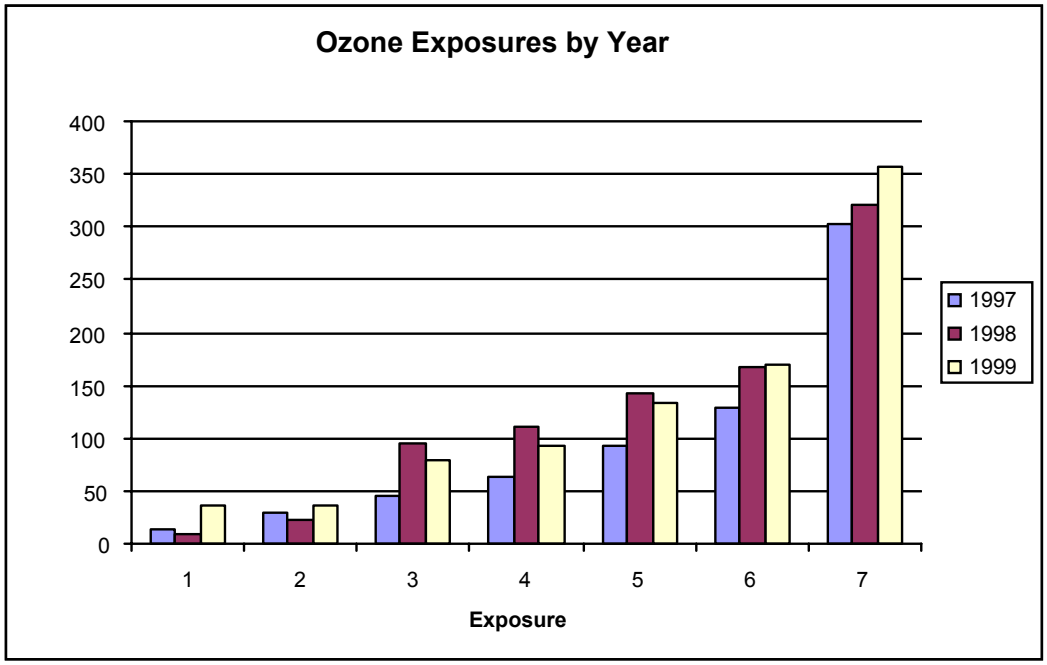

Figure VII-25. Ozone exposures (5 month SUM06) for each of the three simulation years. Treatment 3 is the 1997-1999 monitored ambient exposure at Big Meadows.

matched that of the original target tree (within at least ±10%). Basswood, chestnut oak, and white ash were parameterized for TREGRO for the first time in this study. Details of the parameterizations and growth rate targets are given in Appendix G.

Of the eight species used in this study, a large-tree O_3 response function has been reported in the literature for black cherry (Weinstein et al. 2001), red maple (Weinstein et al. 2001), red oak (Weinstein et al. 1998), sugar maple (Retzlaff et al. 1996), and yellow poplar (Weinstein et al. 2001). The O_3 response of basswood, chestnut oak, and white ash were set to those of red maple, red oak, and red maple, respectively, based upon their physiological and ecological similarities.

TREGRO Simulations

A three-year TREGRO simulation for each species was conducted using meteorological data for Big Meadows and the seven O_3 scenarios illustrated in Figure VII-24. At the end of the simulations, the results were standardized by expressing the final biomass as:

$$Y = \frac{[\text{Final Biomass(O Ozone)} - \text{Final Biomass(Ozone1)}]}{\text{Final Biomass(Ozone1)}}$$

where O Ozone is any given treatment level and Ozone1 is the first treatment level, the lowest simulated O_3 exposure.

Spline regression was used to fit a linear-linear model to % relative tissue mass (y) as a function of O_3 exposure index (x), as follows:

$$Y = a+bx \ (x \leq x_0)$$
$$= c+dx \ (x > x_0)$$

where x_0 is the join point. The parameter a represents the relative mass at zero exposure and was set to equal 0. Note that $x_0=c/(b-d)$.

All calculations were performed using SAS PROC NLIN (SAS Institute, Cary, NC) using several different initial parameter values. In most cases, the parameter values were not uniquely defined and the minimum RMSE criterion was used to select among several candidate models.

Linkage of TREGRO and ZELIG

In order to provide a physiological basis for the projection of O_3 effects at the stand level, TREGRO and ZELIG were linked through three output variables from the individual tree

simulations (Laurence et al. 2001, Weinstein et al. 2001). At the end of each growing season in each of the three-year TREGRO simulations, the value for total tree mass, leaf mass, and fine root mass to leaf mass ratio were output. The average of the three-year response was calculated and standardized for each treatment by dividing each O_3 treatment by the value for the Ozone 1 treatment. These values (modifiers) were used to scale particular processes in ZELIG, thus incorporating a physiological basis for reduced growth of trees in a stand. Modifiers calculated in this study are shown in Table VII-19. The modifiers were then input to ZELIG to alter (by multiplication) the growth rate, leaf area (and therefore shading), and nutrient and drought sensitivity of each of the species as they occurred in the three forest types. Thus, ZELIG results were all expressed relative to the lowest O_3 exposure (about 87% of monitored ambient Sum 0 and 18% of the ambient 5 month SUM06; Tables VII-17 and VII-18).

ZELIG Parameterizations

ZELIG, a model of forest stand dynamics and succession (Urban 1980, Urban et al. 1991), was used to estimate the effect of O_3 on productivity and composition of major forests in the park. The three forest types that comprise the majority of the forest at SHEN were simulated: Chestnut Oak, Cove Hardwood, and Yellow Poplar. The principal species included in each forest type are shown in Table VII-20.

Long-term weather data for Big Meadows were obtained from the EarthInfo database (EarthInfo 1992) and were used to calculate monthly 30-year means and standard deviations for temperature and precipitation.

ZELIG simulates the establishment of seedlings on the plot as a function of the average annual environmental conditions and the ability of selected species to withstand these conditions. The model produces a projection of the average basal area (m^2/ha) for each tree species for each year of simulation, calculated from a landscape containing 100 forest plots, each 600 m^2 in area.

A species parameter set for use with ZELIG was constructed for each of the three forest types. To assure that ZELIG reproduced the diameter growth rates of trees observed from this region, growth rates of trees reported in the Forest Inventory Analysis (FIA; Hansen et al. 1992) were calculated. Growth records from trees for each of the simulated species in or near SHEN were divided into 5 cm diameter size classes. The mean growth rate of all trees of a given species in a given size class was calculated. A polynomial regression was fitted through points representing the mean plus one standard deviation in each size class in order to estimate the

Table VII-19. Modifiers of ZELIG processes calculated from TREGRO simulations. Reductions in growth, leaf area, and root production are achieved by multiplying the calculated modifier and the appropriate variable in ZELIG for the appropriate ozone exposure treatment.

Species	Ozone Exposure[a]	Total Growth	Shoot	Root:Shoot[b]
Basswood	1	1.00000	1.00000	1.00000
	2	0.99893	1.00000	0.99404
	3	0.99632	1.00000	0.97912
	4	0.99525	1.00000	0.97144
	5	0.99306	1.00000	0.95552
	6	0.99088	1.00000	0.93989
	7	0.97140	0.99796	0.82469
Black Cherry	1	1.00000	1.00000	1.00000
	2	0.99995	1.00000	1.00000
	3	0.99980	1.00000	1.00000
	4	0.99974	1.00000	1.00000
	5	0.99966	1.00000	1.00000
	6	0.99955	1.00000	1.00000
	7	0.99064	0.99902	1.04930
Chestnut Oak	1	1.00000	1.00000	1.00000
	2	0.99893	1.00000	0.99404
	3	0.99632	1.00000	0.97912
	4	0.99525	1.00000	0.97144
	5	0.99306	1.00000	0.95552
	6	0.99088	1.00000	0.93989
	7	0.97140	0.99796	0.82469
Red Maple	1	1.00000	1.00000	1.00000
	2	0.99987	1.00000	1.00000
	3	0.99954	1.00000	1.00000
	4	0.99929	1.00000	1.00000
	5	0.99867	1.00000	1.00000
	6	0.99745	1.00000	1.00000
	7	0.97554	1.00082	0.91828
Red Oak	1	1.00000	1.00000	1.00000
	2	1.00000	1.00000	0.99998
	3	1.00001	1.00000	0.99997
	4	0.99996	1.00000	0.99912
	5	0.99986	1.00000	0.99740
	6	0.99976	1.00000	0.99568
	7	0.98766	0.99957	0.87844
Sugar Maple	1	1.00000	1.00000	1.00000
	2	0.99996	1.00000	1.00000
	3	0.99992	0.99998	1.00002
	4	0.99988	0.99998	1.00002
	5	0.99980	0.99997	1.00003
	6	0.99972	0.99996	1.00003
	7	0.99289	0.99812	1.09320

Table VII-19. Continued.

Species	Ozone Exposure[a]	Total Growth	Shoot	Root:Shoot[b]
White Ash	1	1.00000	1.00000	1.00000
	2	0.99809	1.00000	0.98249
	3	0.99385	1.00000	0.94723
	4	0.99201	1.00000	0.93099
	5	0.98832	1.00000	0.89927
	6	0.98455	1.00000	0.86869
	7	0.95750	1.00254	0.73567
Yellow Poplar	1	1.00000	1.00000	1.00000
	2	0.99986	1.00000	1.00000
	3	0.99965	1.00000	1.00000
	4	0.99950	1.00000	1.00000
	5	0.99913	1.00000	1.00000
	6	0.99840	1.00000	1.00000
	7	0.98031	1.00000	0.84447

[a] Ozone exposures based on 7 scenarios of future ozone concentrations
[b] Values of the root:shoot ratio less than 1.0 suggest an effect of ozone on plant growth

Table VII-20. Species included in three forest types simulated with ZELIG.

Chestnut Oak	*Acer rubrum*, *Carya glabra*, *Fraxinus americana, Quercus alba, Quercus coccinea, Quercus prinus*, *Quercus rubra*, *Pinus strobus*
Cove Hardwood	*Acer rubrum*, *Acer saccharum*, *Betula lenta*, *Fraxinus americana, Liriodendron tulipifera, Prunus serotina, Quercus prinus, Quercus rubra, Robinia pseudoacacia, Tilia americana, Tsuga canadensis*
Yellow Poplar	*Acer rubrum*, *Betula lenta*, *Liriodendron tulipifera, Quercus prinus, Quercus rubra, Robinia pseudoacacia, Tilia americana, Carya glabra, Cornus florida*

average growth rate of trees less likely to be suppressed by shade (in order to more accurately estimate an unstressed growth rate). For most species, the polynomial regression closely fit the points. The growth rates estimated in this fashion represent the actual growth reported from the early 1980s until the early 1990s under existing climatic conditions. Thus, if O_3, or other stresses, were suppressing growth during that time, the effect of the stress is included in the baseline growth for each species.

The parameters for the growth equation used in ZELIG were then estimated using the polynomial regression equation described above. The fitting process continued until the

projected mean growth rates deviated from estimates based on field data by less than 5% in any size class less than 50 cm in diameter. For most species, this process also produced reasonable projections of growth for larger trees as well. For a few species, the estimates of growth derived from the field data suggested that larger trees exhibited greater growth rates. Since this is not likely to be correct, the ZELIG growth equation parameters were set to produce a close calibration to the smaller trees. For these species, the growth equation projected diameter increment to follow a parabola, with highest growth in mid-sized classes, as the other species were found to follow.

To provide meteorologic parameter values for ZELIG, a profile of mean monthly temperature and precipitation was constructed from weather data from Big Meadows at 1,081 m elevation. This meteorology was used to simulate the Chestnut Oak forest type. Using an adiabatic lapse rate of 3°C per 1,000 m elevation, a data file was created for estimating equivalent mean monthly temperatures at 600 m — the elevation used for simulations of the Cove Hardwood and Yellow poplar forests. ZELIG simulates the year-to-year variation in annual weather by using the standard deviations in mean monthly temperature and precipitation calculated from observed long term weather records. These deviations were assumed to be the same at 600 m and 1,100 m.

ZELIG Simulations

The average age following farm abandonment for each forest type was calculated from analysis of the FIA plots from this region. ZELIG was then run for this number of years for each forest type, starting from a bare plot. The projected composition after this simulation period was compared to that observed from field plots in SHEN to assure that the model projected forest composition with reasonable accuracy. For a few species, adjustments were made in their rate of seedling production until their final species composition reproduced the field data as closely as possible. This forest then was used as the initial forest for all simulations involving O_3 exposure.

All further simulations were conducted for an additional 100 years, with the same O_3 modifiers applied for each year of the simulation. Thus, in the best case, the forest received no O_3-induced modification of growth, and in the worst case, the modifiers for the highest exposure were applied every year during the simulation.

Output from the simulations, including basal area of the stand, woody biomass of the stand, and the basal areas of the individual species were plotted for the time course of the simulation.

Spatial Interpolation

A Geographic Information System (GIS) was built in ArcInfo® (version 8.02, Environmental Systems Research Institute Inc., Redlands, CA 92373) in order to visualize the spatial distribution of tree species, forest types, and O_3 exposures within the park. Details of the regional O_3 interpolation are presented in Appendix H.

The forest cover spatial database that depicts the major forest types was obtained from the NPS web page (http://www.nps. gov/gis/park_gisdata/virginia/shen.htm). The forest types are designated based on the dominant tree species in an association of forest species. These polygon data are in the UTM zone 17 projection and have an estimated accuracy of 70%. The coverage metadata indicated the distribution data should not be used at a scale less than 1:12,000. The coverage contains eight forest types plus open areas and rock outcrops: Bear Oak, Black Locust, Chestnut Oak, Cove Hardwood, Hemlock, Pine, Red Oak, and Yellow Poplar. The three most prevalent types in the park were Chestnut Oak, Cove Hardwood, and Yellow Poplar, accounting for 49, 15, and 16% of the total area, respectively. This coverage was used to create the distribution of chestnut oak, red oak, and yellow poplar forests within the park. Since detailed species information was not available in all cases, a map of deciduous versus coniferous trees was made using these data to create TREGRO maps of black cherry, basswood, red maple, sugar maple, and white ash. Maps of ZELIG results were created using Cove Hardwood, Chestnut Oak, and Yellow Poplar coverages from the NPS forest type map.

The interpolated tropospheric O_3 exposures were converted from a tabular database to a GIS database. Then the data were converted to the UTM zone 17 projection using the NAD27 datum and re-sampled to 500-m resolution using ArcInfo® software.

Spatial coverages of tropospheric O_3 impacts on tree growth based on TREGRO model runs were created using the ArcInfo/GRID® software using regression equations reported in Appendix I. The growth change projected by ZELIG was estimated by developing linear regression equations between each reported point within the O_3 range reported at SHEN (150 to 182 ppm·hr). Linear regressions were used to construct lookup tables of values corresponding to the range of O_3 exposures that were applied to the spatial database of O_3 exposures.

c. Vegetation Modeling Results

Because of the design of the simulation study, it is possible to examine the projected response of both individual trees and forest stands. The results from TREGRO simulations provide an estimate of the relative sensitivity of the individual species and likely impact of O_3 on the growth of individuals. ZELIG simulations translate those individual effects into a projection of how entire stands will perform in response to varying levels of O_3 exposure. By studying the results from both sets of simulations, an evaluation of differences in individual and stand performance is possible.

TREGRO Simulations

The results of TREGRO simulations of O_3 effects on components of tree mass are illustrated in Figure VII-26 and discussed below. In addition, regression coefficients for equations describing the simulated effect of O_3 on the total mass of the tree and the masses of shoot, stem, and root are presented in Appendix I.

In general, the greatest simulated effects of O_3 were on the mass of root systems, as has been reported previously (U.S. EPA 1996). At the highest three-year O_3 exposure, the magnitude of the effect ranged from about a 2% increase in the mass of sugar maple roots to an 18% decrease in roots of white ash. Under ambient O_3 exposure, simulated current root mass reductions, compared with the lowest simulated O_3 exposure, were less than 2% for all species except white ash (4% reduction). Decreases in the simulated total mass of the trees ranged from about 0.5% in sugar maple to about 7% in white ash over the three-year simulation (Figure VII-26). Simulated current total mass reductions in response to ambient O_3 exposure compared to the lowest simulated O_3 exposure, were less than 1% for all species except white ash, which was < 2%. The species, in order of most sensitive to least sensitive were:

White ash>basswood=chestnut oak>red maple>yellow poplar>black cherry=red oak>sugar maple

In the regression analysis, the r^2 values were generally greater than 0.98, indicating that the models were adequate in describing the relationships. The r^2 values are simply measures of fit and should not be interpreted as the proportion of total variation explained by the model, since TREGRO has no stochastic component. The equations were incorporated into the GIS to project the likely effect of O_3 on growth of individual trees where the species occur.

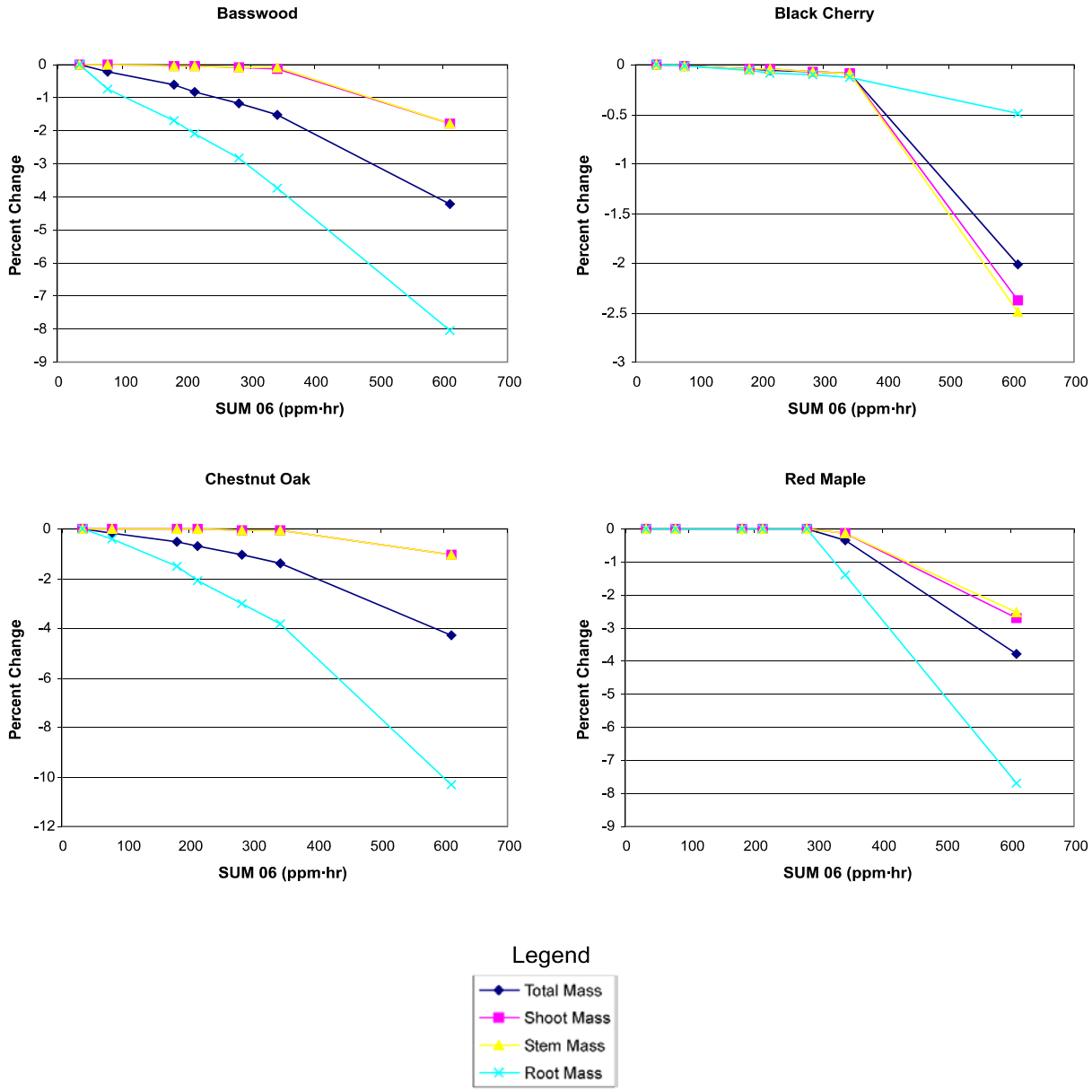

Figure VII-26. Percent change, compared to the lowest ozone exposure, in the mass of the total tree, shoot, stem, and root of basswood, black cherry, chestnut oak, red maple, red oak, sugar maple, white ash, and yellow poplar simulated by TREGRO. The ambient 5-month exposure (total for 1997-1999) was 192 ppm - hr over the three year period of the simulations.

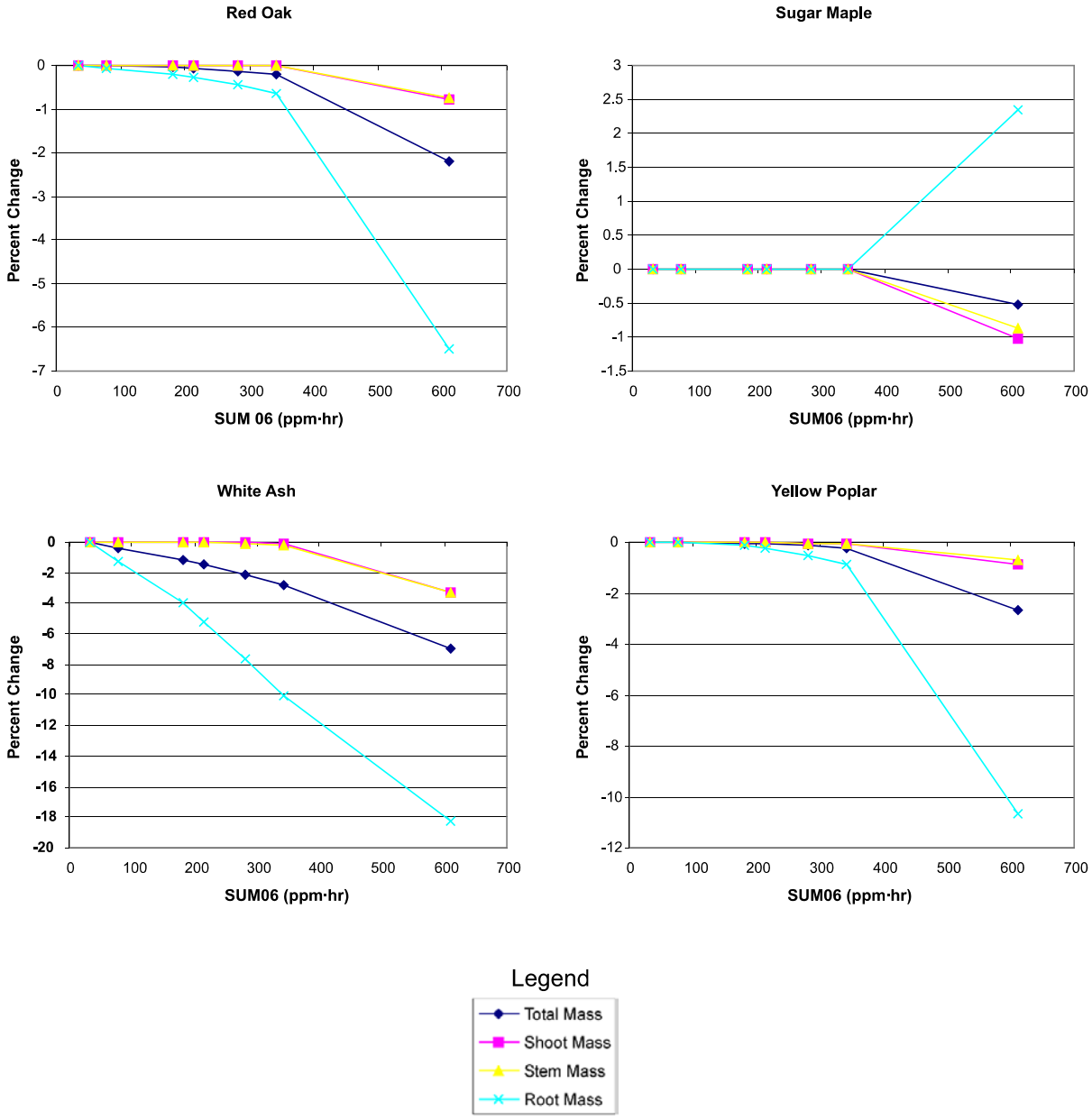

Figure VII-26. Continued.

ZELIG Simulations

The simulated responses of the three forest types to long-term O_3 exposures are illustrated in Figures VII-27 through VII-29. Because of the number of species used in the simulations, and the influence of competition, the results were highly variable, thus preventing the development of regression equations to describe an O_3 exposure-response function. In most cases, the projected effect of O_3 at a wide range of exposure levels on total stand growth and development was less than a 10% reduction in growth. However, some changes were noted in stand composition resulting from the sensitivity of individual species. These results are not surprising given that TREGRO simulated limited impacts of O_3 on growth and ZELIG allows for the possibility that stands will compensate for the loss of sensitive individuals.

The Chestnut Oak forest (Figure VII-27) showed little overall effect of O_3 exposure in terms of total basal area (<1%), woody biomass (<1%), or basal areas of most of the individual species (<10%). White ash, however, was reduced by up to 75% in the final forest due to O_3 exposure. Even at current ambient levels, the simulations indicated that white ash is reduced in growth over what might be expected at low O_3. White ash comprises about 6% of the Chestnut Oak forest in SHEN. Although the simulated impact on white ash growth does not substantially affect the overall growth and development of the chestnut oak forest, protecting sensitive species such as white ash is an important NPS concern.

Simulations of O_3 impact on the Cove Hardwood forest (Figure VII-28) projected a reduction in both total basal area and woody biomass of about 10% at the highest O_3 exposure. These simulated reductions were due primarily to changes in the basal area of yellow poplar and white ash. Yellow poplar and white ash comprise about 22 and 24% of the basal area of Cove Hardwood forests in SHEN, respectively. There was little simulated impact of O_3 at exposures less than the most severe, and stand basal area was not projected to decrease in response to continued ambient O_3 exposure.

There were few, if any differences in the productivity and composition of the Yellow Poplar forest type (Figure VII-29) associated with O_3 exposure. White ash comprises only about 2% of the basal area of Yellow Poplar forests in SHEN.

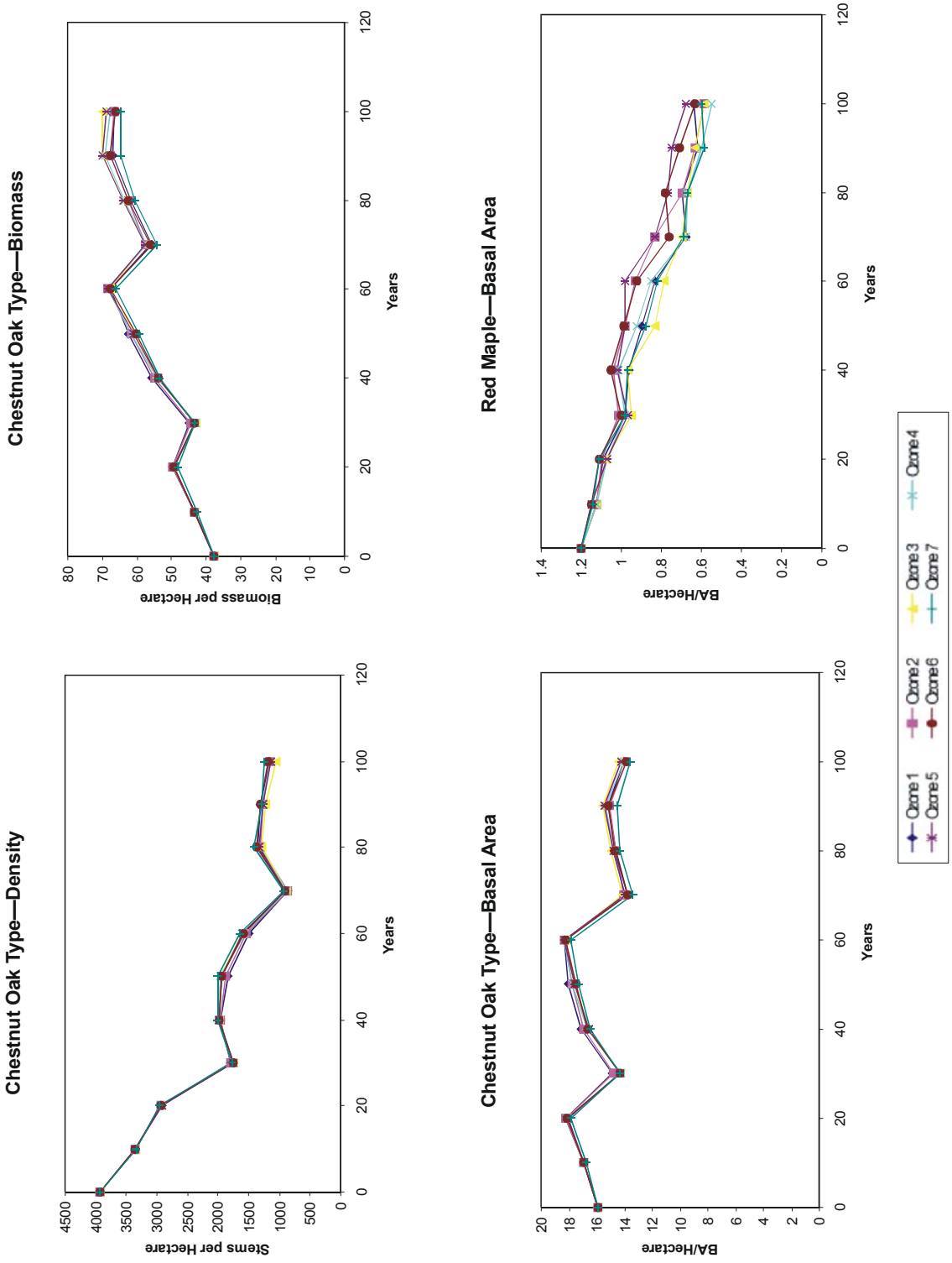

Figure VII-27. Simulated effects of ozone on the density of trees, total woody biomass, and basal area of the stand, and the growth of major species in the Chestnut Oak forest type as affected by ozone. Simulated ozone exposure levels 1-7 correspond to exposures listed in Table VII-17.

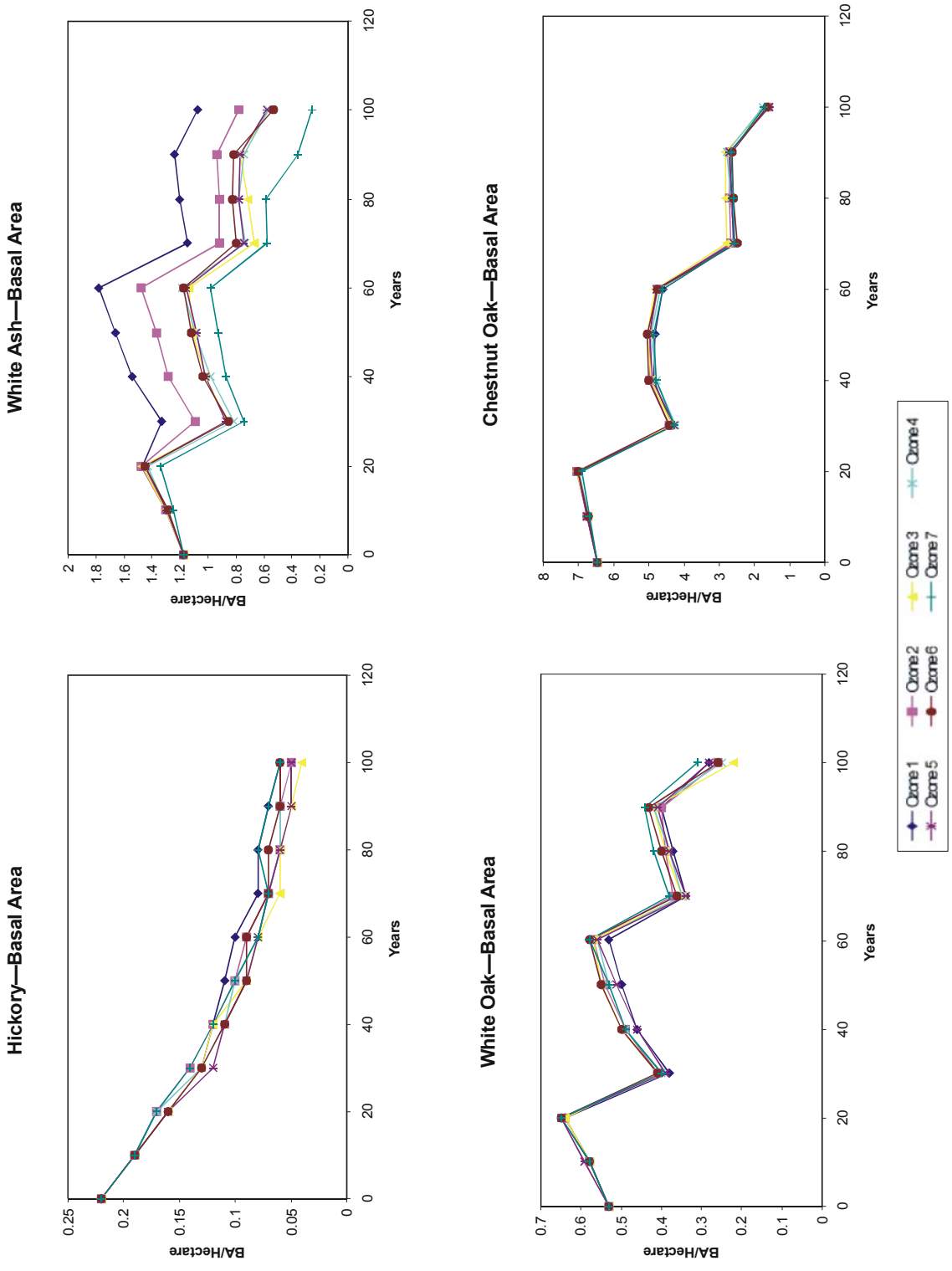

Figure VII-27. Continued.

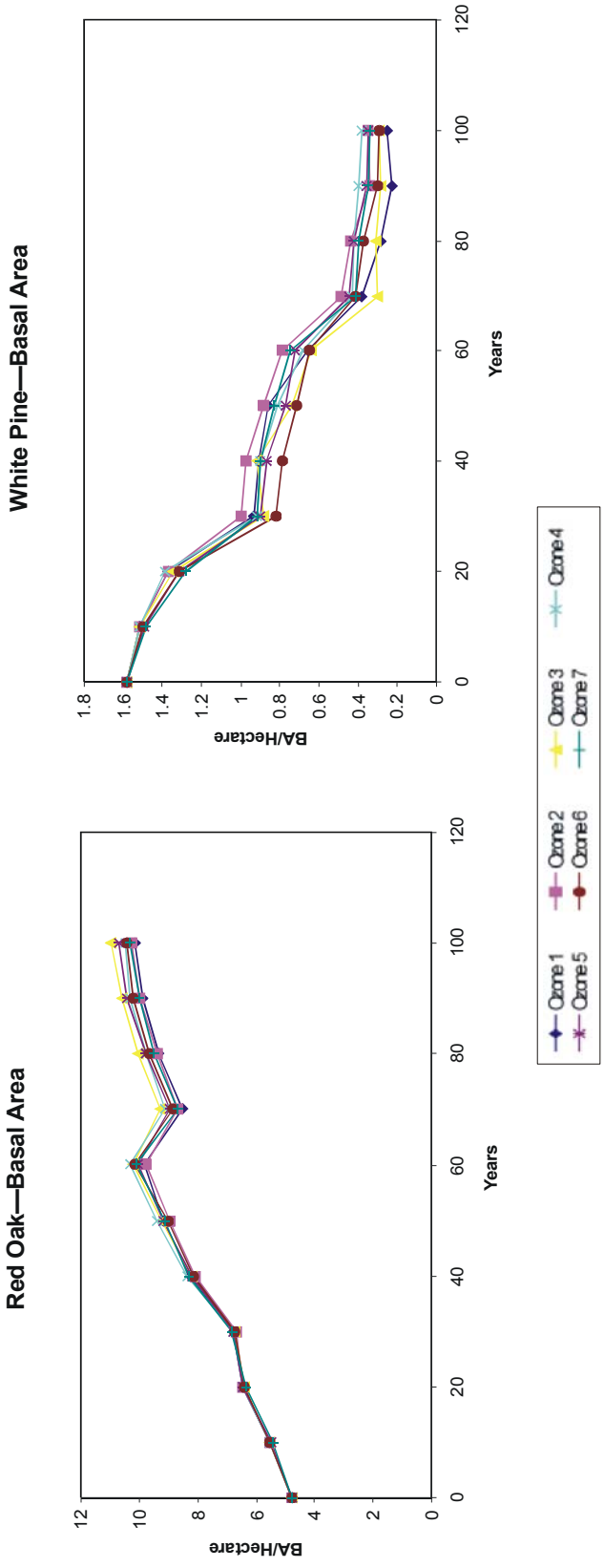

Figure VII-27. Continued.

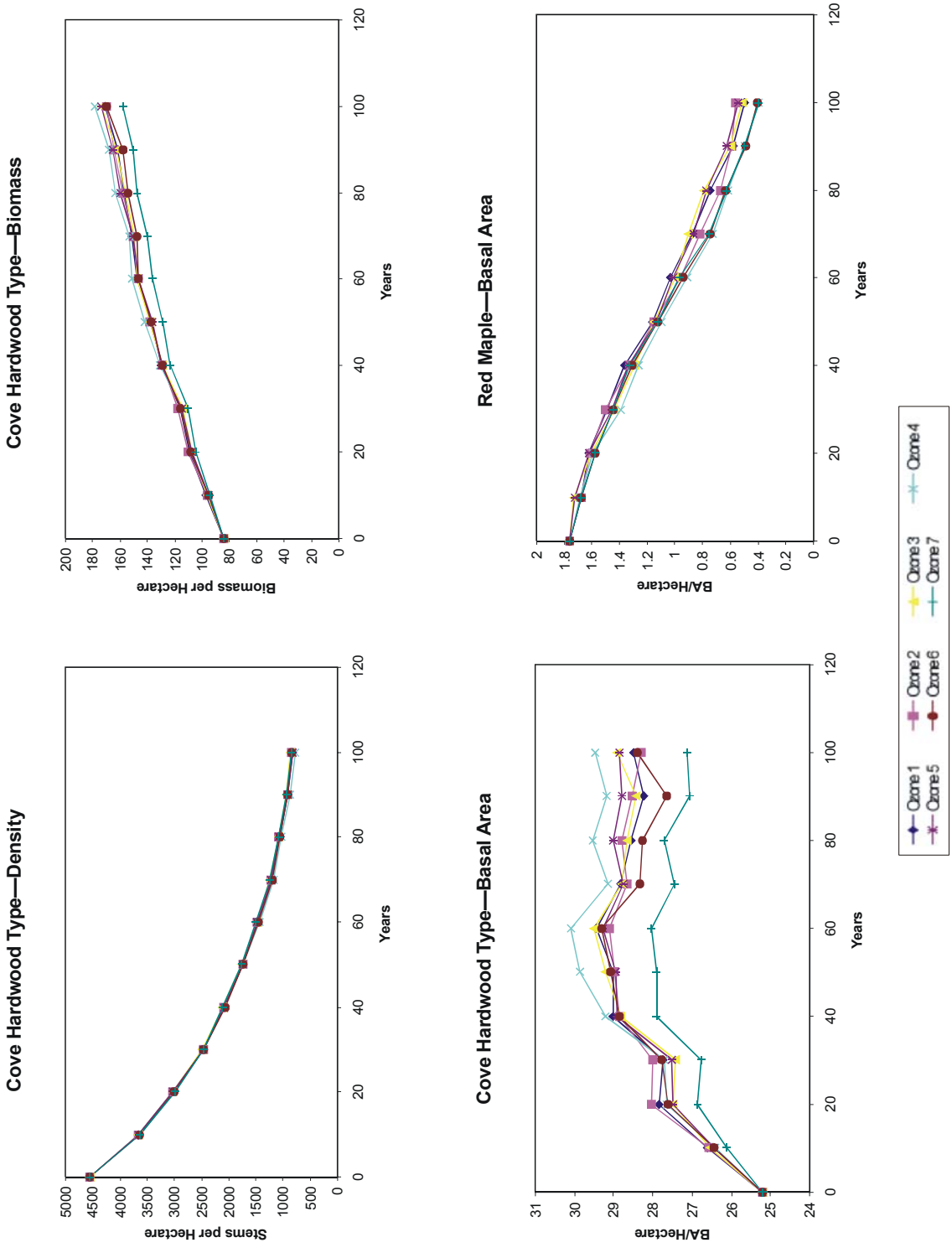

Figure VII-28. Simulated effects of ozone on the density of trees, total woody biomass, and basal area of the stand, and the growth of major species in the Cove Hardwood forest type as affected by ozone. Simulated ozone exposure levels 1-7 correspond to exposures listed in Table VII-17.

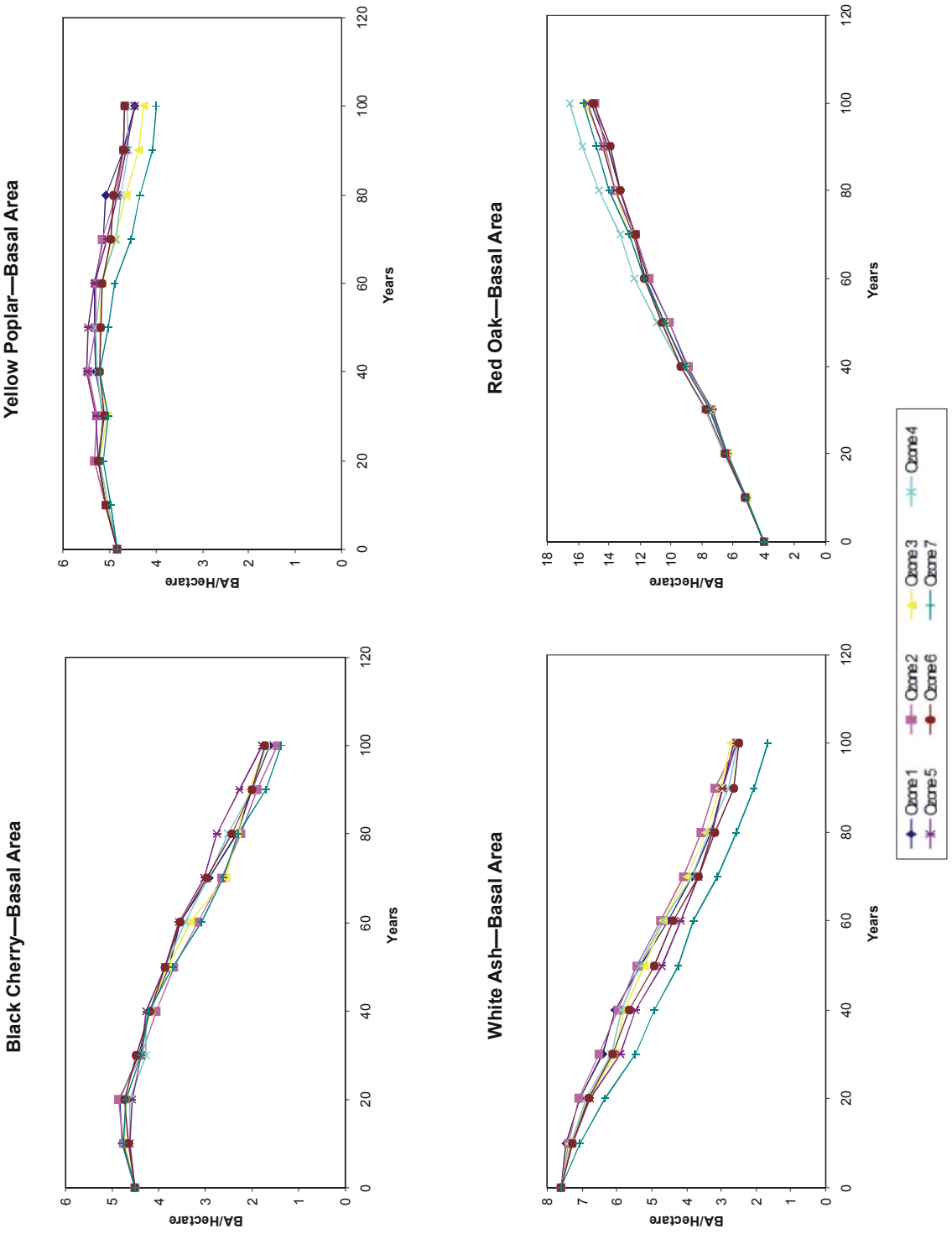

Figure VII-28. Continued.

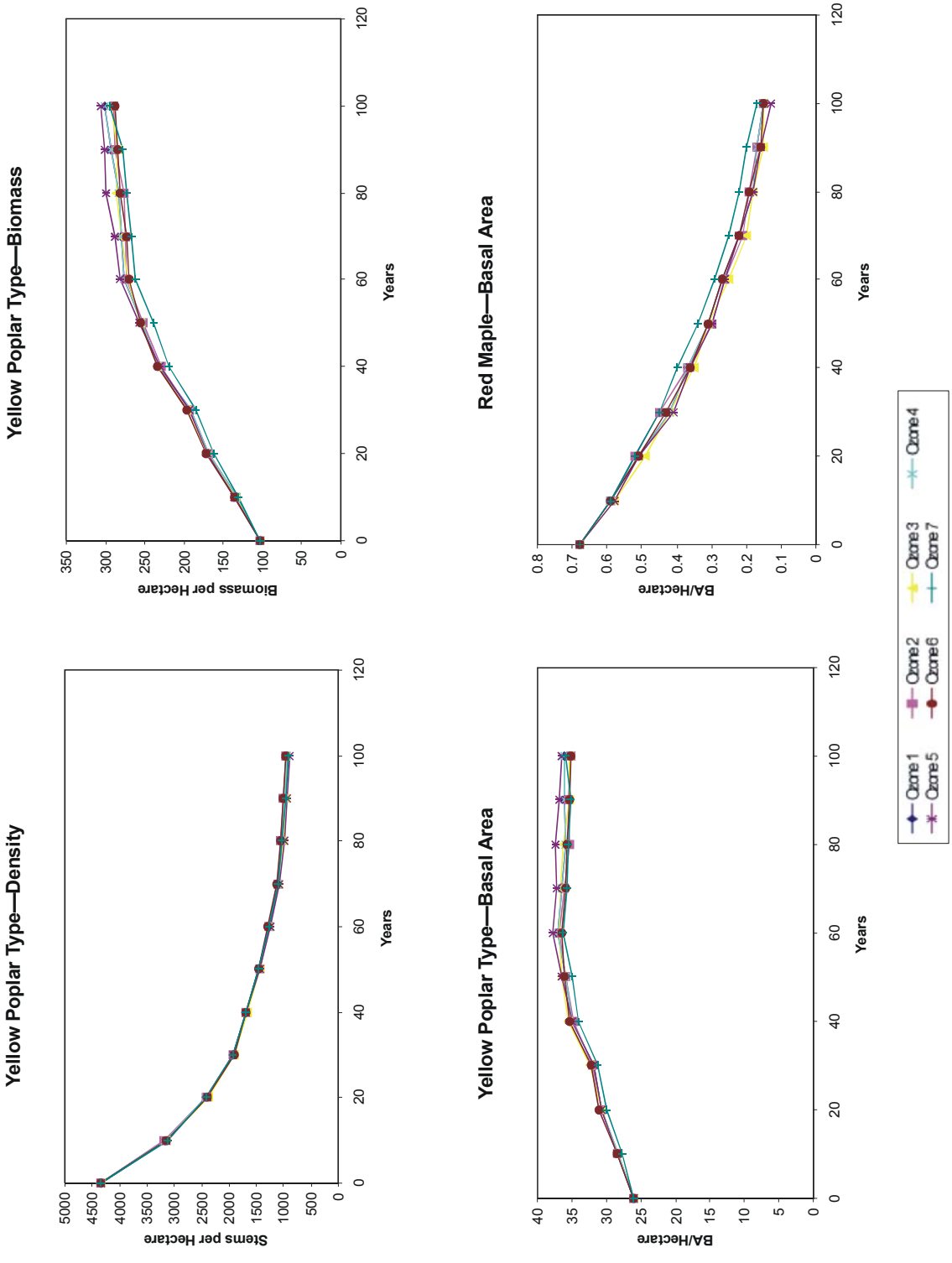

Figure VII-29. Simulated effects of ozone on the density of trees, total woody biomass, and basal area of the stand, and the growth of major species in the Yellow Poplar forest type as affected by ozone. Simulated ozone exposure levels 1-7 correspond to exposures listed in Table VII-17.

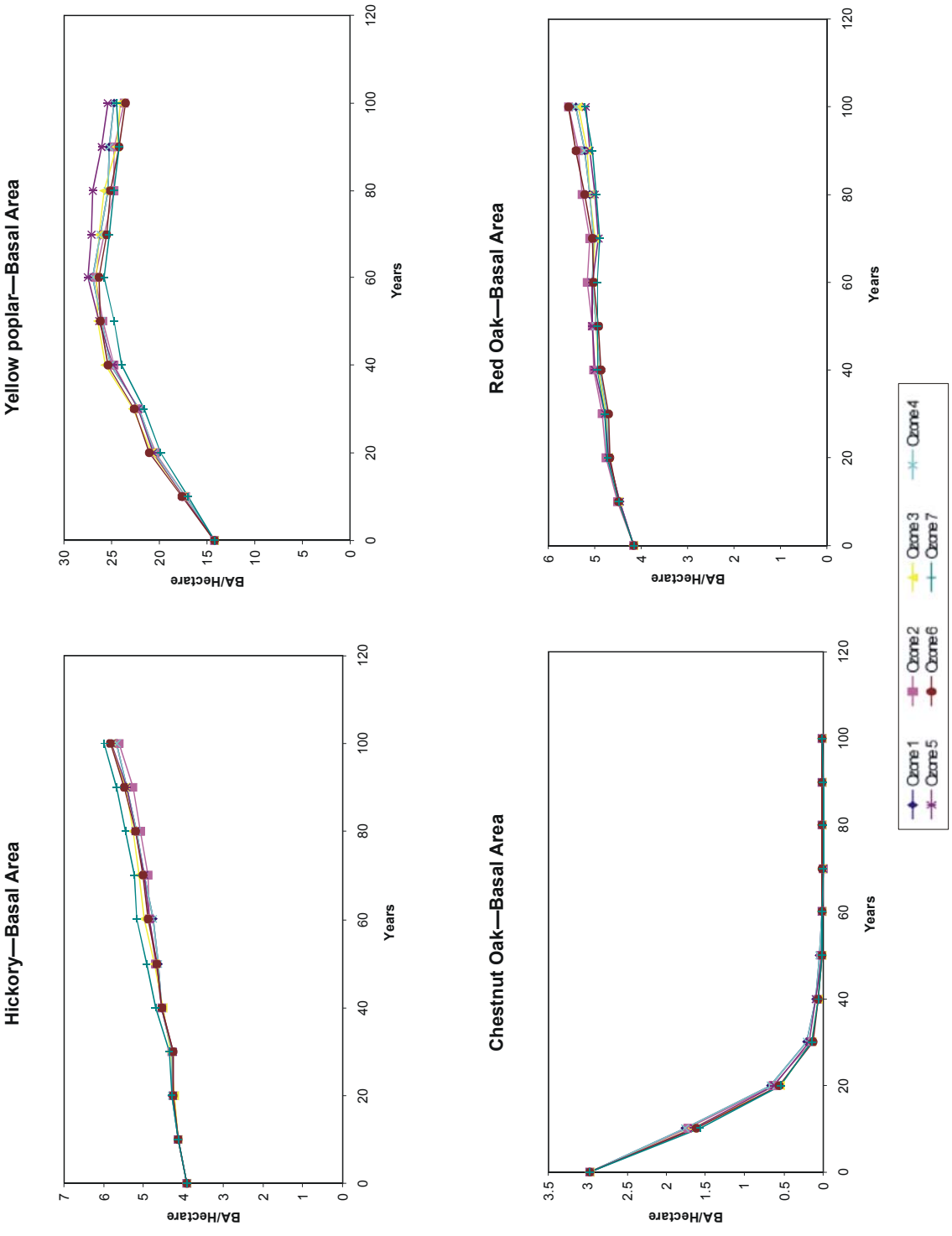

Figure VII-29. Continued.

Comparison of Individual Species versus Response in a Stand

Figure VII-30 illustrates the simulated response of species as individuals (TREGRO) compared to how the same species responded when growing in a stand (ZELIG). It is important to remember that although the responses were standardized, the TREGRO simulations lasted for 3 years whereas ZELIG simulations were for 100 years. Four general types of simulated response were identified. First, there may be a consistent response by the species, regardless of whether simulated as an individual or in a stand. This kind of response was simulated for white ash, which showed a reduction in growth due to O_3 both as an individual and in a stand. The stand response was much greater, illustrating the effect of long-term exposure.

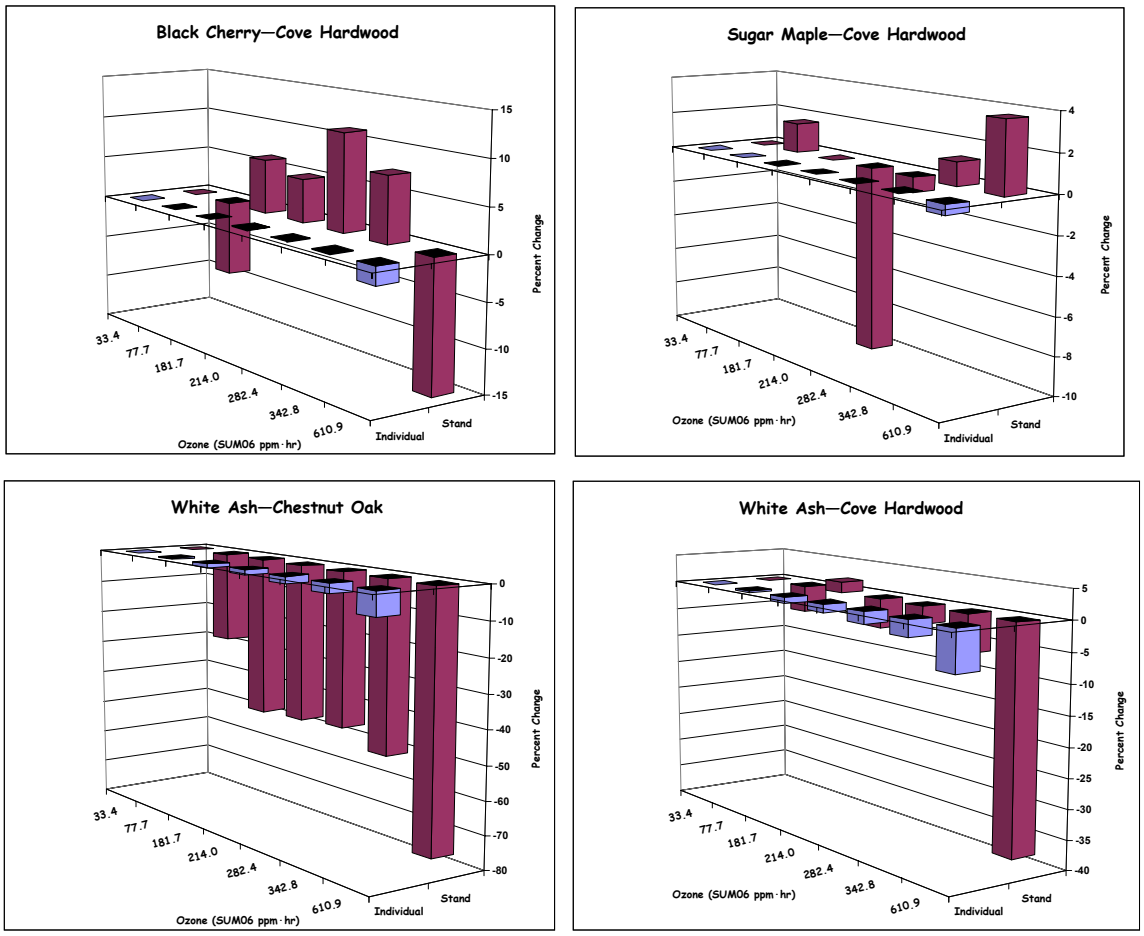

Figure VII-30. Comparison of the effects of ozone on the basal area of species simulated as individuals over three years (blue bars) versus as a member of a stand over 100 years (red bars).

Second, there may be a consistent decrease in growth as an individual, but a variable response in the stand. Such a response was illustrated by chestnut oak, red maple, and yellow poplar; the response in the stand depended upon the relative sensitivities of the other components of the forest and the level of the stress. Thus, growth in the stand may increase in some cases, taking advantage of the demise of other more sensitive species.

Third, a species that is dominant, or becoming so, may increase in growth consistently at the expense of other species, even though its own growth is impaired by O_3. This type of response was illustrated by red oak within the Chestnut Oak forest type.

Finally, some species may show the combined effects of competition and O_3. In the case of black cherry at low O_3, it is not able to compete as well as some other species in the stand. At high O_3, its own growth is diminished, preventing it from taking advantage of slower growth by other species.

The inconsistencies due to the interaction of O_3 with normal stand development would be exacerbated if other stresses such as drought or attack by insect and disease were considered.

Spatial Extrapolation

Maps illustrating the interpolation of O_3 exposures over the extent of the park for 1997-1999, and for the total exposure over three years, are shown in Figures VII-31 through VII-34. The patterns reflect primarily the differences in elevation within the park. These interpolations were used to extrapolate TREGRO and ZELIG projections over the park.

The spatial extrapolations of the effects of ambient levels of O_3 projected by TREGRO on growth of individuals are illustrated in Figure VII-35 and the figures in Appendix G. The simulated effects of current levels of O_3 on the growth of target species ranged from no change in growth to about a 1% decrease in total growth of white ash over the three year simulation. Based on these analyses, it seems likely that only the growth of white ash is significantly affected by O_3 at the present time. It is important to note, however, that although projected growth losses are small, they may accumulate over time. Furthermore, visible injury of leaves may be present at exposures less than those necessary to cause a reduction in growth. Results for white ash are shown in Figure VII-35. Results for other species, which were less pronounced, are shown in Appendix J.

The spatial extrapolations of ZELIG results are shown in Figures VII-36 through VII-38. Virtually no response of forest types to O_3 was projected over the park due to the relatively small

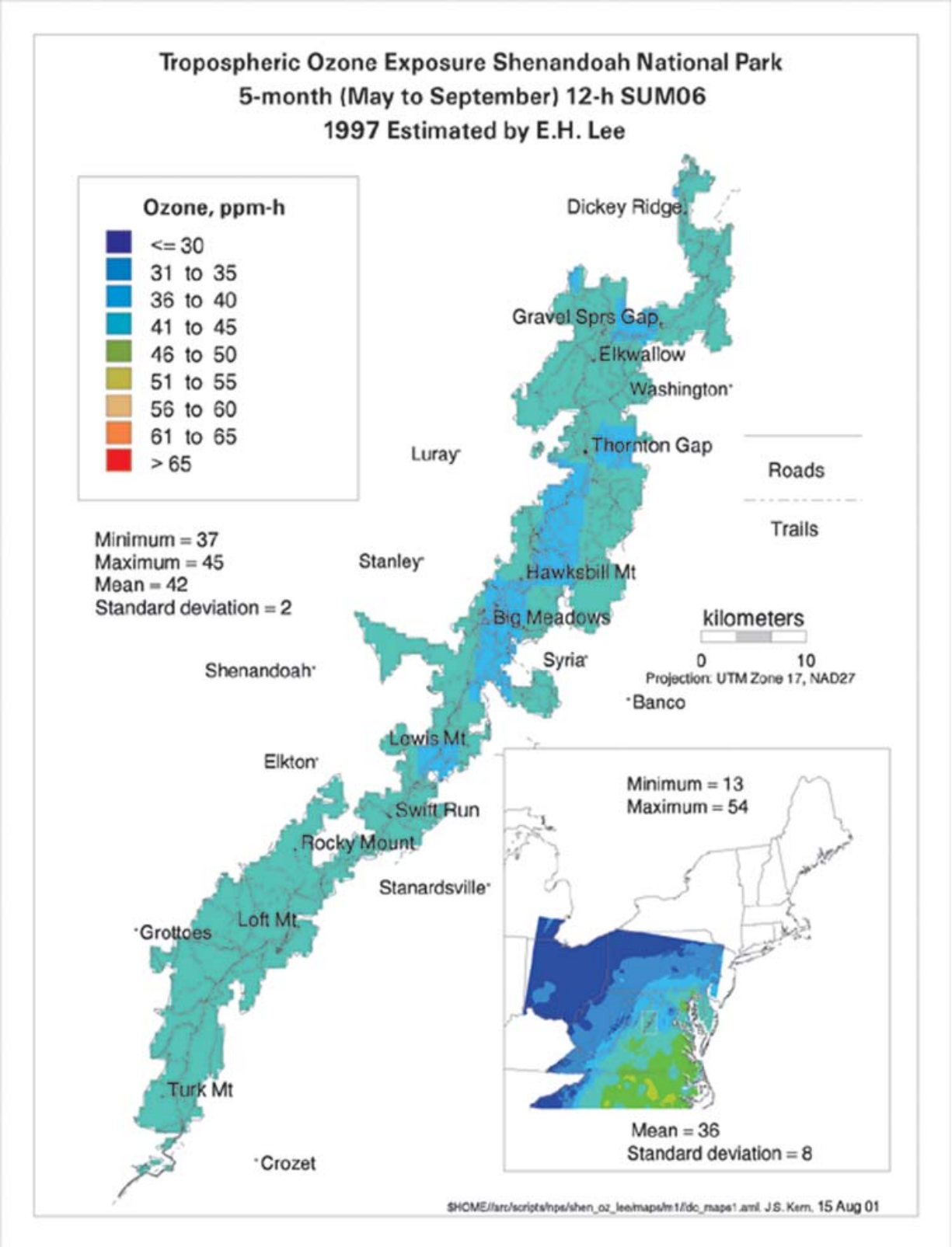

Figure VII-31. Interpolated ozone exposure (on a 4 km grid) for SHEN in 1997.

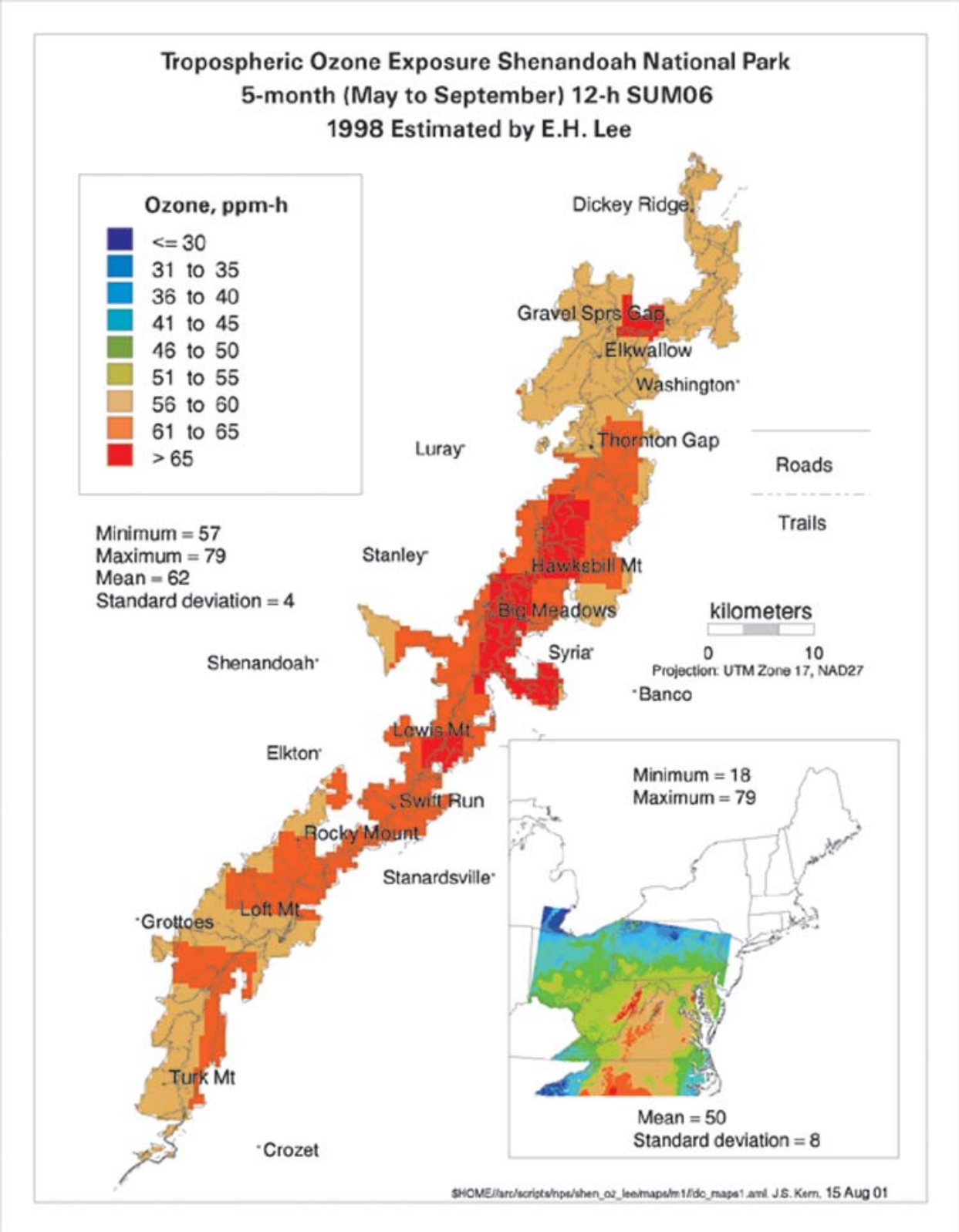

Figure VII-32. Interpolated ozone exposure (4 km grid) for SHEN in 1998.

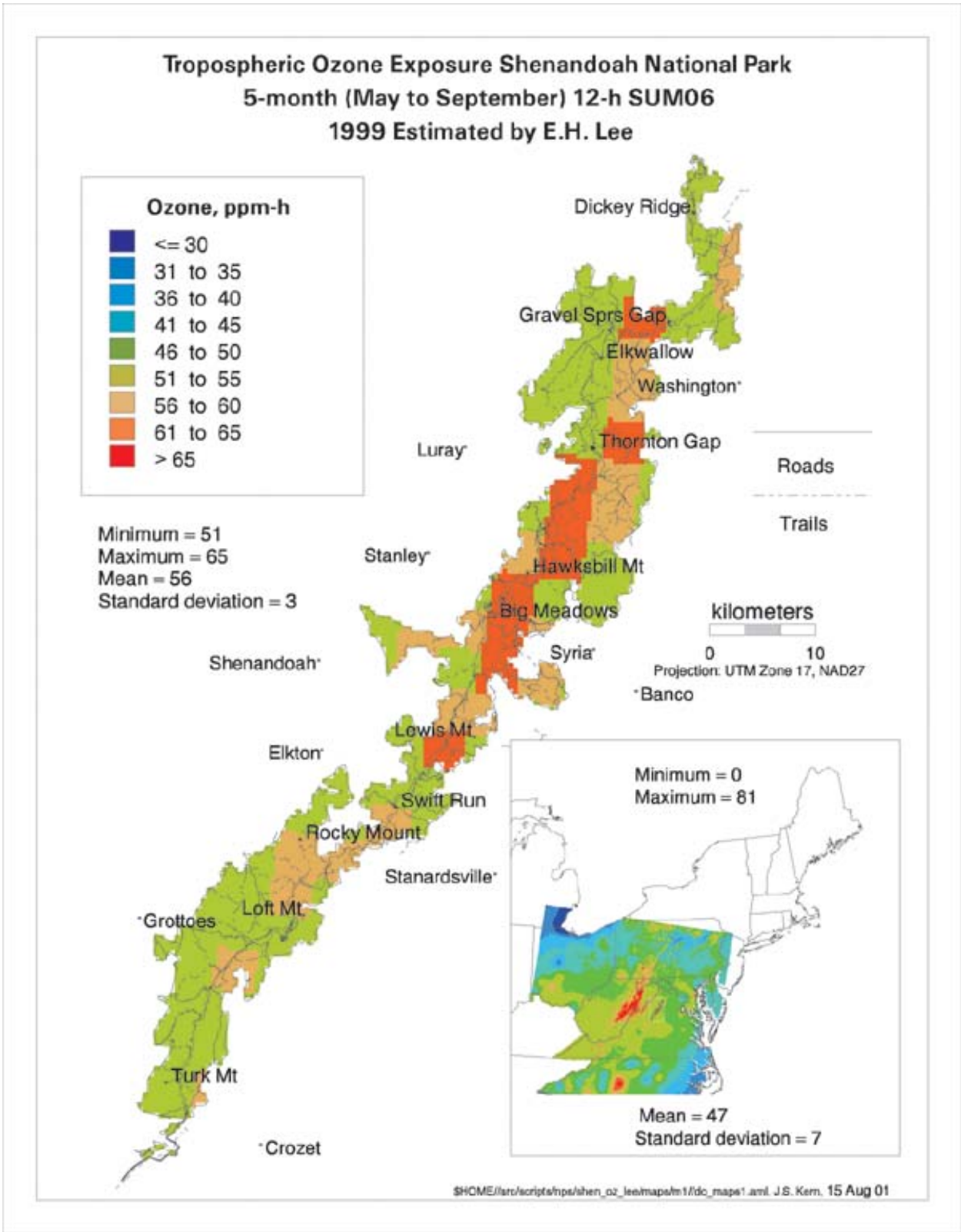

Figure VII-33. Interpolated ozone exposure (4 km grid) for SHEN in 1999.

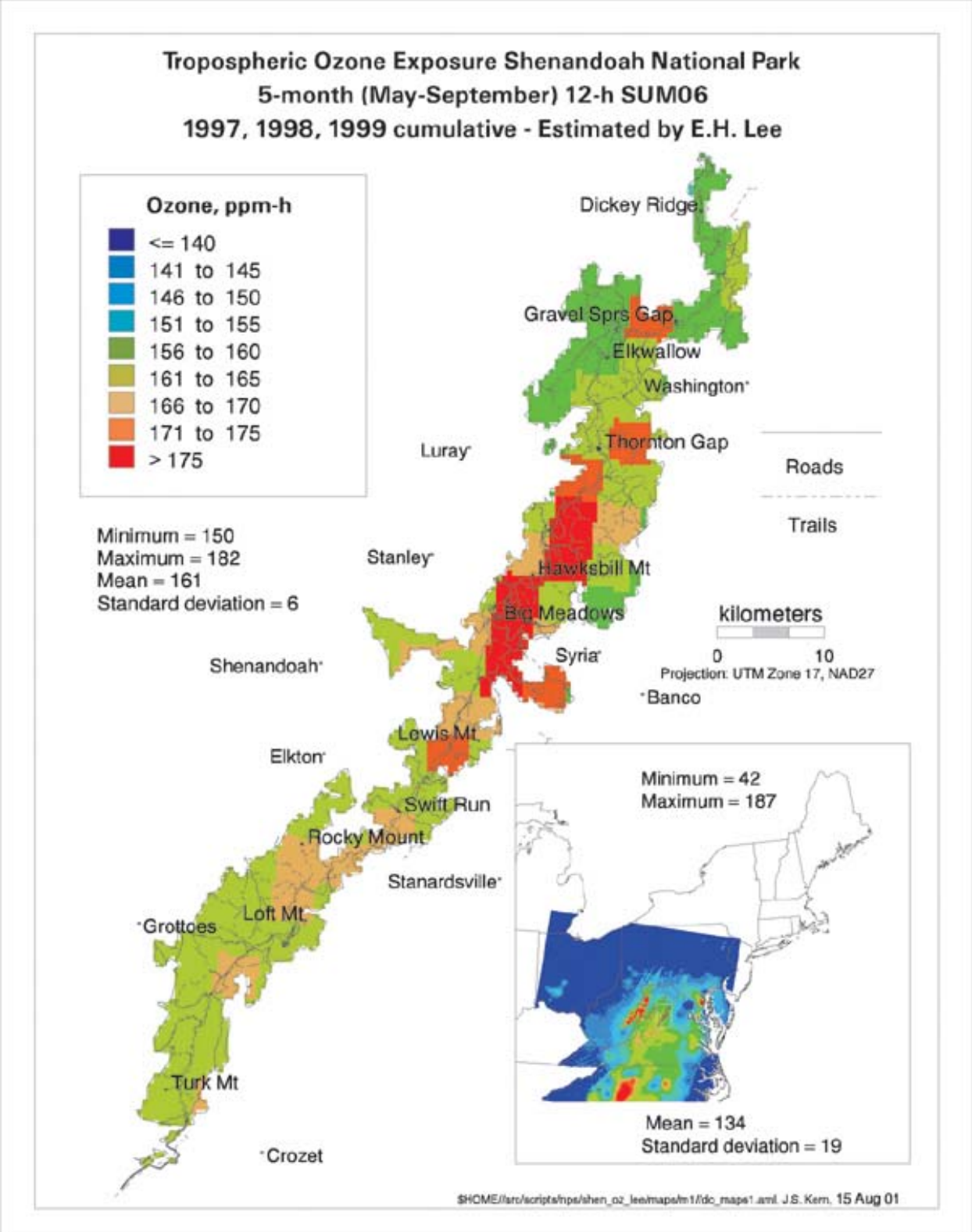

Figure VII-34. Interpolated total ozone exposure (4 km grid) for SHEN, 1997-1999.

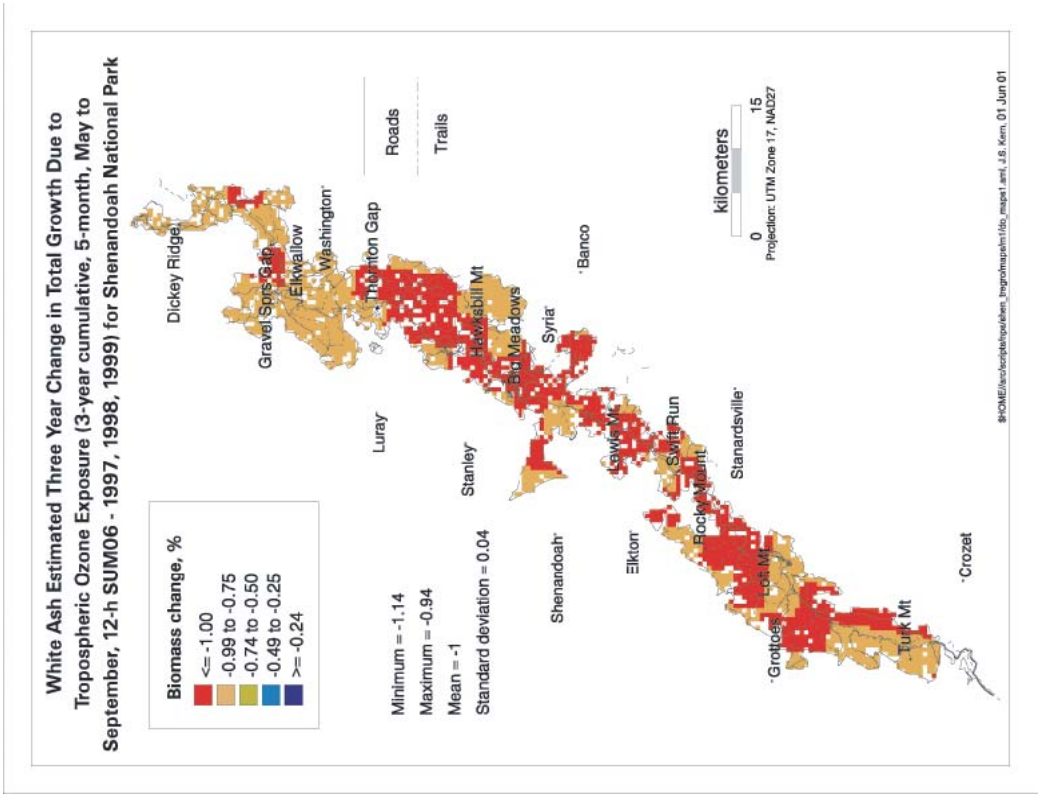

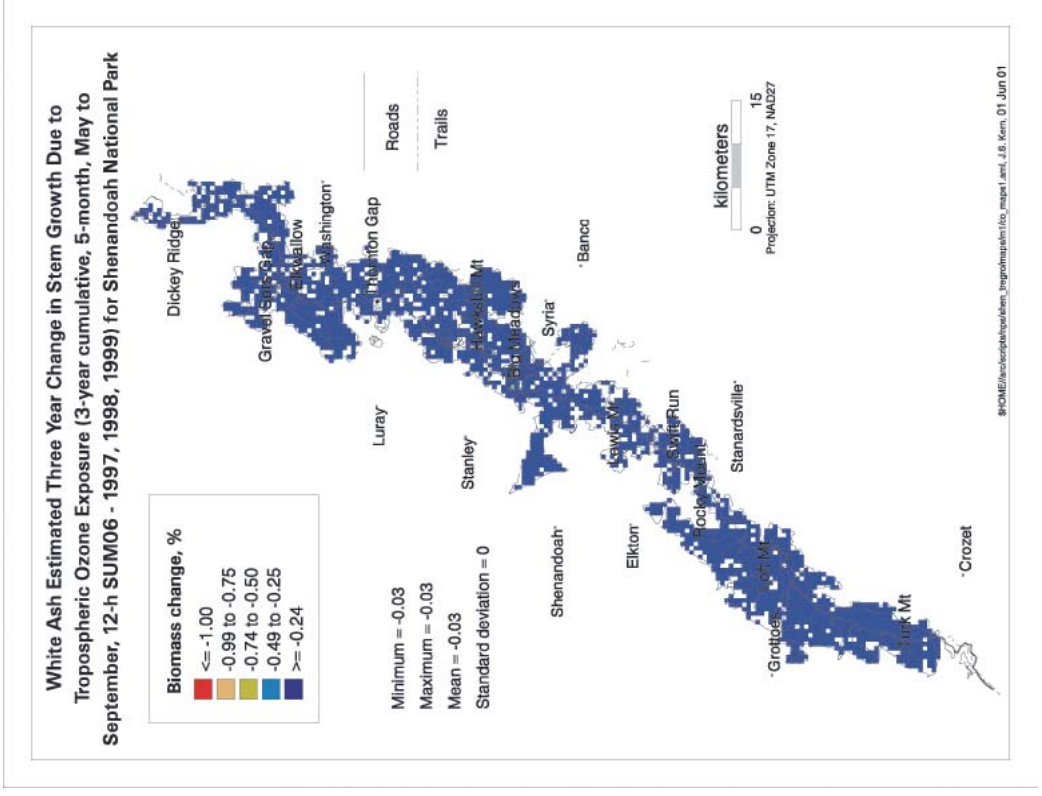

Figure VII-35. Projected change in stem (left) and total (right) mass of white ash in response to ozone exposures in 1997-1999.

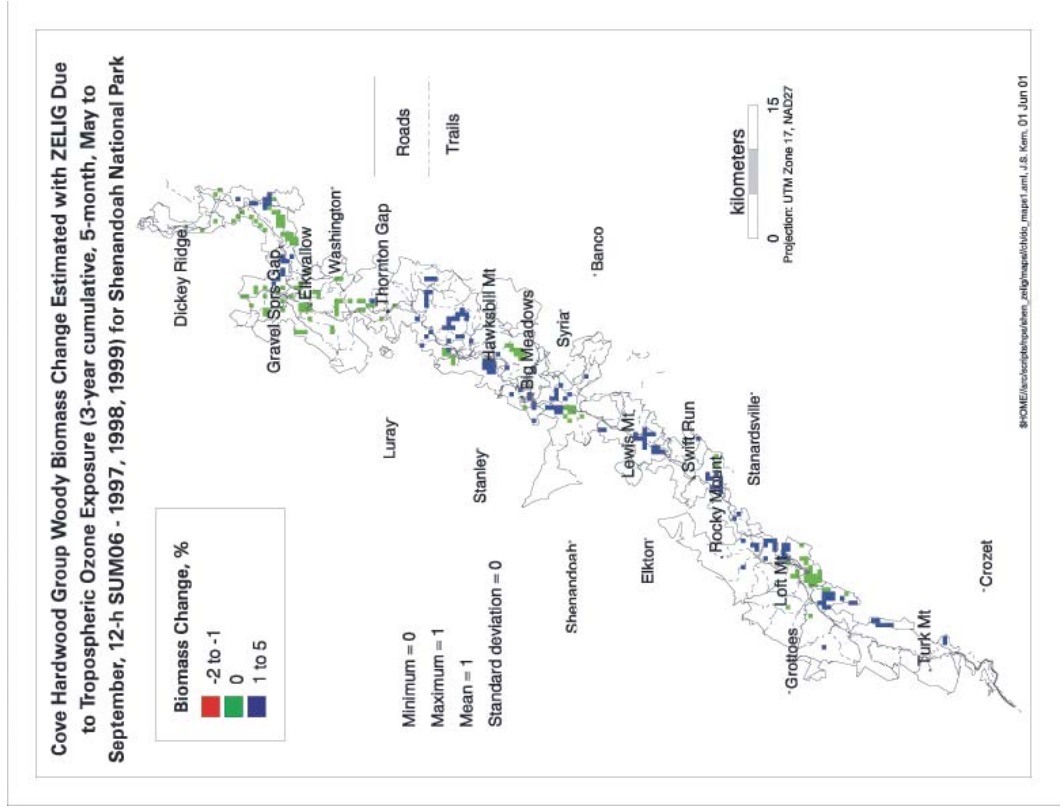

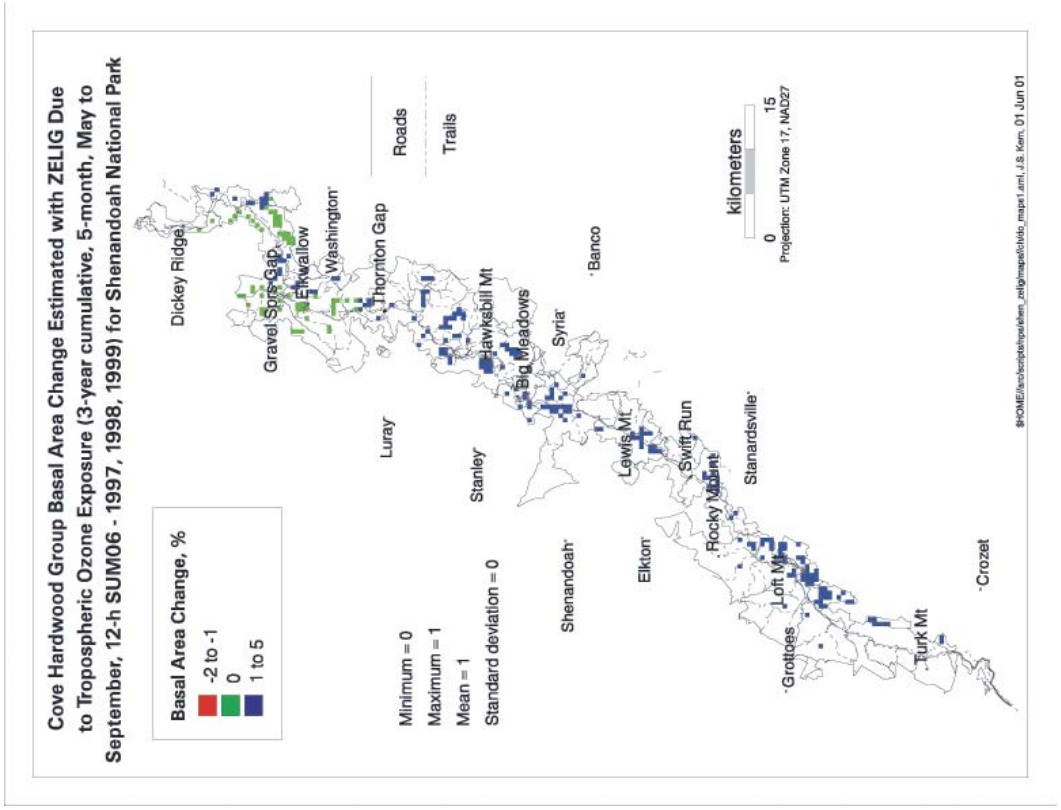

Figure VII-36. Projected change in basal area (left) and woody biomass (right) in Cove Hardwood forests in response to ozone over 100 years.

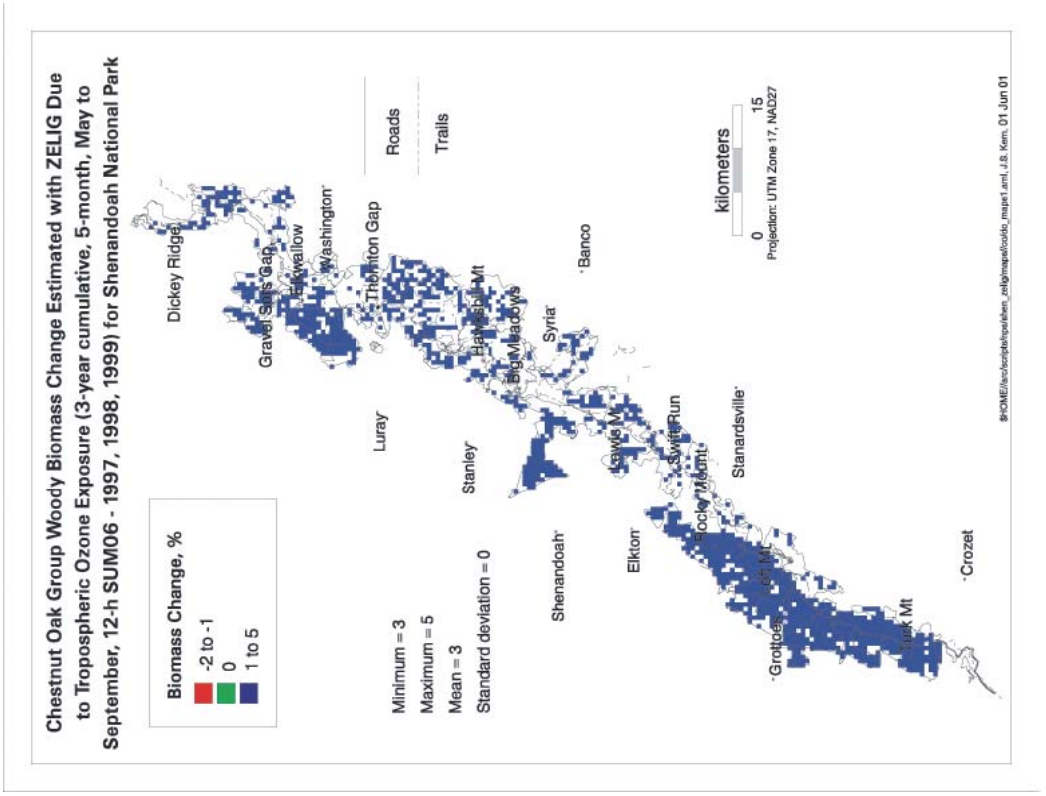

Figure VII-37. Projected change in basal area (left) and woody biomass (right) in Chestnut Oak forests in response to ozone over 100 years.

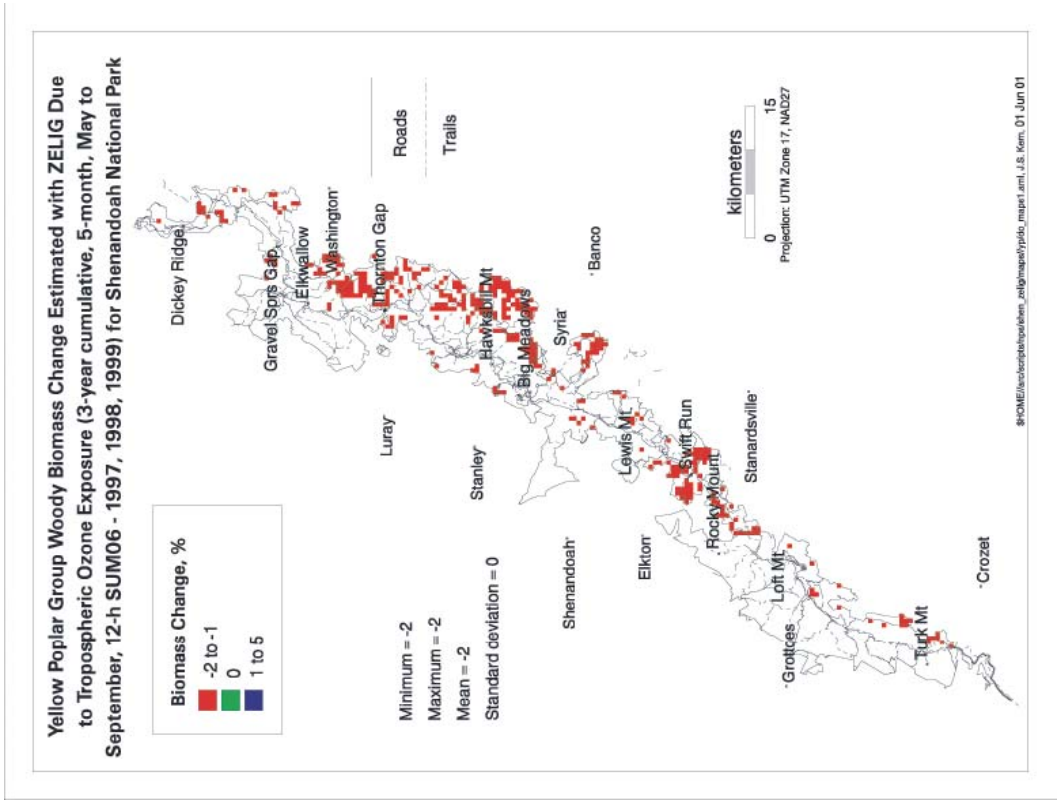

Figure VII-38. Projected change in basal area (left) and woody biomass (right) in Yellow Poplar forests in response to ozone over 100 years.

changes in growth and composition simulated by ZELIG at ambient O_3 concentrations. No changes were observed in the total projected productivity or composition of species or forests.

Uncertainties and Limitations in the Analysis

There are a number of recognized limitations in this analysis. The limitations fall into four general categories: species response, simulation methodology, model linkages, and extrapolation.

In this analysis, we assume that the species response to O_3 determined experimentally is correct, and further, that it applies to all mature individuals. We ignore potential genetic differences in sensitivity and possible influences of variable environmental conditions on the exposure-response relationships. To address this limitation, we conducted simulations at seven O_3 exposure levels. Potential differences in sensitivity can be addressed by assuming a greater or lesser exposure.

The simulation methodology has been tested and verified extensively. However, it must be remembered that simulation models are simplifications of reality, and we obviously do not simulate all processes that occur in trees and forest stands. Based upon years of use and comparisons with controlled experiments or known tree and forest growth, we believe the results reasonably reflect responses in the field.

In this assessment, we linked TREGRO to ZELIG using only three modifiers of stand processes. It would be possible to use many more linkages, but the research necessary to establish those linkages was beyond the scope of this project. The TREGRO-ZELIG linkage has been subjected to peer-review and we believe it is a reasonable approach to provide a physiological mechanism for estimating O_3 impact on stand growth.

Finally, we extrapolated the results of our simulations across SHEN. This extrapolation assumes that the O_3 exposures we hypothesize to occur do, in fact, occur; that the trees and forest types are found where the maps indicate they are found; that the exposure-response relationships developed from the simulations hold at all locations in the park; and that there are no interactions with other stresses. We do not believe these assumptions limit the validity and usefulness of the assessment. It is important to note, however, that pollutant stresses do not act individually. Trees and forest stands are exposed simultaneously to multiple air pollutants and also to multiple diseases, insects, and other disturbance mechanisms. Multiple stresses probably affect the structure and function of park ecosystems beyond the effects of one stressor in isolation.

d. Prognosis for Recovery of Terrestrial Ecosystems

Based on the results of this simulation study, it seems unlikely that reductions in the growth of forest trees in excess of about 1%, or in the composition of forest stands, are occurring as a result of O_3 exposure at SHEN. An exception to this is white ash, which seems to be more sensitive, both as an individual and in a stand, than the other species.

In general, these results are in agreement with other simulations of O_3 effects on the growth of mature trees and forests. For instance, Laurence et al. (2001) reported a simulated decrease in growth of about 0.7% for loblolly pine and 0.2% for yellow poplar over the southern United States. Woodbury et al. (1995) also reported relatively small growth reductions in loblolly pine using a different simulation system. Ollinger, in Laurence et al. (2000), found reductions in net primary productivity of about 5 to 9% over a five-year simulation of forests in the northeast United States. His analysis showed that drought stress had a greater impact on growth than O_3, and in the driest conditions, drought reduced the O_3 response by 25%.

On the other hand, large reductions in growth have been simulated in some studies elsewhere. Tingey et al. (2001) simulated reductions in growth of ponderosa pine (*Pinus ponderosa*) due to O_3 ranging from close to 0 to greater than 40% under the most severe conditions in southern California. Weinstein et al. (2001) reported no change in the simulated growth of black cherry in the Great Smoky Mountains, but large reductions in the growth of yellow poplar and red maple (>40% and 20%, respectively). Their simulations used essentially the same parameter values for the species as we used in this study.

There are two potential explanations for these differences in model output. First, we used three years of actual meteorological observations from Big Meadows whereas Weinstein et al. (2001) used the same weather (1992), repeated three times. We know that both 1998 and 1999 were warm years, which could reduce the effect of O_3 in the model (Tingey et al. 2001). The second difference relates to the construction of O_3 profiles. Our method increases the exposure in proportion to the annual maximum O_3 concentration. Weinstein et al. (2001) applied a multiplier to all concentrations; in their 0.5 x ambient profiles, the lowest concentrations were also decreased by 50% whereas our lowest exposure was reduced by only 13% of the total O_3 exposure. This makes a substantial difference in the "background exposure" that is used to calculate projected growth decrease. Differences in the elevated O_3 exposure, calculated using a constant multiplier versus proportional increase, could affect the dynamics of carbon gain,

particularly when there is heavy demand on stored carbohydrates for growth, and this could account for differences in our projections.

There are few field studies of the effects of O_3 on mature trees. McLaughlin and Downing (1995) projected circumference growth reductions due to the interaction of O_3 and soil moisture of from 0 to about 30%, depending on the year. For conditions similar to those in this study, the projected growth loss was 7% or less. Samuelson and Kelly (1996) compared the response of seedling and mature red oak to O_3 and found, in general, that mature trees had a greater uptake rate of O_3 than did seedlings. However, in a three-year study, they did not find the growth of mature trees to be reduced by ambient O_3 at Norris, Tennessee.

Duchelle et al. (1982) exposed seedlings of eight tree species to ambient and charcoal-filtered air in open-top chambers at Big Meadows. They reported a substantial decrease in height growth of yellow poplar seedlings under ambient O_3 conditions, but did not report total growth or foliar injury. Neufeld et al. (1995) exposed black cherry seedlings to O_3 in open-top chambers at Great Smoky Mountains National Park. They reported seasonal losses of 1-2% in growth at ambient O_3. Effects on seedlings do not necessarily translate to effects on mature trees, however.

Recently, Chappelka and Samuelson (1998) reviewed the literature and concluded that growth losses in the eastern United States from ambient O_3 are likely less than 10% and are affected by a multitude of factors. Intuitively, it seems unlikely that the growth reductions of up to 40% reported by Weinstein et al. (2001) for the Great Smoky Mountains could have been occurring over long periods of time without such differences being measured in forest inventories. We believe O_3 is more likely to be a long-term debilitating stress, causing relatively small changes in growth on an annual basis, but some potentially large changes in species composition, such as for white ash in SHEN.

Ozone causes visible injury on many plant species in SHEN, an endpoint that cannot be addressed in this simulation study. Hildebrand et al. (1996) reported that O_3, at approximately the same levels as reported for SHEN in this study, caused visible injury on yellow poplar, black cherry, and white ash. Although a high percentage of the trees had symptoms of O_3 exposure, the amount of leaf area injured was relatively small. They did not make measurements of growth that could be compared to our results.

Results of the analyses performed for this assessment suggest that further deterioration in air quality at SHEN would begin to take a toll on the growth of forest trees and the composition of

stands. In addition, whereas the current impacts of O_3 seem to be small, it is important to remember that O_3 does not act alone. The O_3 effects modeling analysis is an attempt to isolate the effects of O_3 from those of other stresses, but other stresses do occur, potentially exacerbating the relatively small, direct growth effects of O_3 at current concentrations.

The results of the O_3 effects modeling suggest that up to a 20% increase in current ambient O_3 could be tolerated in the absence of other significant stressors before substantial effects on tree growth and stand composition would occur. However, it is likely that some species, such as white ash, would begin to decline further in growth with any increase in ambient concentrations. We would also expect impacts to occur on stand composition, primarily through the effects on white ash. Visible foliar injury to sensitive species would certainly increase beyond what currently occurs. Given these results, it seems that the critical exposure level for sensitive species like white ash is likely below current ambient levels. Simulation results suggest that critical O_3 exposures ranging from about 15% less than current ambient levels to up to 20% greater that current ambient levels should protect against growth and species composition impacts to sensitive (e.g., white ash) and less sensitive (e.g., sugar maple) species, respectively. The critical level to protect against visible foliar O_3 injury or growth effects on tree seedlings would be substantially lower than current ambient exposure, probably in the range of 8 to 12 ppm·hr SUM06 (3 month, 12-hour) or 10 to 15 ppm·hr, respectively, as suggested by Heck and Cowling (1997).

3. Visibility

As shown in Section V, visibility at SHEN, while showing some indications of improvement, is presently much worse than estimated natural conditions. In order to assess the sensitivity of visibility to changes in emissions, future visibility conditions at the park were estimated from modeling analyses of expected and hypothetical emissions scenarios described in Section IV. Emissions and ambient conditions from 1990 were selected as the base case for this projection. The 1996 column in Table VII-21 reflects visibility improvements related to SO_2 emissions reductions mandated by Phase I of the Title IV Acid Rain Program of the CAAA of 1990.

The visibility condition associated with each emissions (modeling) scenario was calculated using the expected reduction in particle concentrations (see Table VII-21, top half) and the

Table VII-21. Degree of visibility improvement associated with the emission reductions scenarios given in Section IV, relative to the 1990 Base Case.

Attribute	1996	Scenario 1 2007/10	Scenario 2 2020	Scenario 3 2020	Scenario 4 2020
Combined Reduction of Fine Particle Ammonium Sulfate and Nitrate Relative to the 1990 Base Case					
Annual Mean	-6.9%	-15.7%	-17.5%	-41.7%	-50.4%
Warm Season Mean	-15.0%	-28.5%	-30.8%	-55.7%	-63.6%
Expected Visibility Improvement[a]					
Annual Mean	5.1%	11.7%	13.0%	31.0%	37.5%
Warm Season Mean	12.4%	23.5%	25.4%	45.9%	52.4%

[a] Relative humidity adjustment factors of 3.65 and 4.31 were used for annual and warm season means, respectively

corresponding change in light extinction coefficient (see Appendix B for calculation method). The observed 1990 annual mean and warm season mean visibility conditions at SHEN were 111 Mm^{-1} (35 km visual range) and 187 Mm^{-1} (21 km visual range), respectively. Expected improvements from this base case are presented in Table VII-21 (bottom half). The estimated annual mean improvement in atmospheric extinction ranged from 105 to 69 Mm^{-1} (visual ranges from 24 to 44 km). Although these visibility improvements represent progress toward the national visibility goal (Section I), they fall substantially short of the nearly 80% improvement in extinction needed to restore natural conditions (Section IV) as is required by the 1999 Regional Haze Rule. An interesting comparison can be made between the model projections of improvements for 1996 of 5.1 and 12.4% for the annual and warm season mean and the actual changes estimated from ambient data collected in the park in 1990 and 1996 of 12 and 10% for the same respective averaging times (Table V-11). The improvements estimated by the model for 1996 as compared to 1990 Base Case were generally similar to the actual differences in the "measured" extinction at the park for the years 1990 and 1996.

The encouraging recent trend in visibility at the park, notwithstanding, current visibility conditions still represent a significant departure from what a visitor could experience if natural conditions were more prevalent. The park certainly has benefitted (Malm et al. 2002), and should continue to benefit, from emission reductions contained in Scenario 1 (primarily Title IV emissions reductions at EGUs and Federal Tier II standards; Section IV). However, these conditions are forecasted to achieve only an 11.7 % improvement in annual average visibility (Table VII-21). Only emissions scenarios 3 and 4, which have more stringent controls

(including over 90% reductions for EGUs), would make significant progress towards the national visibility goal. For the warm season, the degree of needed improvement is nearly 85%, but even the most stringent scenario (4) was forecasted to achieve only a 52.4% improvement in visibility (Table VII-21).